

GPSS | Global Program
for Safer Schools

GLOSI THE GLOBAL LIBRARY
OF SCHOOL INFRASTRUCTURE

Fragility and Vulnerability Assessment Guide

October 2019



GLOSI THE GLOBAL LIBRARY
OF SCHOOL INFRASTRUCTURE

Fragility and Vulnerability Assessment Guide

October 2019



© 2019 International Bank for Reconstruction and Development / The World Bank

1818 H Street NW

Washington DC 20433

Telephone: 202-473-1000

Internet: www.worldbank.org

This work is a product of the staff of The World Bank with external contributions. The findings, interpretations, and conclusions expressed in this work do not necessarily reflect the views of The World Bank, its Board of Executive Directors, or the governments they represent.

The World Bank does not guarantee the accuracy of the data included in this work. The boundaries, colors, denominations, and other information shown on any map in this work do not imply any judgment on the part of The World Bank concerning the legal status of any territory or the endorsement or acceptance of such boundaries.

Rights and Permissions

The material in this work is subject to copyright. Because The World Bank encourages dissemination of its knowledge, this work may be reproduced, in whole or in part, for noncommercial purposes as long as full attribution to this work is given.

Any queries on rights and licenses, including subsidiary rights, should be addressed to World Bank Publications, The World Bank Group, 1818 H Street NW, Washington, DC 20433, USA; fax: 202-522-2625; e-mail: pubrights@worldbank.org.

Graphic and design: Miki Fernández



Acknowledgements

The Global Library of School Infrastructure (GLOSI) was created by **Fernando Ramirez Cortes** (Senior Disaster Risk Management Specialist), **Carina Fonseca Ferreira** (Disaster Risk Management Specialist), **Laisa Daza Obando** (Consultant), and **Jingzhe Wu** (Consultant) from the World Bank's Global Program for Safer Schools (GPSS).

The original analytical framework and content of the GLOSI was prepared by a technical team led by **Dina D'Ayala** (Project Director) from University College London, United Kingdom, and **Luis Eduardo Yamin** (Project Director) from Universidad de Los Andes, Bogotá, Colombia. The technical team comprised **Rohit Kumar Adhikari** (Project Specialist) from University College London, **Rafael Ignacio Fernández** (Project Specialist), **Angie Garcia** (Project Specialist), **Miguel Rueda** (Project Specialist) and **Gustavo Fuentes** (Project Specialist) from Universidad de Los Andes.

The GLOSI was developed with grant support from the Global facility for Disaster Reduction and Recovery (GFDRR), including the Japan-World Bank Program for Mainstreaming Disaster Risk Management in Developing Countries. The team is especially thankful to **Francis Ghesquiere**, **Julie Dana**, **Luis Tineo**, **Sameh Naguib Wahba**, **Maitreyi B Das**, and **David Sislen** who provided overall guidance and support in the preparation of the GLOSI. The team would also like to thank **Juan Carlos Atoche Arce**, **Diana Katharina Mayrhofer**, **Maria De Los Angeles Martinez Cuba**, **Nathalie Judith Karine Tchorek**, and **World Bank Rapid Application Development Team** who provided valuable input and contributions to this document.

Contents

Global Library of School Infrastructure	1
1. GLOSI for Seismic Risk Assessment	3
2. Fragility/Vulnerability Assessment Methodology	4
2.1 Hazard Definition.....	6
2.2 Definition of Index Buildings.....	6
2.3 Numerical Modelling.....	7
2.4 Non-Linear Pushover Analysis and Pushover Curve Derivation	9
2.5 Damage States and Thresholds	11
2.6 Seismic Performance Assessment: N2 Methodology.....	16
2.7 Derivation of Fragility Functions	21
2.8 Derivation of Vulnerability Functions.....	23
3. Illustrative examples	31
3.1 Example Analysis for an LBM Index Building	31
3.1.1 Hazard Definition	31
3.1.2 Index Building Definition	32
3.1.3 Numerical Modelling, Pushover Analysis and Seismic Behavior.....	33
3.1.4 N2 Analysis.....	36
3.1.5 Fragility Analysis.....	37
3.1.6 Vulnerability Analysis.....	37
3.2 Example Analysis of an RC Index Building	38
3.2.1 Hazard Definition	38
3.2.2 Index Building Definition	39
3.2.3 Numerical Modelling and Pushover Analysis.....	40
3.2.4 N2 Analysis.....	41
3.2.5 Fragility Analysis.....	42
3.2.6 Vulnerability Analysis.....	42

4. Catalog of Fragility/Vulnerability Assessment Results	44
5. Sensitivity Analysis	46
5.1 Load Bearing Masonry	46
5.1.1 Seismic Design Level.....	48
5.1.2 Diaphragm Type.....	51
5.1.3 Irregularities	54
5.1.4 Wall Panel Length	56
5.1.5 Wall Opening	59
5.1.6 Effective Seismic Retrofitting.....	61
5.1.7 Structural Health Condition.....	63
5.2 Reinforced Concrete	67
5.2.1 Geometrical variations	67
5.2.2 Ground motion records for different soil types.....	69
5.2.3 Foundation-soil flexibility	70
5.2.4 Masonry infill quality	72
5.2.5 Non-structural vulnerable elements.....	74
5.2.6 Analysis type	76
References.....	78



Global Library of School Infrastructure

The World Bank's Global Program for Safer Schools (GPSS) launched in 2019 the Global Library of School Infrastructure (GLOSI). The GLOSI is a live global repository of evidence-based knowledge and data about school infrastructure and its performance against natural hazard events. A one-stop-shop with open access to global indicators on school infrastructure exposure and risk to natural hazards, taxonomy of school buildings, catalog of building types, fragility and vulnerability information, case studies on vulnerability reduction solutions applied around the world, and data collection tools. In-country data is also available with restricted access. The GLOSI is updated over time through World Bank-funded safer school projects and contributions from development partners with interest in this field.

Why do we need GLOSI?

Safer school projects have taught us that there are three main challenges to global dissemination of knowledge surrounding school building performance: communication to decision makers, the lack of a common language, and facilitation of quantitative risk assessment.

Global knowledge about school infrastructure performance needs to reach decision makers

The engineering community has achieved immense progress in the past few decades towards understanding building performance against natural hazards and devising scalable risk-reduction solutions. However, this knowledge has not reached decision makers nor has it been used to drive school infrastructure investments. Without this knowledge, the opportunity to maximize benefits from intervention and optimize investments in school safety can be lost.

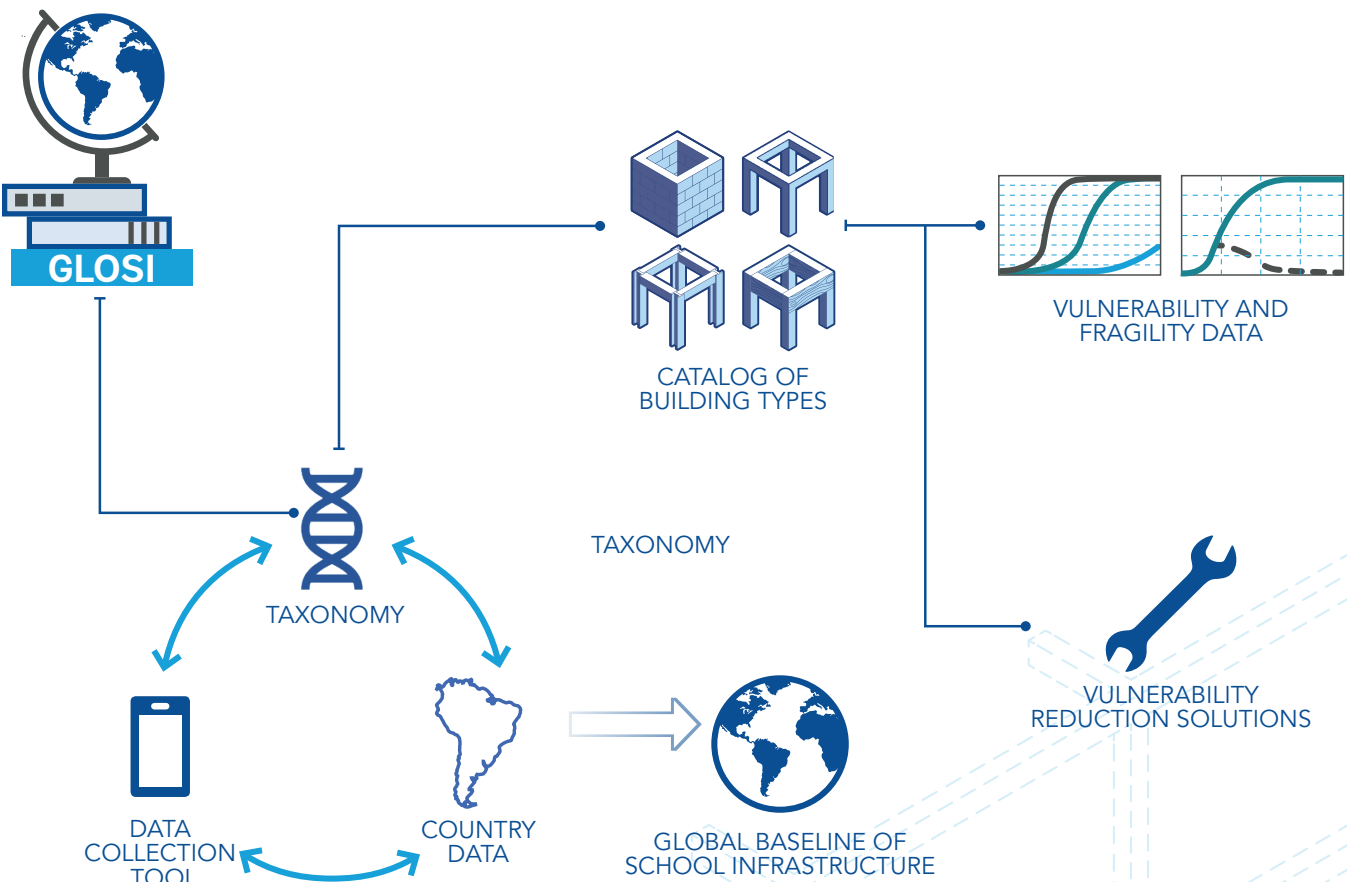
The first objective is to create a universal "language"

School buildings tend to follow standard designs, yet buildings with similar vulnerability are still difficult to identify in different countries, or even within a country. This is largely due to the lack of a systematic classification system and consistent vulnerability assessment framework. The GLOSI offers a solution by making a taxonomy and vulnerability assessment framework for school buildings globally applicable, and oriented to produce quantitative risk information that will inform large investments in school safety and resilience.

The GLOSI is a tool to mainstream quantitative risk assessment in investment planning

By using a systematic taxonomy, the GLOSI includes a catalog of typical school building types found in different parts of the world with the respective vulnerability data needed to conduct quantitative risk assessments. Countries can map their school facility portfolios with the catalog and use the GLOSI data to perform quantitative risk assessments or vulnerability analyses to identify cost-efficient retrofitting solutions. The availability of this information will ensure that results are scalable across countries and safer school engagements in each country begin with a solid existing technical foundation.

Global Library of School Infrastructure (GLOSI)



1. GLOSI for Seismic Risk Assessment

As part of the GLOSI initiative, a methodological approach has been defined to derive both the seismic fragility and vulnerability (F/V) of selected school index buildings (IBs). Considering that each of those IBs represents a typology that can be found in several countries, a reliable analytical assessment of expected seismic performance is an important contribution toward a robust seismic risk assessment process in any country or region around the world.

Globally used risk assessment platforms (HAZUS, CAPRA, OpenQuake, RISK-UE) typically provide, for each building typology, a quantitative probabilistic relationship between a given seismic intensity and expected damage expressed in terms of either a fragility or vulnerability function:

- **Fragility function**

It establishes the probability of reaching or exceeding a particular damage state given a hazard intensity parameter. Damage states are usually defined in terms of global or local parameters, which identify the loss of physical integrity and structural capacity of the building. In an analytical fragility assessment, the damage states are defined with respect to damage thresholds, i.e. specific values of an Engineering Demand Parameter (EDP), such as roof or inter-story drift, which characterize the onset of a particular damage state.

- **Vulnerability function:**

It correlates the Mean Damage Ratio (MDR) and its variance with a hazard intensity parameter. The MDR is usually expressed in economic terms, as the ratio of the expected total repair cost to the total replacement cost of the building. Within the GLOSI library, the total

replacement cost of the building has been defined as the actual reconstruction cost of the building according to local price conditions in the country or zone under analysis.

GLOSI Informs Future Seismic Risk Assessment –

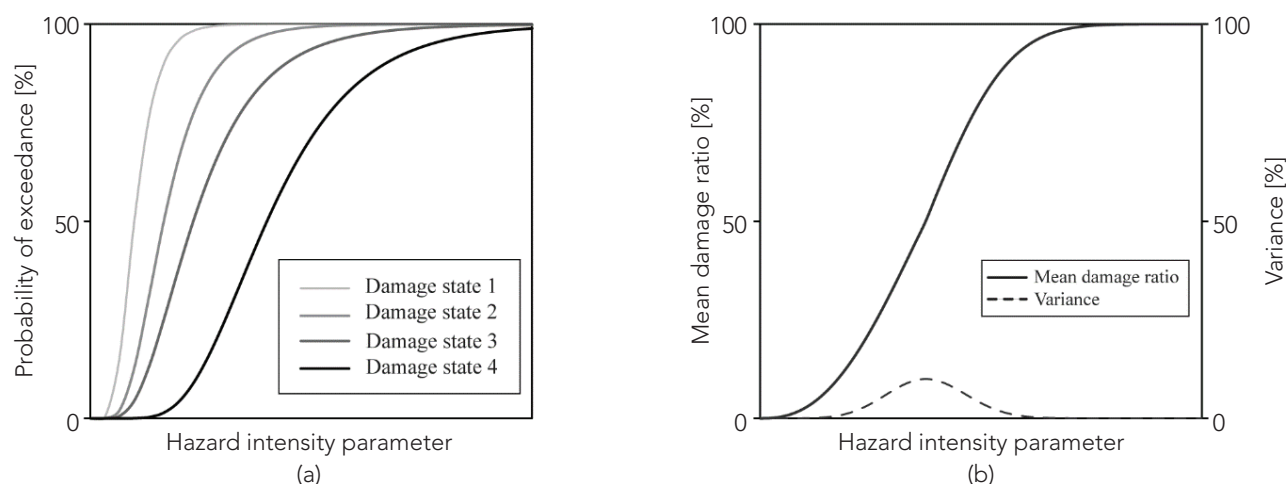
GLOSI provides a collection of F/V functions for all IBs considered, together with their uncertainty and possible sensible variations with selected critical parameters. The GLOSI methodology can be easily adopted by the structural engineering community to generate F/V functions for particular local conditions in developing countries worldwide.

The hazard intensity parameter used for the GLOSI corresponds to peak ground acceleration (PGA (g)) for load bearing masonry (LBM) structures and spectral acceleration at a given structural period T ($Sa(T)$) for reinforced concrete (RC) structures. Figure 1 presents the general conception and representation of the fragility and vulnerability functions used in a risk assessment process.

The main sources of uncertainty considered in the vulnerability assessment include both aleatory and epistemic uncertainties. Aleatory uncertainties are associated with the seismic input, the soil response, the frequency content of seismic records used, and the variability in the materials and design of the building stock. The epistemic uncertainty is associated with lack of knowledge of some aspects of the problem and limitation of the numerical modelling methodology, the estimation of the damage states, the repair cost estimation, and other analytical parameters used in the assessment. All uncertainties are represented in the probability distribution function of each damage state of the fragility functions or in the variance function indicated for the vulnerability function.

Finally, sensitivity analyses are performed in order to quantify the expected variations in the resulting F/V functions for a given IB, when particular critical taxonomy parameters take different values.

Figure 1. Typical representation of (a) fragility and (b) vulnerability.



2. Fragility/Vulnerability Assessment Methodology

A great diversity of methodologies can be considered to derive F/V function, including empirical, expert opinion-based, analytical, or hybrid methods. The analytical vulnerability approach has been adopted for the GLOSI, allowing unbiased and consistent assessment worldwide. The analytical approach is independent of historic seismic damage data and local expertise on specific typological building performance, which avoids introducing any potential bias. The analytical methods allow fragility and vulnerability functions to be easily updated, complemented, and modified, once more refined data on exposure or refined analytical approaches become available. Notwithstanding its generic essential quality, the analytical approach also allows a comprehensive consideration, covering structural modelling and hazard specification, local geographical and seismic conditions, and particular characteristics of each IB. Such comprehensive consideration supports the construction of more specific and region dependent vulnerability curves. For each IB, pushover curves are derived for both principal directions (longitudinal and transverse) of the building to identify the weakest direction. F/V functions are then generated and documented for the weaker direction only. Note that specific detailed strengthening/retrofit strategies to reduce fragility/vulnerability should depend on a full 3D analysis of the vulnerability of the building.

The general methodology of GLOSI to develop representative and comprehensive F/V functions for an IB using the analytical approach is briefly outlined below:

- a) **Seismic hazard definition:** hazard is defined in terms of the acceleration spectra of a set of 22 earthquake ground motion records given by FEMA P-695 that represent the following typical seismic environment:
 - a. High seismicity
 - b. Both subduction and shallow type of seismicity
 - c. Peak ground acceleration greater than 0.2g
 - d. Peak ground velocity greater than 15 cm/sec
 - e. Magnitude greater than $M_w=6.5$
 - f. Rock and soft soils sites
- b) **Definition of index buildings:** an index building is defined through the taxonomy parameters and intrinsic characteristics (geometrical characteristics and material properties) representing a group of buildings with a similar seismic behavior.
- c) **Numerical modelling and non-linear pushover analysis:** reliable 3D numerical models of index buildings are generated, and non-linear pushover analyses are performed to obtain the pushover curves. Any acceptable methodology and/or software can be used for the pushover curve derivation. It should be noted that for flexible diaphragm type LBM structures, the pushover curves are separately generated with respect to global in-plane (IP) and global out-of-plane (OOP) behaviors.
- d) **Seismic performance assessment:** the non-linear static approach is selected based on the latest version of the N2 method. For each pushover curve, the thresholds of discretized damage states represented by the roof drift are determined in terms of specific

element and global damage indicators. The definition of damage states and associated threshold limits can be code-based from available literature or IB specific. In GLOSI, the adopted approach is to identify IB specific damage states validated through experiments and field observations available in literature. This is preferred to code prescriptions. The code prescriptions are affected by expert opinion, which is not easily traceable. For each IB, the building or multi degree of freedom (MDoF) pushover curves are converted to bilinear idealized pushover curves of the equivalent single degree of freedom system (SDoF) following standard rules. This is intersected to the demand spectrum of each different ground motions suite (scaled to different values of earthquake intensity measure (IM)) to generate a group of seismic performance points (identified through IM versus EDP) ranging from slight damage to complete damage thresholds.

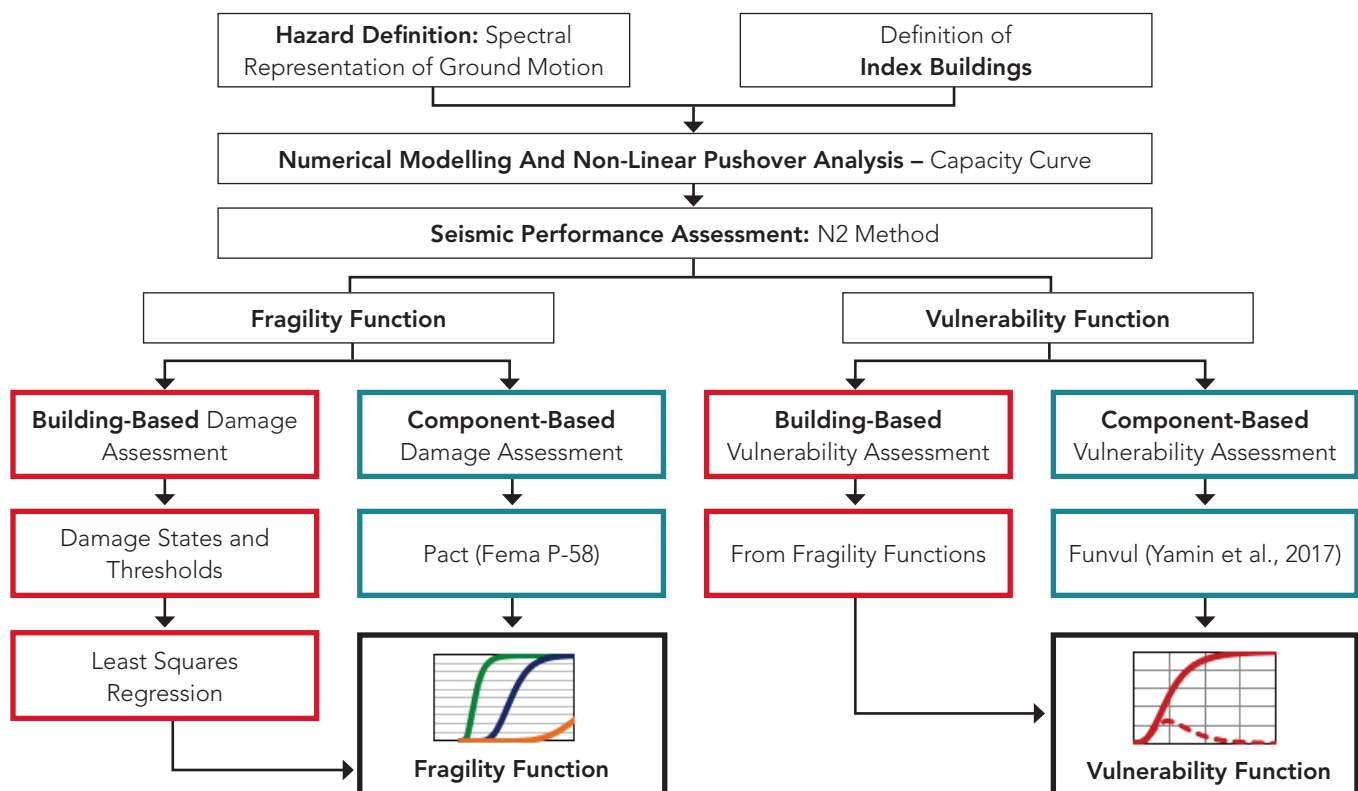
- e) **Derivation of fragility functions:** a building-based fragility assessment is conducted for the derivation of fragility functions for each damage state based on the identified performance points. For the

derivation of fragility functions, the least square regression method is used to obtain the best fit to the performance points for each damage state. It should be noted that for flexible diaphragm type LBM structures, the fragility curves are separately generated with respect to global IP and global OOP behaviors.

- f) **Derivation of vulnerability functions:** the derivation of vulnerability function for LBM IBs follows either the building-based method or the component-based method. The building-based method is used for structures with a rigid diaphragm type, while the component-based method is adopted for structures with a flexible diaphragm type. The building-based method implies convolving building-level fragility curves with the cumulative distribution of the total cost. The component-based methodology is followed to derive vulnerability functions for all RC IB cases.

Figure 2 summarizes the main steps of the methodology used in the present study to derive F/V functions. Each component of the proposed methodology is described in detail in the following sections.

Figure 2. General fragility/vulnerability assessment methodology. Note that the red and blue colors represent steps for building-based and component-based fragility/vulnerability assessment methodology, respectively.



2.1 Hazard Definition

The proposed hazard definition is based on the FEMA P-695 approach, which considers a set of pre-selected

seismic records for two different distance criteria: far field and near field. Table 1 presents the selection criteria for these two groups of records.

Table 1. FEMA P695 ground motion selection criteria.

	Far Field	Near Field
PGA	>0.2 g	>0.22 g & <1.43 g
PGV	>15 cm/sec	>30 cm/sec & < 167 cm/sec
Distance	-	>1.7 km & <8.8 km
Minimum Mw	Mw>6.5	Mw>6.5
Soil Type	Soft rock and stiff soil sites (C&D)	Soft rock and stiff soil sites (C&D)

Figure 3 presents the collection of acceleration response spectra for the far field and near field records. In GLOSI, the F/V assessment uses far field records only and the sensitivity analysis includes near field sets. For country-specific assessments, it is advisable to use ground motion sets obtained from local seismological networks or historic records, wherever available.

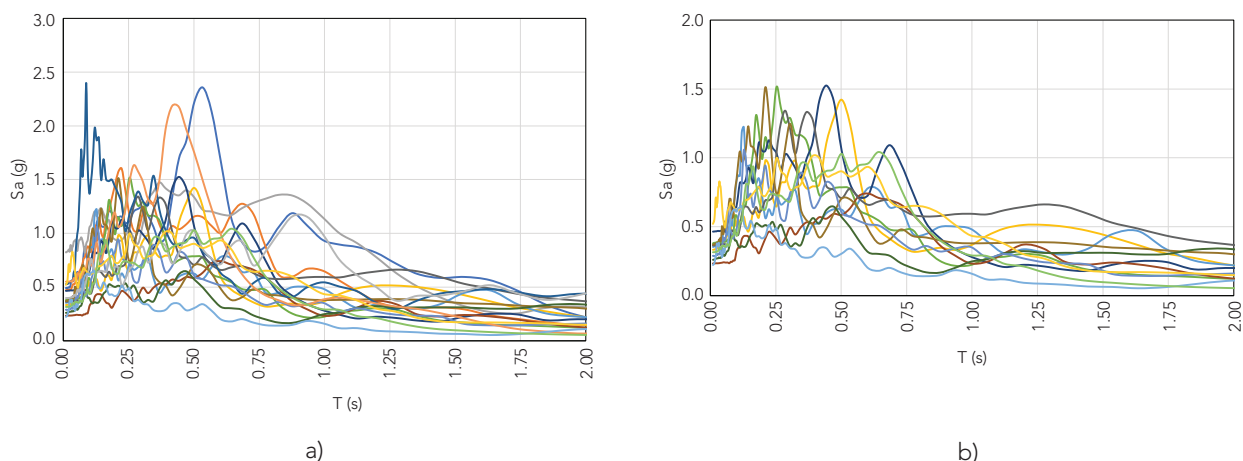
No specific additional consideration is given to the type of soil. A site-specific F/V assessment is needed for buildings located in particularly vulnerable soil conditions such as very soft soils (NHERP E or F type of soils) or with specific topographic conditions, such as steep slopes, for which the above selected records would not be applicable.

2.2 Definition of Index Buildings

Index buildings of different building types of common LBM and RC school buildings around the world are selected for the F/V assessment. A total of 14 LBM and 23 RC IBs are identified considering the main lateral load structural resisting system, the height range and the level of seismic design. Each IB is further characterized by:

- The most applicable attribute range of the secondary taxonomy parameters such as diaphragm type, structural irregularities, slenderness, structural health conditions, etc.
- The intrinsic characteristics which include the plan characteristics, geometrical details of the main structural components, and the material properties.

Figure 3. a) Far field ground motion response spectra and b) Near field ground response spectra.



2.3 Numerical Modelling

2.3.1 LBM Index Buildings

The assumption and strategy adopted for the structural modelling of LBM School IBs are as follows:

- a) Full 3D numerical models are developed for LBM IBs, with an element-by-element, non-linear modelling approach resulting in a simplified micro-modelling technique, based on the applied element method (AEM). In the AEM, masonry is modelled using a simplified micro-modelling technique (Figure 4), in which the applied elements are modelled as rigid elements whereas the joint and the mortar-unit interfaces are sandwiched into one element represented by the joint springs. If the units are expected to be damaged, the units can be divided into several elements (usually two) by having unit springs in between the applied elements of the units. All the stresses, deformation, and non-linearities in the material behavior are thus represented in the joint springs. The AEM has been used in several studies conducted on masonry structures under static and dynamic analysis. Reasonable accuracy of the AEM has been demonstrated for the study of the complete response of structures from the initiation of cracking to the final collapse. The version of this approach codified in the Extreme Loading for Structures® (ELS) software is used in the work performed under GLOSI. However, it is possible to develop the numerical model and perform pushover analysis with any other software such as macro-element based approaches (e.g. TREMURI) or finite element method (FEM) based software (e.g. ABAQUS).
- b) As shown in Figure 5, the layout of the masonry units and the resulting bond (e.g. running bond or English bond) are accurately modelled. The construction details such as lintels and the diaphragm structure (e.g. slab) are also modelled appropriately. The lintels are modelled as elastic continuous elements. Further, in the numerical model of confined masonry IBs, the tie-beams and tie-columns are modelled explicitly. Similarly, in the numerical model of reinforced masonry IBs, the reinforcements along with the grout are also modelled explicitly inside the concrete blocks.
- c) Foundation flexibility is not considered in the present work.
- d) The mechanical characteristics and parameters needed for the numerical model of each IB are calibrated using validation against experimental results on tested masonry walls for the specific masonry fabric considered.
- e) The elastic and non-linear material properties (modulus of elasticity, compressive strength, tensile strength, friction coefficients, etc.) for units, mortar and the masonry are established from available literature based on experimental test results.
- f) Dead loads and live loads are considered in the analysis. The total dead load consists of the self-weight of all the structural elements as well as the weight of the non-structural elements such as roof, ceiling, etc. In multi-story buildings, 25% of the design live load is considered in the total seismic weight of the structure (ASCE, 2013).

Figure 4. Simplified micro modelling technique for masonry adopted in the numerical modelling.

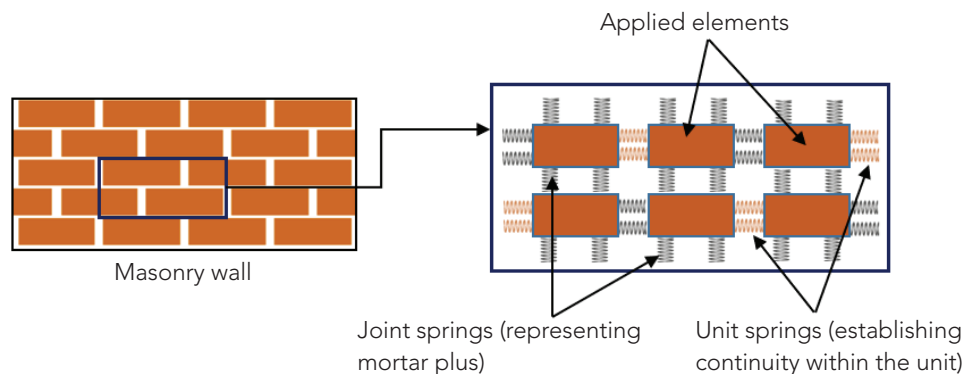
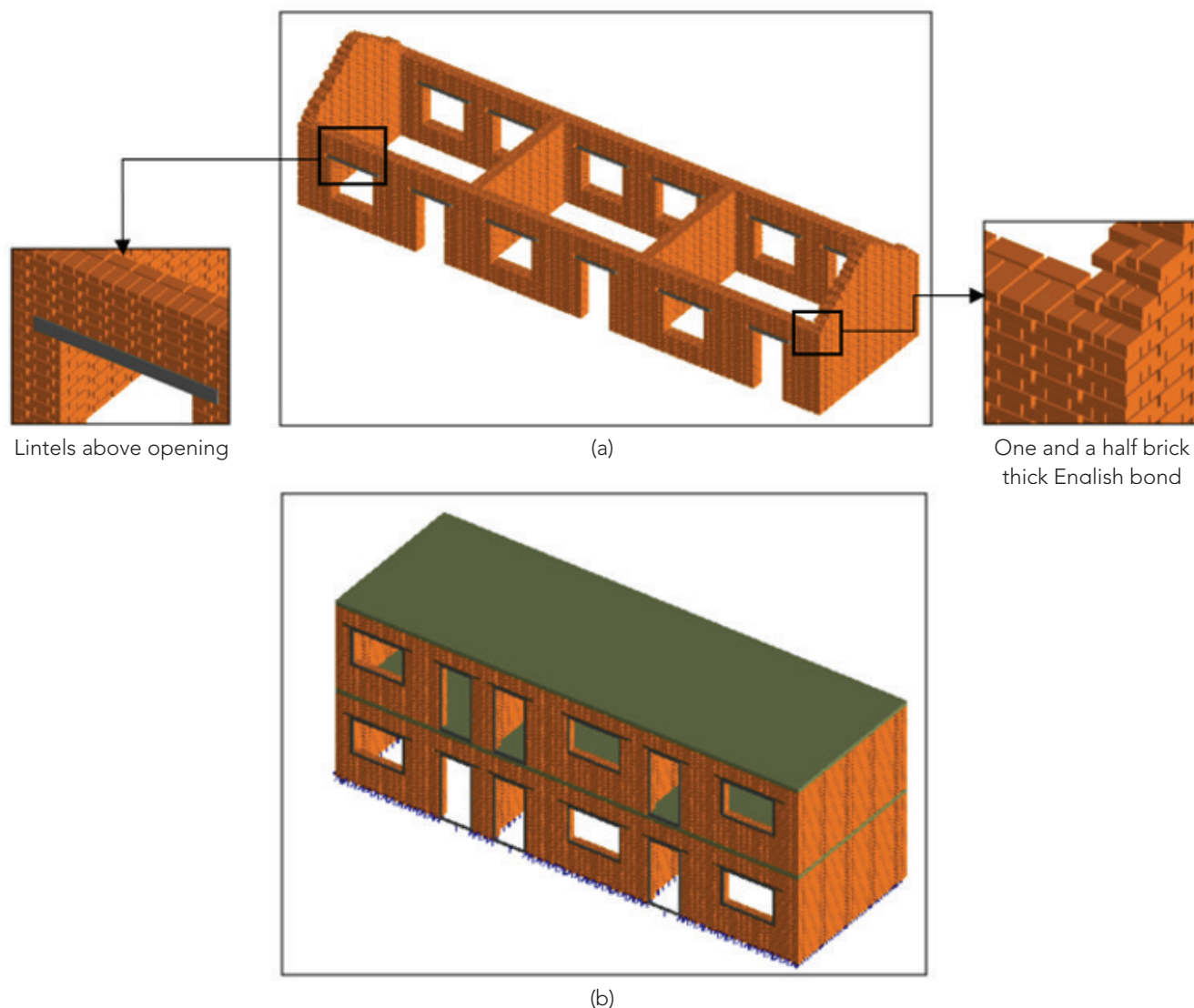


Figure 5. Example of 3D numerical models of a) a single-story brick in mud mortar (UCM-URM4) IB and b) a two-story brick in cement mortar (UCM-URM7) IB.



2.3.2 RC Index Buildings

For the RC structures, the modelling considerations are as follows:

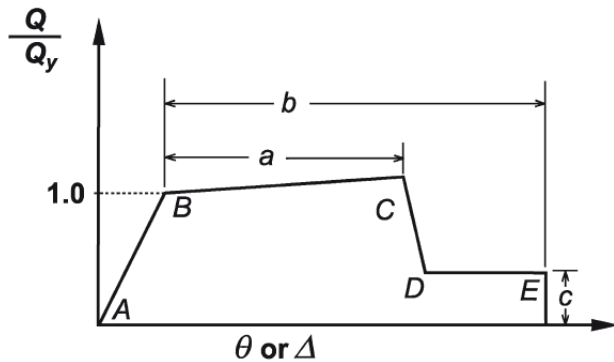
a) General considerations:

- » 3D model.
- » Concentrated plasticity for beams and columns (hinges) and distributed plasticity for walls (fiber model).
- » Consideration of P-Delta effects.
- » Concrete beam and column and masonry infills modeled as FRAME elements and concrete walls as SHELL elements.

- » Consideration of rigid zones for RC.
- » Rigid diaphragms in floors and roofs when a concrete slab is present (for particular cases of very thin slabs or irregular plan shapes, diaphragm flexibility considerations may be required).
- » Cracks are considered in the sections for the main structural elements.

Figure 4-6 illustrate a typical model of a plastic hinge for a representative structural component model such as a beam, a column, a wall or any other.

Figure 6. ASCE 41-17 general shear or flexural plastic hinge behavior (ASCE, 2017).



- b) Loads considered in the analysis:
 - » Self-weight of all elements.
 - » Additional dead loads (slabs, nonstructural walls, roofs, ceilings, etc.).
 - » A permanent 25% of the design live load is considered for the non-linear analysis.
- c) Foundation flexibility considerations:
 - » In general, a fixed based condition is adopted.
 - » Flexible foundation conditions are considered in a particular sensitivity analysis for one IB. To that end, linear springs are included in the base of the main structural elements.

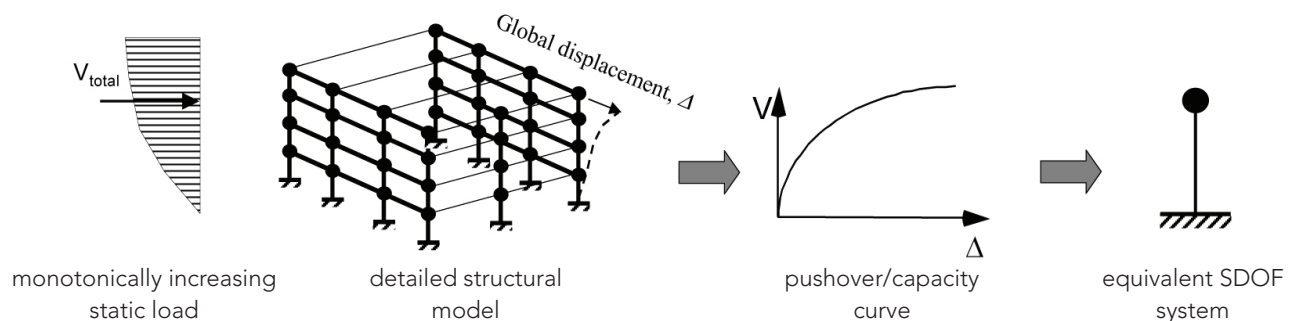
- d) Considered software: Perform3D, SAP2000 or SeismoStruct.

2.4 Non-Linear Pushover Analysis and Pushover Curve Derivation

The first phase of the assessment consists of determining the capacity curve for the IB using pushover analysis. A pushover curve relates the total horizontal base shear of the building with respect to the corresponding roof displacement. Figure 7 illustrates a typical pushover analysis procedure and the resulting curve for a building. For LBM and RC structures with rigid diaphragms, usually the fundamental mode shape is used for the application of pushover loading. The derivation of pushover curves for these types of structures is straightforward and simply derived by summing up the total base shear and plotting it with respect to the roof master node displacement.

The pushover curve is used as an input for non-linear static seismic performance assessment procedures (here the N2 Method is used) to predict the seismic performance of a building to a specific ground motion. During such assessments, the quantities in the building pushover curve are transformed into response measurements of an equivalent single-degree-of-freedom (SDoF) system (Figure 4-7). In addition, the pushover curve is also used for the determination of building-specific damage state threshold definitions.

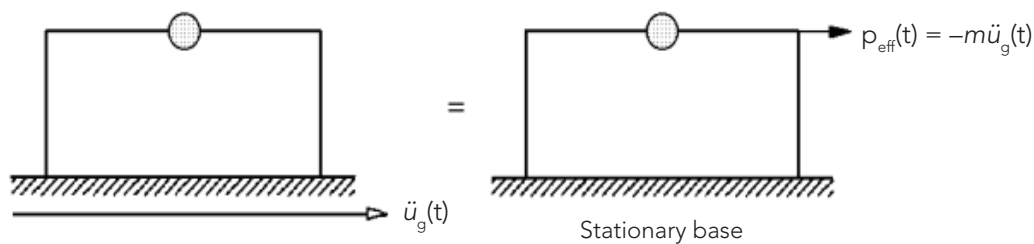
Figure 7. Schematic representation of static pushover analysis (excerpted from: FEMA 440).



Conventional pushover analysis of blocky masonry structures modelled using an element-by-element modelling technique, with discontinuous joints represented by finite strength and stiffness springs, is a complex task as the application of pushover forces/displacements on the structure often causes strain concentration on a particular element or region, thereby causing local failure without affecting the rest of the structure. Thus, the numerical models of

LBM IBs are subjected here to a non-linear pushover analysis under linearly increasing ground acceleration (rather than a force pattern on the structure) until collapse. This causes an application of an increasing 'effective earthquake force' on the structure as illustrated in Figure 8. Such analysis represents a force-based non-linear pushover analysis, as opposed to the displacement-based pushover analysis, usually implemented for frame structures.

Figure 8. Illustration of an effective earthquake force applied to a structure under the application of a ground acceleration (Adapted from Chopra, 1995).

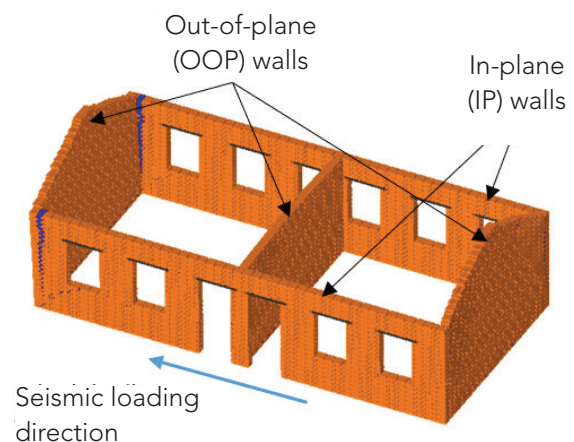


Observations from post-earthquake damage surveys in literature show that the walls subjected to OOP deformations (OOP walls) sustain heavy damage before the walls subjected to IP deformations (IP walls) suffer any significant damage when the diaphragm is of a flexible type. This is mainly due to the weaker stiffness in the OOP direction compared to that in the IP direction, and the absence of diaphragm action at the floor/roof level to control the global displacement. At a given instant of seismic loading, the OOP walls are subjected to more displacements than IP walls, and structural damage is directly related to the drift. Figure 9 and Figure 10 show the OOP walls have already been heavily damaged while the IP walls have not suffered any serious damage yet.

Moreover, because of the substantial difference in stiffness, IP and OOP walls tend to have a different natural frequency of vibration. Therefore, it can be inaccurate to represent the whole building with one SDoF, as this would necessarily have characteristics averaged among the ones with differing walls. As a result, the procedure presented here for the application of the N2 method is also separately conducted with respect to OOP and IP walls.

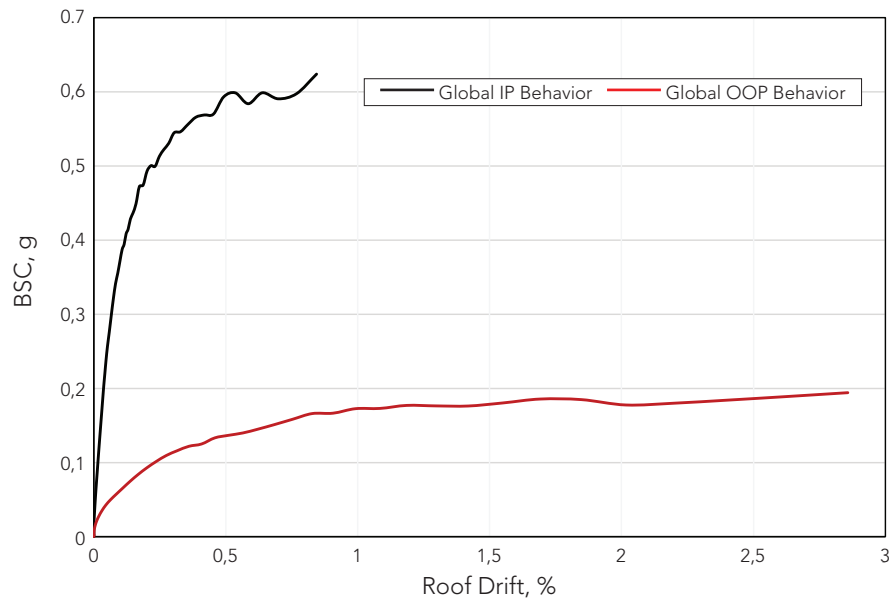
For the reasons discussed above, pushover curves and fragility functions are derived separately with respect

Figure 9. Damage due to seismic loading in an unreinforced masonry building with a flexible diaphragm.



to OOP behavior and IP behavior. Nonetheless, although the pushover curves and hence fragility functions are separately generated with respect to IP and OOP walls, the interaction among walls in the two orthogonal directions is correctly simulated by the 3D numerical models developed, depending on the level of connection among the two sets of walls observed in the IB under consideration. Such interaction affects the pushover curves and the identification of damage thresholds, and ultimately both fragility and vulnerability functions.

Figure 10. Typical capacity curves for an unreinforced masonry building when loaded in the longitudinal direction.



In line with the above discussion, the following procedure is applied to generate pushover curves for LBM IBs with flexible diaphragm types:

- The pushover curve for individual walls (in-plane and out-of-plane) are extracted by recording the base shear at the base of the walls vs the roof displacement of the corresponding wall.
- The threshold for different damage states of individual walls is identified along the respective pushover curve based on the progressive damage associated with the wall response. Corresponding drift limits for different damage state thresholds are identified.
- All the pushover curves of the walls acting in IP behavior are integrated by summing up the base shear and averaging the roof displacement of each IP wall at each instant of loading to generate the global pushover curve for IP behavior in a particular loading direction. Similarly, all the pushover curves in the walls acting in OOP behavior are integrated by summing up the base shear and averaging the roof displacement of each OOP wall at each instant of loading to generate the global pushover curve for OOP behavior in the same loading direction.

- Finally, the fragility curves are also developed with respect to global IP and OOP behavior, respectively.

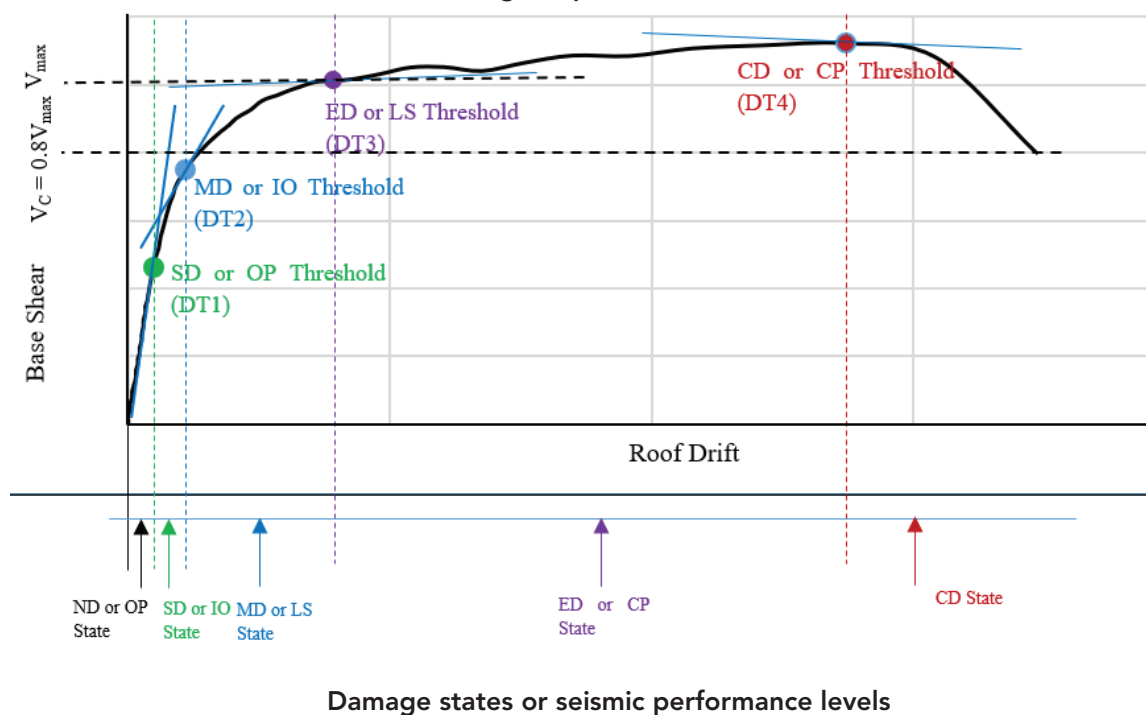
2.5 Damage States and Thresholds

Five different discretized damage states are considered for each structural component (column or wall) or at a building level: no damage (ND), slight damage (SD), moderate damage (MD), extensive damage (ED) and complete damage (CD) or collapse state. Table 2 presents the general definition of the damage states (ND, SD, etc.) and their corresponding damage thresholds (DT) or performance points (DT1, DT2, etc.). The damage threshold defines the particular event which can be identified in the pushover analysis and which determines a change in structural response, and hence a new damage phase. The threshold of each damage state for global building behaviors is defined as the point when the first structural component (wall or column) starts to enter the corresponding damage state. For example, the threshold for a slight damage state is the point when one of the structural components (e.g. a masonry pier/wall or an RC column) enters the slight damage state (e.g. hairline cracks have started to appear). Table 2 shows the seismic performance levels according to ASCE 41-13, equivalent to the different damage states considered. These definitions are also illustrated in Figure 11.

Table 2. Definition of Damage States and Damage Thresholds.

Damage Threshold or Performance Point	Definition of Threshold of Damage State	Damage State	Equivalent Seismic Performance Level (ASCE 41-13)
–	–	No Damage (ND): up to DT1	Operational (OP): up to DT1
Slight Damage Threshold (DT1)	Elastic (cracking limit), a slight reduction in initial stiffness starts.	Slight Damage (SD): DT1 to DT2	Immediate Occupancy (IO): DT1 to DT2
Moderate Damage Threshold (DT2)	Strength is increasing, stiffness starts to reduce noticeably as all the structural components have achieved a slight damage state.	Moderate Damage (MD): DT2 to DT3	Life Safety (LS): DT2 to DT3
Extensive Damage Threshold (DT3)	Peak strength is achieved as all the components have attained a moderate damage state, stiffness changes from positive to zero. The structure now enters a plastic deformation state, i.e. it will withstand a certain deformation at a constant capacity.	Extensive Damage (ED): DT3 to DT4	Collapse Prevention (CP): DT3 to DT4
Complete Damage Threshold (DT4)	Some structural components start to fail (loosing load resisting capacity), stiffness and strength start to degrade considerably. Further lateral deformation will cause the structure to collapse.	Complete Damage or Collapse (CD): after DT4	Collapse after DT4

Figure 11. Definition of damage states (or seismic performance levels) and damage state thresholds along the pushover curve.



For masonry buildings, the damage state thresholds are identified based on the crack pattern, extent and maximum width of cracks occurring on each wall. The dominant image threshold depends on the prevalent seismic response of the wall (i.e. in shear or bending, which depends on in-plane or out-of-plane prevalent loading). These elements' damage thresholds, obtained from literature, experiments and standards, are marked on each elements capacity curve and correlated to the drifts and changes in strength and stiffness as obtained from the 3D analysis. In the global pushover curves, each global damage state

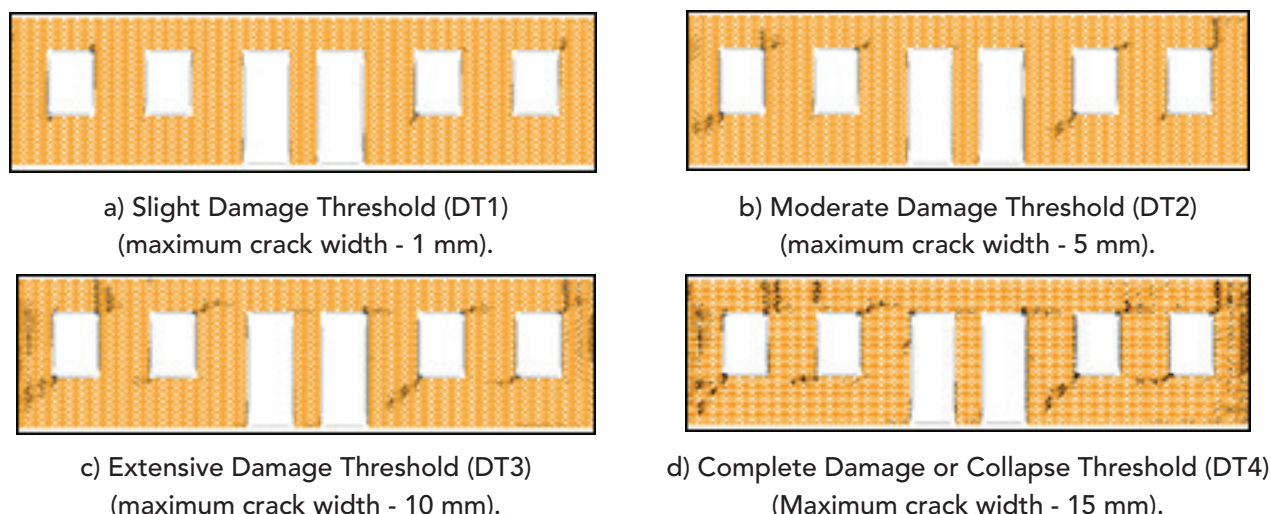
threshold (expressed in terms of roof drift) is reached and overcome when the first wall enters the respective damage state. For each global IP or OOP behavior, the global collapse is defined when one of the walls reaches the collapse damage state.

Table 3 and Figure 12 illustrate the physical definition of four different damage state thresholds for an unreinforced masonry wall under IP behavior. It should be noted that the crack pattern development and width at different damage state thresholds depends on the masonry fabric and connections between walls for each IB.

Table 3. Example of the physical definition of damage states for an unreinforced masonry wall under IP behavior.

Damage Threshold Definition	Physical Damage Definition
Slight Damage Threshold (DT1)	Hairline cracks (about 0.1 - 1 mm width) on a few corners around the openings.
Moderate Damage (MD) Limit (DT2)	Hairline to minor cracks appear on all the corners around opening, minor flexural cracks of about 1 mm - 5 mm width appeared in a few spandrels, diagonal shear cracks (about 1 mm - 5 mm maximum width) start to appear in some piers.
Extensive Damage (ED) Limit (DT3)	Most of the piers and spandrels have developed minor flexural/diagonal shear cracks (about 5 mm in width). Several spandrels and piers start to develop major flexural/shear cracks of 10 mm maximum width.
Complete Damage (CD) or Collapse Limit (DT4)	Most of the spandrels and piers have already developed a major crack of about 10 mm width. Several spandrels damaged with an extensive crack width of 10 mm to 15 mm and a few piers start to develop extensive cracks in shear or a combined shear-flexure mechanism with a maximum crack width of about 15 mm.

Figure 12. Illustration of different damage state thresholds for an unreinforced masonry wall under IP behavior (black lines represent the cracks; figures are shown in reduced scale to better represent the cracks).



For RC structural systems, it is rather difficult to precisely define the limits of each damage threshold if there is no detailed model developed. In literature, different approaches have been adopted. One of them consists in establishing different ranges in the non-linear part of the pushover curve. For instance, document FEMA-356 recommends some fixed limits for reinforced concrete frames such as the following: Immediate occupancy: 1% Roof drift, Life safety: 2% Roof Drift, and Collapse prevention: 4% Roof Drift. However, those limits will only be applicable to frames with specific characteristics. Another way to define damage states is based on recommendations from SEAOC whereby the thresholds are defined by identifying the first yield and the collapse point first,

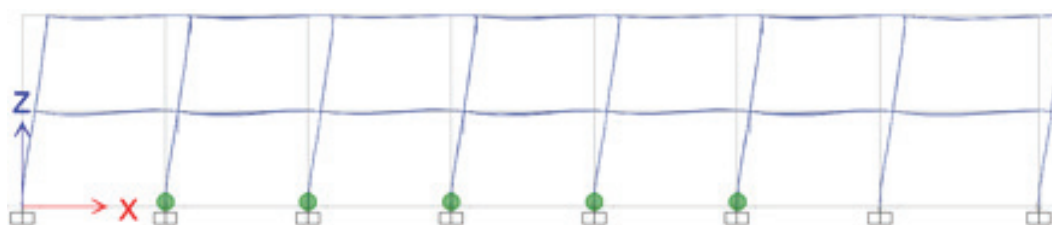
and then the intermediate points as percentages of the plastic displacement range.

For RC school buildings, the definition of damage limit thresholds and corresponding drift limits for each of the damage states are extracted here from the damage progression analysis under increasing seismic action. Each damage state is defined by the limit state of the plastic hinges developing in the model's elements. For instance, when the first hinge in the first column reaches the yielding threshold, as per Figure 6, the whole building is considered in slight damage threshold. In this way the approach for RC structures and for LBM structures is consistent. The description of each damage threshold for RC buildings is shown in Table 4 and illustrated in Figure 13.

Table 4. Example physical definition of damage states for an RC school building.

Damage Threshold Definition	Physical Damage Definition
Slight Damage Threshold (DT1)	When the first plastic hinges exceed Immediate Occupancy (IO) performance point defined by ASCE 41-17.
Moderate Damage (MD) Limit (DT2)	When the first plastic hinges exceed Life Safety (LS) performance point defined by ASCE 41-17.
Extensive Damage (ED) Limit (DT3)	When the first plastic hinges exceed Collapse Prevention (CP) performance point defined by ASCE 41-17.
Complete Damage (CD) or Collapse Limit (DT4)	When a collapse mechanism is developed and the structure loses its capacity (negative stiffness).

Figure 13. Example illustration of different damage states for RC IB.



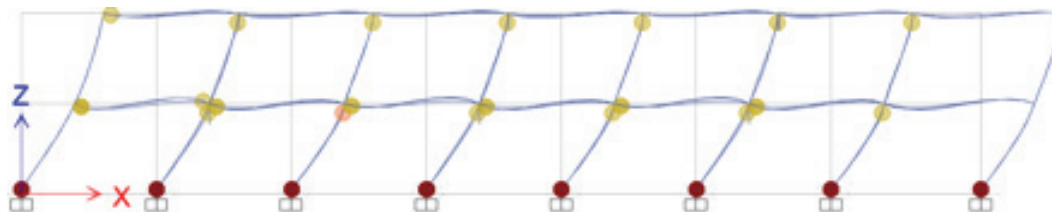
Slight Damage Threshold (DT1): First columns plastic hinge exceeds IO limit (green).



Moderate Damage Threshold (DT2): First columns plastic hinge exceeds LS limit (yellow).



Extensive Damage Threshold (DT3): First columns plastic hinge exceeds CP limit (orange).



Complete Damage Threshold (DT4): Collapse mechanism developed.

The roof drift is considered here as the engineering demand parameter (EDP). The seismic performance assessment and fragility derivation are carried out with respect to the roof drifts and each limit of the damage state is represented by the corresponding roof drift. As mentioned before, some judgement is required to define the limits for each damage state and therefore the final fragility functions shall be used and interpreted with this clear limitation. Also, specific IB types may have a slightly different definition of damage limit states, which will be specified in the analysis of the respective IBs.

2.6 Seismic Performance Assessment: N2 Methodology

A simplified, non-linear, static, seismic performance assessment methodology is adapted here based on the N2 method. The seismic performance assessment procedure using the N2 method is detailed in the subsequent steps, each of which is thoroughly described in the following sections:

- Convert the MDoF pushover curve (obtained with the procedure described in Section 4.2.4) to SDoF pushover curve and then transform the resultant capacity curve to ADRS (acceleration displacement response spectra) format.
- Idealize the capacity curve into a bilinear curve based on the principle of equivalent energy (Eurocode 8).
- Compute the elastic and inelastic spectrum for the ground motion record. Obtain the expected performance point using the N2 methodology, which will correspond to the maximum spectral displacement of the structure.
- Calculate the corresponding horizontal roof displacement and then the roof drift (EDP) which are back-calculated from the maximum spectral displacement at the performance point.
- Repeat the procedure to generate the EDPs (i.e. roof drift) for each IM with a number of scaled ground motion spectra.

For the seismic performance assessment and the generation of IM vs EDP results for a number of ground motions, a Microsoft Excel® based program named "N2_Bilinear_Capacity_Curve.xlsx" has been developed and made available in the GLOSI.

2.6.1 Derivation of Equivalent SDoF Capacity Curves

The SDoF system is a virtual oscillator, which has the same natural frequency and elastic properties (e.g. stiffness) as that of the MDoF system building. More precisely, the applied load is translated into spectral acceleration, and the lateral deformation is translated into spectral displacement. The pushover curve represented by these two parameters is called the capacity curve. A building's capacity curve reflects various seismic characteristics of the building, such as its stiffness, its material brittleness or ductility, and its strength. This curve correlates the lateral deformation of the building (in terms of spectral displacement) to a specific level of dynamic demand (expressed in terms of spectral acceleration). The transformation of the Force-Displacement (F-D) curve to Acceleration-Displacement Response Spectra (ADRS) format is done using the modal participation factors and effective modal weight ratios, determined from the fundamental mode of the structure. The procedure is summarized below:

- Run Eigen value analysis and extract the fundamental mode shapes of the multi-degree-of-freedom (MDoF) system.
- Obtain the F-D relationship (pushover curve) as a result of non-linear static pushover analysis of MDoF system.
- Derive the equivalent SDoF-based capacity curve by dividing the base shear and displacement of the MDoF-based capacity curve by the transformation factor.

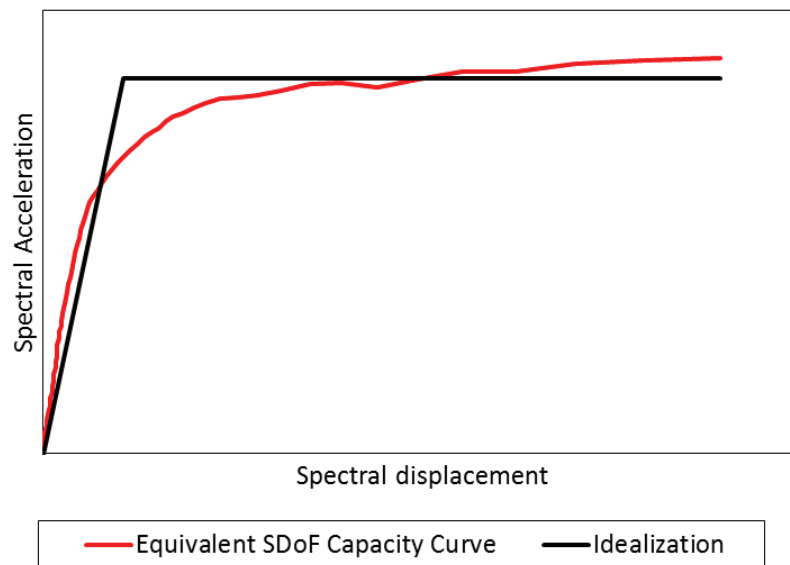
The conversion of a MDoF system to an equivalent SDoF system is an established engineering procedure and the readers are referred to well established literature such as FEMA 440 and Fajfar (2000) for more details.

2.6.2 Idealization of SDoF Capacity Curve

The application of the nonlinear static-based procedure (N2 method) depends on the determination of an idealized capacity curve of the equivalent SDoF system. This curve is derived by using the equal energy principle, imposing that the areas under the SDoF capacity and idealized curves are equal. Several forms of capacity curve idealization models exist in literature, including the simple bilinear elastic-perfectly plastic

model and the multilinear elastic-plastic, among others. It is assumed here that the idealized curve follows a simple bilinear elastic-perfectly plastic form (EPP hereafter). In EPP idealization of the capacity curve, the elastic segment is defined from ordinate zero to the yielding point, and the plastic segment is a plateau from the yielding point to ultimate deformation at the collapse (Figure 14).

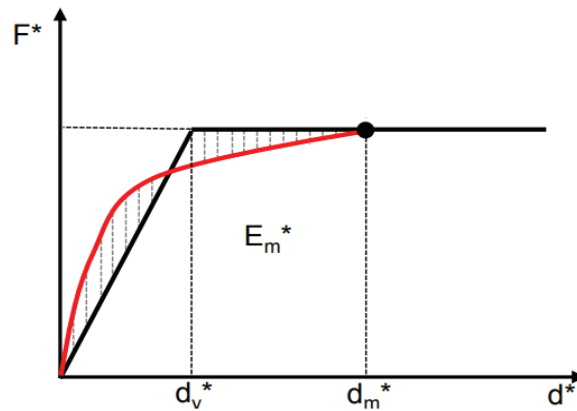
Figure 14. Example bilinear idealization of a capacity curve.



The choice of the idealization approach is of high importance for the determination of the seismic response of a structure. Although several variations of multilinear idealization models exist in literature, most design codes/guidelines (e.g. FEMA-440, EC8 etc.) recommend the simple bilinear idealization model fitting (elastic-plastic or elastic strain-hardening). The simplicity of the bilinear shape means that one only needs to estimate the position of the nominal 'yield point' and the 'ultimate point'.

A summary of some of the most commonly used fitting capacity idealization approaches found in design codes/guidelines are discussed below. Eurocode 8, following the original N2 method, suggests an elastic-perfectly plastic idealized capacity curve based on the balancing of the area discrepancy above and below the fit (equal energy rule), optionally using an iterative procedure. In this case, the capacity corresponding to the idealized yield point i.e. F_y^* is taken as $1 \cdot F_u$, where F_u is the maximum capacity of the actual pushover curve (Figure 15).

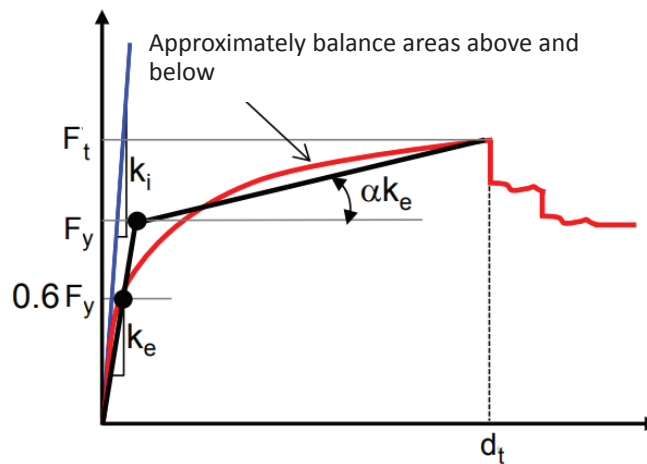
Figure 15. Bilinear fitting procedure according to EC8 (excerpted from De Luca et al 2013a).



Federal Emergency Management Agency (FEMA) documents (e.g. FEMA 440 and ASCE/SEI 41-06) generally employ a bilinear model with an initial slope and a post-yield slope (either positive or negative) up to the target point. The initial effective slope is calculated

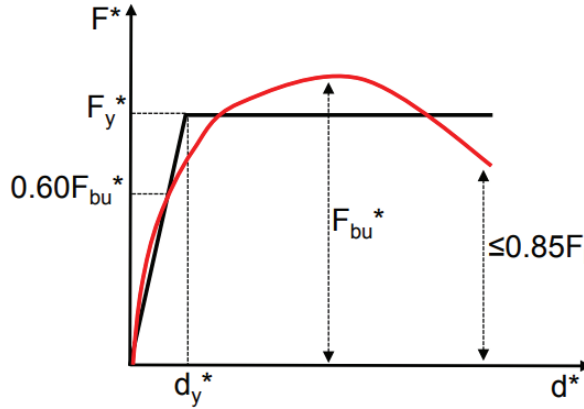
at a capacity equal to 60% of the nominal yield strength. In all cases, the idealized elastic-hardening shape is fitted through an iterative procedure approximately balancing the area above and below the fitted curve (Figure 16).

Figure 16. Bilinear fitting procedure according to FEMA 440 (excerpted from De Luca et al 2013a).



Italian guidelines (Decreto Ministeriale del 14/01/2008) suggest an elastic-plastic fit that may also account for a limited softening behavior up to a point of a 15% degradation of maximum capacity in the capacity curve. The initial stiffness fit is also based on the 60% rule¹, as in all FEMA documents. An equal energy criterion is then applied to derive the plateau of the bilinear fit. When that structural model does not reach a negative stiffness, it becomes equivalent to the Eurocode 8 fitting model. In this case, the capacity corresponding to the idealized yield point i.e. F_y^* is taken as $0.85 \cdot F_u$. (Figure 17).

Figure 17. Bilinear fitting procedure according to Italian guidelines (excerpted from De Luca et al 2013a).



There are comparisons in literature between the results obtained from the above-mentioned fitting procedures and incremental dynamic analysis (IDA) results. These comparisons showed that the bilinear fitting proposed in the FEMA and Italian guidelines provided the most acceptable errors for capacity curves with strain hardening and strain softening in the IDA results.

The index buildings analyzed in GLOSI showed a great variety of capacities. Therefore, an alternative strategy for capacity idealization is used, based on the principles of some of the fitting approaches discussed above. Specifically, a bilinear elastic-perfectly plastic model using the equal energy rule and the 60% capacity rule for the initial stiffness principle is employed. To that end, a sensitivity test for the determination of the

optimal value of F_y was carried out and it was found that a value of F_y^* equal to $0.95 \cdot F_u$ satisfies the 60% capacity rule for the initial stiffness principle for all index buildings in average. Thus, it is suggested to idealize the capacity curves into a bilinear elastic-perfectly plastic curve with equal energy principle and the recommended value of F_y^* is $0.95 \cdot F_u$.

2.6.3 Determination of Seismic Performance Point

Once the idealized capacity curve has been determined, one needs to select a seismic record, or a suite of seismic records to represent the seismic demand. For each selected record and the associated 5% damped elastic response spectrum ($S_{ae}(T)$, $S_{de}(T)$), the inelastic response spectrum ($S_a(T)$, $S_d(T)$) is derived by means of an $R - \mu - T$ relationship, where R is the reduction factor, μ is the ductility and T is the natural period of vibration of the SDoF system:

$$S_a(T) = \frac{S_{ae}(T)}{R} \quad (5)$$

$$S_d(T) = \frac{m}{R} S_{de}(T) = \frac{m}{R} \frac{T^2}{4p^2} S_{ae}(T) = m \frac{T^2}{4p^2} S_e(T) \quad (6)$$

The seismic performance can be obtained graphically by extending the elastic branch of the idealized capacity curve up to the intersection with the elastic demand spectrum (see Figure 18). By performing a number of iterations, the intersection of the capacity curve with the inelastic demand spectrum for the correct value of ductility is then identified. This point is known as the performance point and links the seismic performance of the building, expressed in terms of EDPs, with the seismic demand, expressed in terms of ground motion intensity measures (IMs).

For a given earthquake ground record, the performance point of the equivalent SDoF system can be calculated with respect to the following two conditions:

- For a medium and long period range: $T^* \geq T_C$
- For a short period range: $T^* < T_C$

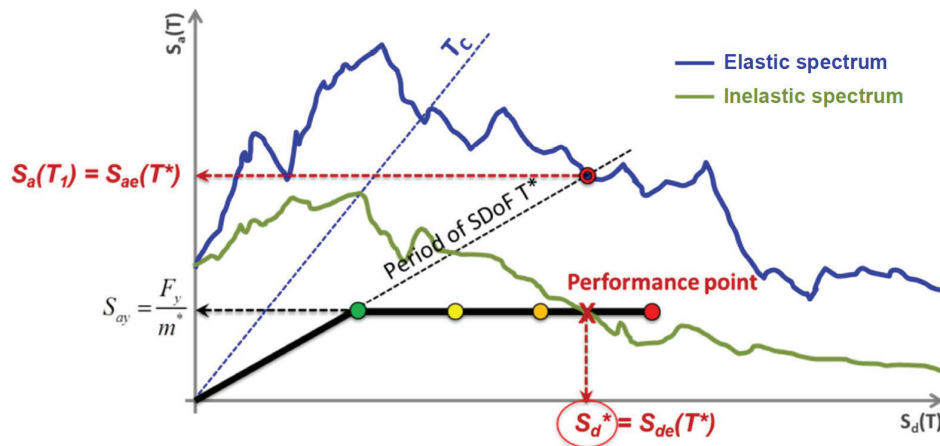
¹ The ratio of the base shear at the intersection of idealized and exact capacity curve over the maximum (ultimate) base shear of the exact capacity is equal to 60%.

where T_c (also known as the corner period) is the characteristic period of the ground motion, which identifies the transition from constant acceleration (corresponding to the short-period range) to constant velocity (the medium-period range) section of the elastic spectrum. A detailed description of the performance point calculation for each of the above conditions can be found in D'Ayala et al. (2015) damage, or loss for any single structure, or for a class of buildings defined by the GEM Taxonomy level 1 attributes. At the same time, sufficient flexibility is incorporated to allow full exploitation of cutting-edge methods by knowledgeable users. The basis for this effort consists of the key components of the state-of-art PEER/ATC-58 methodology for loss assessment, incorporating simplifications for reduced effort and extensions to accommodate a class of buildings rather than a single structure, and multiple damage states rather than collapse only considerations. To inject sufficient flexibility into the guidelines and accommodate a

range of different user needs and capabilities, a distinct hierarchy of complexity (and accuracy. Using this process, a set of spectral displacement and spectral acceleration values corresponding to the performance point can be obtained.

The corresponding horizontal roof displacement and then the roof drift (EDP) can be obtained through the back-calculation from the maximum spectral displacement at the performance point. In order to determine the structure's performance under increasing ground motion intensity, the analysis described above should be repeated for multiple accelerograms scaled up until all the limit states are reached. The selected number of accelerograms/ground motions should be sufficient to provide stable estimates of the median capacities. The resulting cloud of performance points is then used to determine the median EDP for each damage state threshold and its dispersion, and then create a fragility curve by fitting a statistical model, as described in the following section.

Figure 18. N2 graphical procedure (D'Ayala et al, 2015).



2.7 Derivation of Fragility Functions

The proposed methodology considers the assessment of fragility functions using a building-based damage assessment methodology. To generate fragility functions for the different damage levels defined, the following procedure is followed:

- Select all resulting performance points (IM vs EDP) as obtained from N2 analysis in the corresponding range of values to each particular damage state.
- Using a least square method (LSM), calculate the mean and variance of the resulting collection of seismic intensity values.
- Performing piece-wise regression over these different IM intervals, assign a lognormal probability distribution function for each particular damage state.

- Conform the collection of fragility functions for the building under consideration.

A MATLAB® based software package has been developed for the calculation of fragility functions, given a collection of EDP resulting from the seismic performance assessment at different intensity levels, and is available in GLOSI. Figure 19 shows the cloud of IM versus EDP points (expressed in terms of PGA and roof drift ratio (RDR) in this example), divided into five bins based on the four damage state thresholds corresponding to SD, MD, ED and CD damage states. Figure 20 illustrates the resultant LSM obtained fragility curves for the given collection of EDP values at different intensity levels.

Figure 19. LSM Methodology (excerpted from D'Ayala et al, 2015).

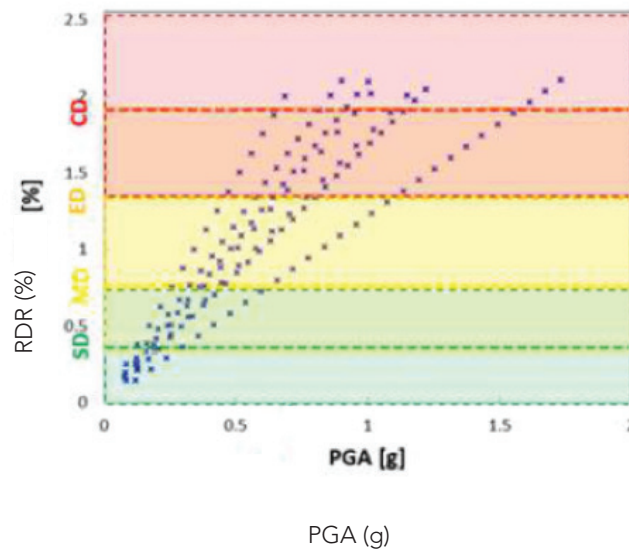
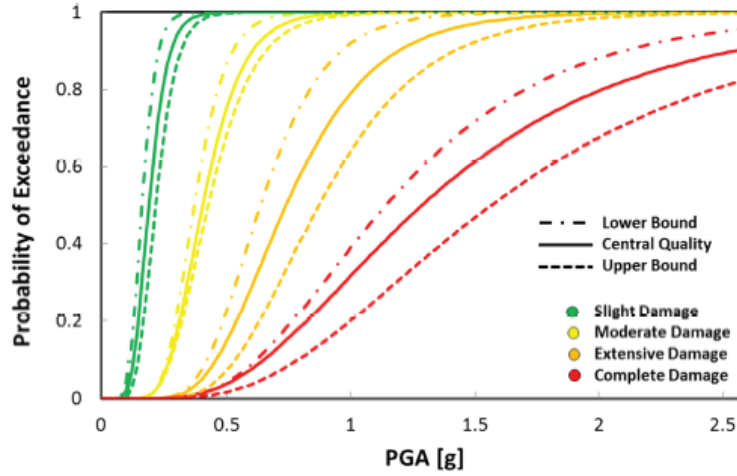


Figure 20. Example of a fragility function obtained by LSM Methodology (excerpted from D'Ayala et al, 2015).



Least Squares regression is a widely used technique to estimate the probabilistic relation between EDPs and IMs for each damage threshold. Assuming a lognormal distribution between EDP and DS, the predicted median demand is represented by a normal cumulative distribution:

$$\Phi \left[\frac{\ln IM - \ln \alpha}{\beta} \right] \quad (7)$$

where Φ represents the standard normal cumulative distribution function, and β is the global standard deviation for the predicted median demand α . For an assumed probabilistic damage threshold, IMs are chosen in such a way that roughly half the points are below that damage threshold and half above, determining

an interval of IMs values, which are assumed to be lognormally distributed within each interval.

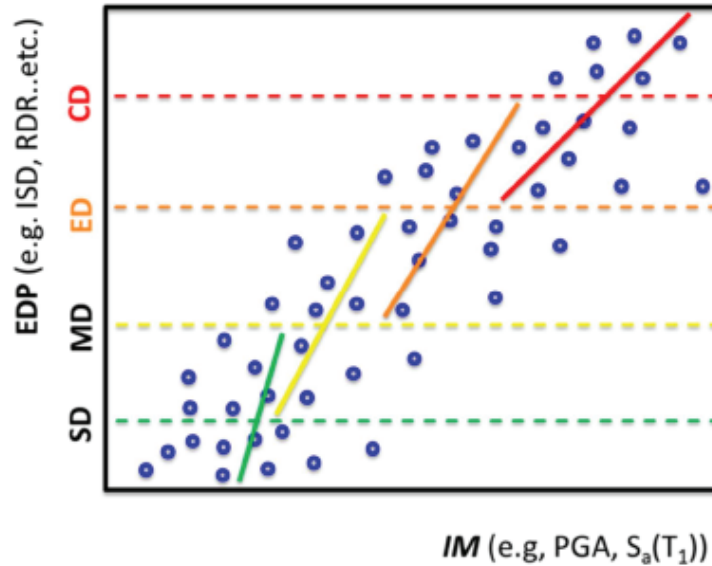
Performing piece-wise regression over these different IM intervals, the fragility parameters are computed using the corresponding relation (Figure 21):

$$\ln(EDP) = a \ln(IM) + \ln(b) \quad (8)$$

The median demand ds_i and its dispersion ds_i , for each assumed threshold ds_i , can be written as:

$$ds_i = \exp \frac{\ln \frac{ds_i}{b}}{a} \quad \text{and} \quad ds_i = \frac{STDEV(\ln IM_i)}{a} \quad (9)$$

Figure 21. Derivation of fragility functions (median demand and dispersion) using Least Squares regression technique (excerpted from D'Ayala et al, 2015).



This fragility assessment methodology is associated with some advantages and limitations. Here are the main advantages of the methodology:

- It is a simple and rapid approach which does not require a significant level of detailed information.
- It is an established approach which has been used in several scenarios and applications worldwide and appears to perform well in vulnerability assessment applications of similar scope.

However, this approach is also associated with the following limitations:

- It does not allow for the direct inclusion of damage levels for non-structural components.
- The definition of the damage levels is rather subjective and therefore high uncertainty shall be associated to the final qualification in a particular damage state.
- Only one parameter is used as reference for damage assessment and it corresponds to the roof horizontal displacement (either the maximum value or a combined mean value when flexible diaphragms are present).

2.8 Derivation of Vulnerability Functions

There are two approaches for the derivation of vulnerability functions: building-based or component-based. As mentioned previously, the component vulnerability models are not available/well established for LBM IBs, thus the building-based vulnerability function derivation is employed, while the component-based methodology is followed for RC IBs.

2.8.1 Building-Based Vulnerability Assessment Approach

For the generation of building-based vulnerability curves, the procedure suggested in the GEM analytical vulnerability guideline is employed. With the building-based fragility curves for different damage states obtained in the above section, the transformation of these curves into vulnerability curves is conducted with the following total probability relation:

$$E(C > c | im) = \sum_{i=1}^n E(C > c | ds_i) \cdot P(ds_i | im) \quad (10)$$

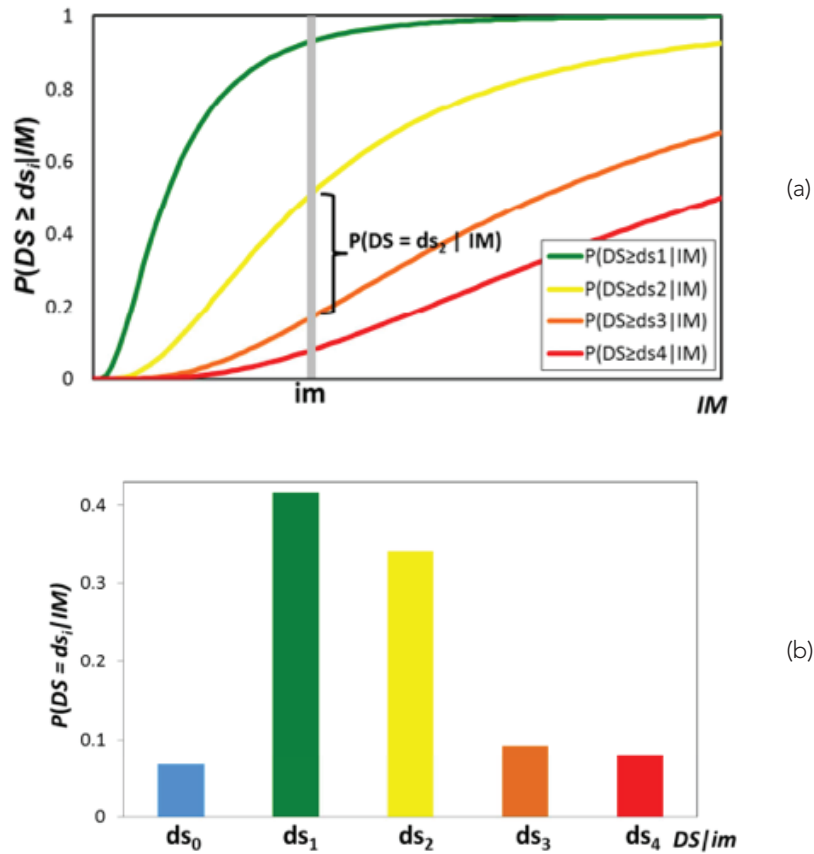
where, n ($= 4$) is the number of damage states considered; $P(ds_i | im)$ is the probability of a building sustaining a damage state ds_i given an intensity level im ; $E(C > c | ds_i)$ is the complementary cumulative

distribution of the cost (or loss) given ds_i ; $E(C > c | im)$ is the complementary cumulative distribution of cost (or loss) given an intensity level im .

The probability of a building sustaining a particular damage state requires the calculation of damage probabilities from the fragility curves for specific intensity levels.

Figure 22. Calculation of damage probabilities from the fragility curves for a specific level of intensity measurement, im : a) Fragility curves corresponding to $n=4$ damage limit states and b) Column of the damage probabilities for different damage states given an intensity (adapted from D'Ayala et al. 2015).

ds_0 = No Damage; ds_1 = Slight Damage State; ds_2 = Moderate Damage State; ds_3 = Extensive Damage State; ds_4 = Collapse State



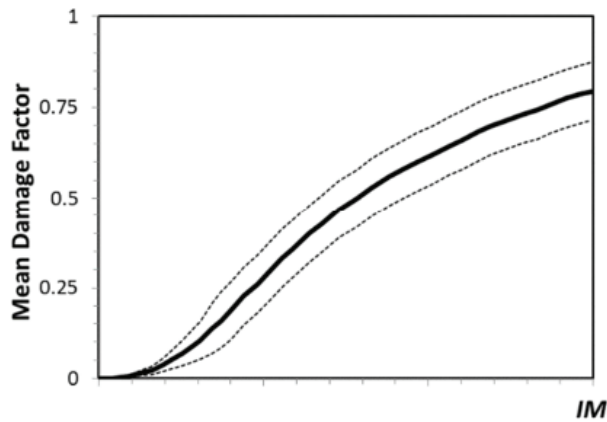
Each element (or bar) in the damage probabilities is defined as the difference between two successive fragility curves for a given intensity im , as shown in Figure 22. The mean, $E(C|im)$, and the variance, $var(C|im)$ of the vulnerability, given an im can then be obtained by the following expressions (where n = is the number of damage states considered):

$$E(C|im) = \sum_{i=1}^n E(C|ds_i).P(ds_i|im) \quad (11)$$

$$var(C|im) = \sum_{i=1}^n [E(C|ds_i) - E(C|im)]^2.P(ds_i|im) \quad (12)$$

Repeating the application of these two equations (11) and (12) for different levels of im (0.01g, 0.02g, 0.03g,...) will result in the vulnerability curve for the IB, similar to the one shown in Figure 23.

Figure 23. Example illustration of transformation of the fragility curves into vulnerability curve, with confidence boundaries (excerpted from D'Ayala et al. 2015).



For the cases of flexible diaphragm LBM IBs where the capacity curves and fragility functions are derived with respect to global OOP and global IP behavior, vulnerability curves are also computed separately with respect to global OOP and global IP behavior. Then, the global building vulnerability curve is computed by adding these two vulnerability curves with appropriate vulnerability factors depending on the mass of the masonry (and the roof portion supported), for OOP and IP walls respectively.

2.8.2 Component-Based Vulnerability Assessment Approach

The proposed methodology considers the assessment of vulnerability functions using a component-based damage assessment. The methodology is partially based on the component-based fragility assessment method proposed in document FEMA P-58 and is explained in detail in Yamin (2017). The proposed methodology is more suited for RC buildings as compared to LBM, where the interaction between structural and non-structural components defines the level of damage at different intensities. It includes the following steps:

- Define a model of structural and non-structural components at each story of the building.
- Assign a particular fragility function to each component in terms of different damage levels and the EDP that best corresponds to the damage qualification. Each damage level is associated with a repair cost and time for calculating the vulnerability functions.
- For each seismic intensity level, estimate the total repair cost and time of repair for all the collection of seismic records, all possible variations of damage states, and costs of all individual structural and non-structural components.

2.8.2.1 Component model of the building

A component model, with both structural and non-structural elements, is to be assembled for each building under consideration. It shall include all structural and non-structural components at each story. For each type of component, the unit of measure, the quantity of elements, the fragility in terms of repair cost and time at different damage states, the controlling EDP, and the correlation of damage between all the same components at the same story, have to be defined. Table 5 illustrates a typical component model for a two-story building.

Table 5. Typical component model for a two-story building.

Group	Subgroup	Unit	Quantity	Fragility specification code	EDP	DS correlation between components
Structural	Columns and beam end nodes	Node	8	B1041.001a	Drift	No
Structural	Column and beam central nodes	Node	8	B1041.001b	Drift	No
Non-structural	Confined masonry facade	5mx3m	3	C1011.006b	Drift	Yes
Non-structural	Confined masonry partition wall (veneer)	5mx3m	1	C1011.005b	Drift	Yes
Non-structural	Confined masonry partition wall	5mx3m	2	C1011.004b	Drift	Yes
Non-structural	Plastered ceiling	5mx5m	9	C3032.005a	Acceleration	No
Non-structural	Gas piping	22ml	1	D2022.025a	Acceleration	Yes
Non-structural	Electrical piping	110ml	1	D2021.011a	Acceleration	Yes
Non-structural	Water piping	62ml	1	D2022.011a	Acceleration	Yes
Contents	Contents (acceleration controlled)	5mx5m	8	E2022.010	Acceleration	No
Contents	Contents (drift controlled)	5mx5m	8	E2022.010a	Drift	No

Note: Confined masonry refers to infill walls built with additional confinement elements in a framed RC building.

2.8.2.2 Component fragility functions

Fragility functions are to be assigned to each component type in the building. They represent the probability of being in a given damage state (usually slight, moderate or extensive) as a function of the

corresponding EDP (as defined previously). Each damage state is assigned a probability density function of repair cost and time. Figure 24 illustrates a typical fragility definition for a beam-column connection and Table 6 presents the fragility function parameters for a confined masonry partition.

Figure 24. Beam-column joint damage states (FEMA, 2013).

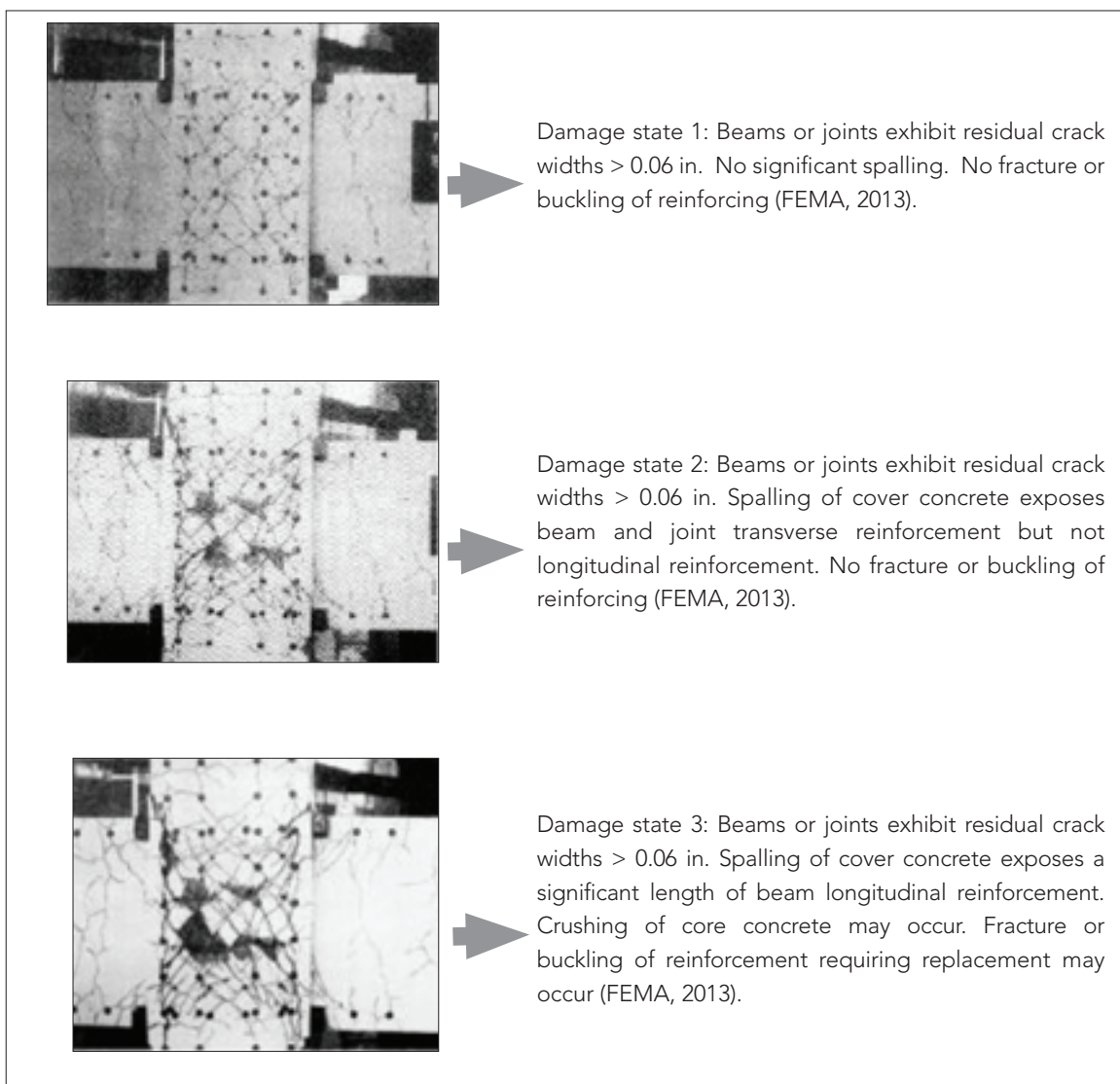


Table 6. Typical fragility functions parameters. Adapted from Yamin (2017).

Fragility Functions Parameters General Data				Date
				5/10/2015
Code	C1011.004b			
Description	Confined masonry partition wall isolated from the structure			
# Damage States	3			
Demand Parameter	Story Drift Ratio			
Standard Unit	5m x 3 m			

Fragility Function Parameters			
Damage State	DS1	DS2	DS3
Median Demand, θ	0.05	0.01	0.015
Total Dispersion, β	0.60	0.45	0.45

Damage Associated	
DS1	Minor cracking
DS2	Crack at joints and plaster
DS3	Partial collapse

Cost Model			
Damage State	DS1	DS2	DS3
Lower Quantity (LQ)	1	1	1
Upper Quantity (UQ)	10	10	10
Cost LQ, US\$ Dollars	404	694	1350
Cost UQ, US\$ Dollars	249	427	830
Best Fit	Normal	Lognormal	Lognormal

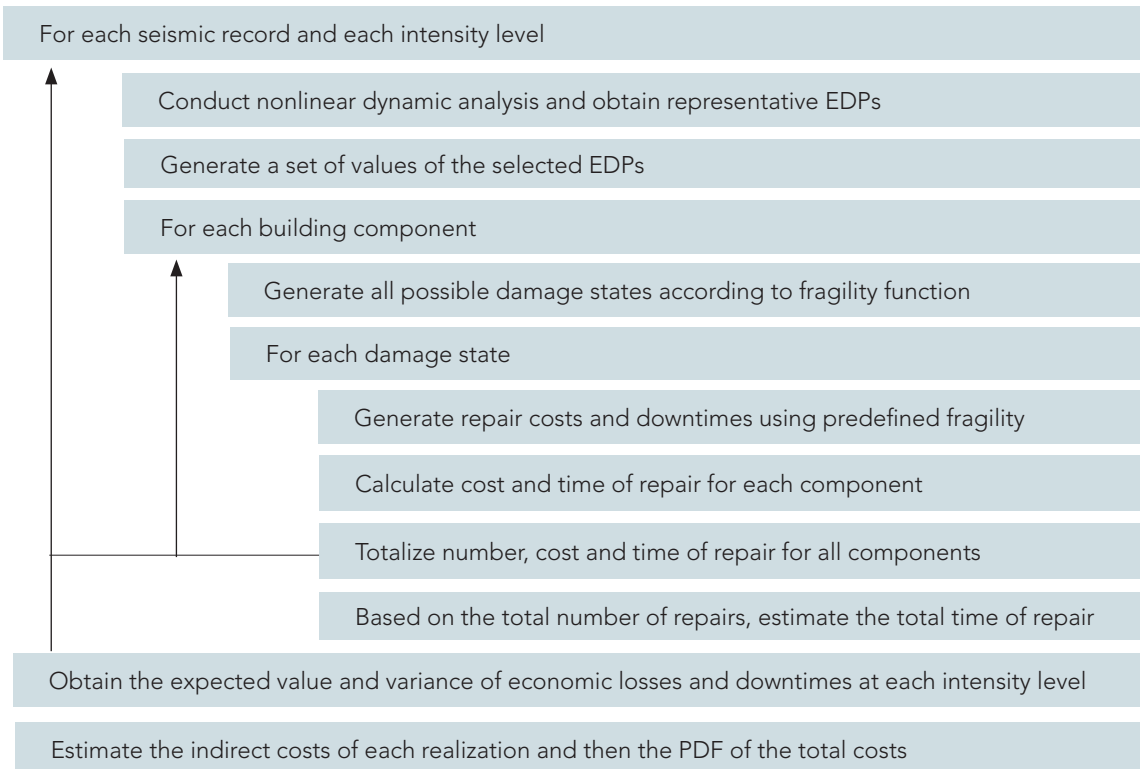
Time Model			
Damage State	DS1	DS2	DS3
Lower Quantity (LQ)	1	1	1
Upper Quantity (UQ)	10	10	10
Time LQ, days	9.5	15.5	60.8
Time UQ, days	7.8	12.7	49.8
Best Fit	Normal	Lognormal	Lognormal

2.8.2.3 Repair Cost Integration

Using Monte Carlo simulation techniques, the integration of repair costs from all components in the model is performed considering all possible sources of uncertainty (for details, see Yamin et al. 2017). For

each specific building type, a sufficient number of realizations is used to obtain the total expected repair costs and the variance at each intensity level. Figure 25 summarizes the procedure followed.

Figure 25. Monte Carlo simulation procedure to obtain total repair costs. Adapted from (Yamin et al., 2017).



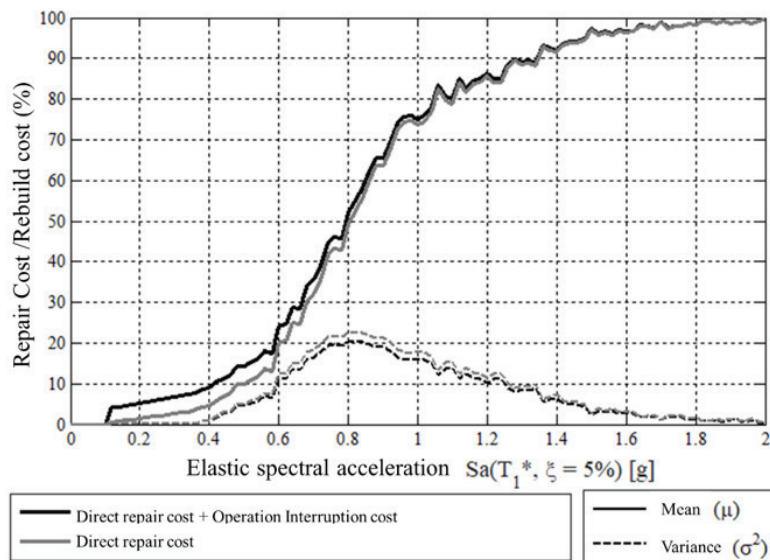
Once the results are available for a sufficient number of realizations, the following considerations are included in the vulnerability and loss assessment procedure:

- Residual drift in order to consider if the building is irreparable.
- Excessive repair costs to consider a complete replacement.
- Minimum seismic intensity level for initial damages.
- Specific considerations for the estimation of indirect costs which are related to business interruption.

Repair costs and time (including the time needed to initiate, execute and finalize repair works and to re-occupy the building after completion of works) are estimated considering the economic capacity and efficiency of a society to recover from a shock.

A software package has been developed to facilitate the calculation of vulnerability functions, given a collection of EDP resulting from the analysis at different intensity levels (Software IT-Funvul V2.0, available at www.ecapra.org). Figure 26 illustrates a typical vulnerability function obtained with the proposed methodological approach.

Figure 26. Example of vulnerability curve computed using IT-FUNVUL V2.0 (www.ecapra.org).



2.8.2.4 Advantages and limitations of the component-based vulnerability assessment method

The following are the advantages of the proposed vulnerability assessment method:

- It is a component-based damage assessment method, enabling the consideration of simultaneous damages occurring in different structural and non-structural components.

- No subjective assessment is directly demanded by the method.
- Multiple EDPs can be used to define damage states for different component types.

The main limitations are:

- It requires the definition of information that may not be readily available.

3. Illustrative examples

This section presents an illustrative example of the application of the proposed F/V assessment methodology for one IB of LBM school construction type and one IB of RC school construction type, respectively. Results for all the IBs are documented in GLOSI.

3.1 Example Analysis for an LBM Index Building

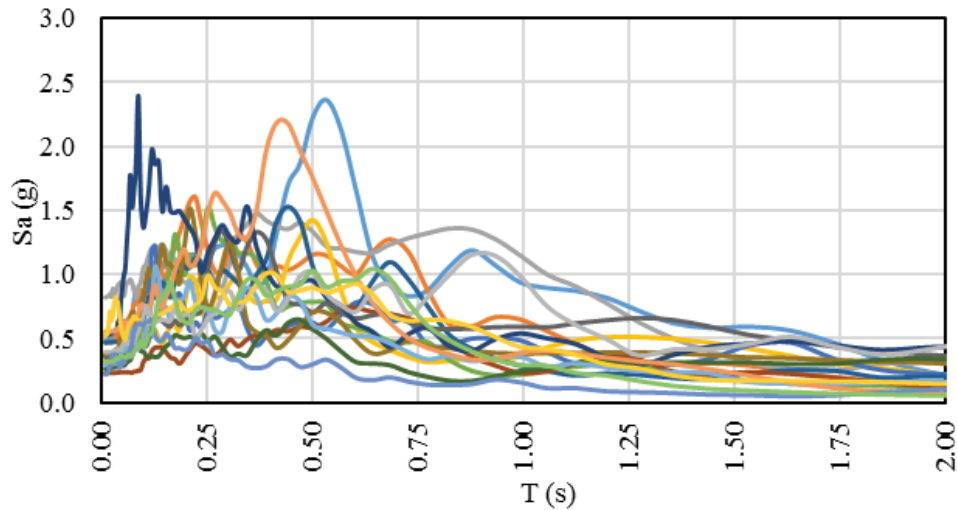
An example application of the discussed methodology to an LBM IB is presented in this section. To that end,

an UCM-URM7 IB is considered to carry out the fragility and vulnerability analysis following the steps described in the previous sections.

3.1.1 Hazard Definition

The group of far field records are selected for the analysis. Figure 27 presents the response spectra of the 22 ground motions.

Figure 27. Response spectra of 22 far field ground motion suite.



3.1.2 Index Building Definition

Figure 28 shows representative photographs of the IB considered. A single story two-classroom rectangular

plan school building is chosen for the analysis of an UCM-URM7 IB.

Figure 28. Photographs representative of an IB of the UCM-URM7/LR(1)/LD school building type: (a) outside front view and (b) Inside view showing the flexible roof diaphragm. (Photo from Nepal, Copyright: The World Bank).



Table 7 presents the GLOSI taxonomy string for the selected UCM-URM7 IB.

Table 7. IB Taxonomy parameters.

Building Type	GLOSI Taxonomy String
UCM-URM7/LR/LD	UCM-URM7/LR(1)/LD/FD/NI/LP/LO/RF/NP/OS/PC/VN

3.1.3 Numerical Modelling, Pushover Analysis and Seismic Behavior

Figure 29 shows the element-by-element 3D numerical model developed in ELS using the applied element method. Table 8 presents the geometrical characteristics of the building and Table 9 the average material properties for the UCM-URM7 construction in Nepal. This model is subjected to an equivalent pushover analysis as explained previously.

Figure 29. Numerical model of the UCM-URM7 IB in ELS using simplified micro-modelling technique.

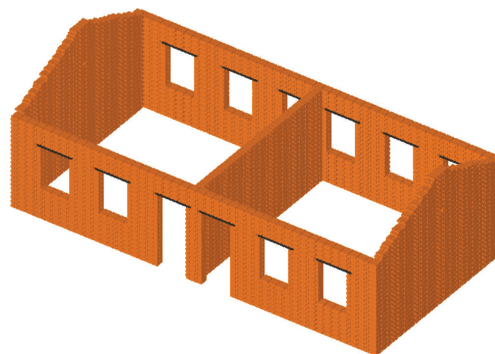


Table 8. Geometrical characteristics of the UCM-URM7 IB.

Characteristic	Value
Building plane area (m ²):	60
Building total area (m ²):	60
Number of stories:	1
Story height (m):	2.8
Number of spans in long direction:	2
Typical span length in long direction (m):	5.7
Number of spans in short direction (m):	1
Typical span length in short direction (m):	5.3
Wall Thickness (mm):	250
Wall Construction:	English Bond
Thickness:	One brick

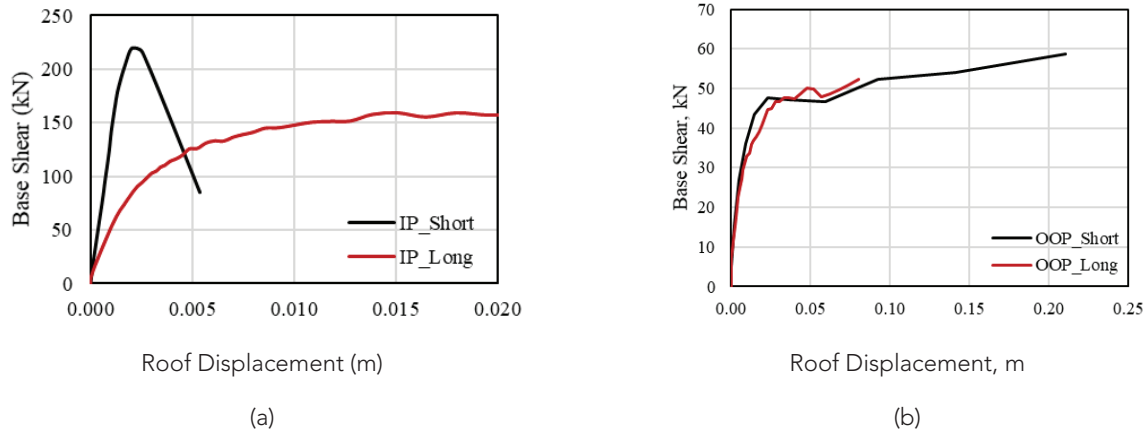
Table 9. Elastic and non-linear material properties of masonry.

Masonry Material Properties	Average Value
Unit Weight	1920 kg/m ³
Modulus of Elasticity	263 MPa
Shear Modulus	158 MPa
Compressive Strength	4.14 MPa
Cohesion	0.17 MPa
Flexural Tensile Strength	0.069 MPa
Friction Coefficient	0.6

Figure 30 shows the pushover curves for the selected IB in two principal directions with respect to global IP

and OOP behavior, respectively.

Figure 30. Pushover curve comparison of the UCM-URM7 IB in long and short direction with respect to (a) global IP and (b) global OOP behavior.



As shown in Figure 30, it is clear that the building is weaker in the longitudinal direction in comparison to the transverse direction (under IP behavior, initial stiffness and peak strength are both higher in the transverse direction; while under OOP behavior, although the initial stiffness and peak strength are comparable, the ductility is lower in the longitudinal direction). Thus, the F/V analysis is conducted in the longitudinal direction only.

Figure 31 presents the global capacity curves for the selected IB in the longitudinal direction with respect to global IP and global OOP behavior, respectively. The thresholds for different damage states are also shown in the figures. As explained in the methodology, analysis with respect to IP and OOP behavior will be conducted for this structure with a flexible diaphragm type which lacks global behavior.

Figure 31. Capacity curves and associated damage state thresholds for the UCM-URM7 IB: (a) global IP behavior and (b) global OOP behavior. (Damage state thresholds: green – DT1, blue – DT2, Windigo – DT3 and red – DT4).

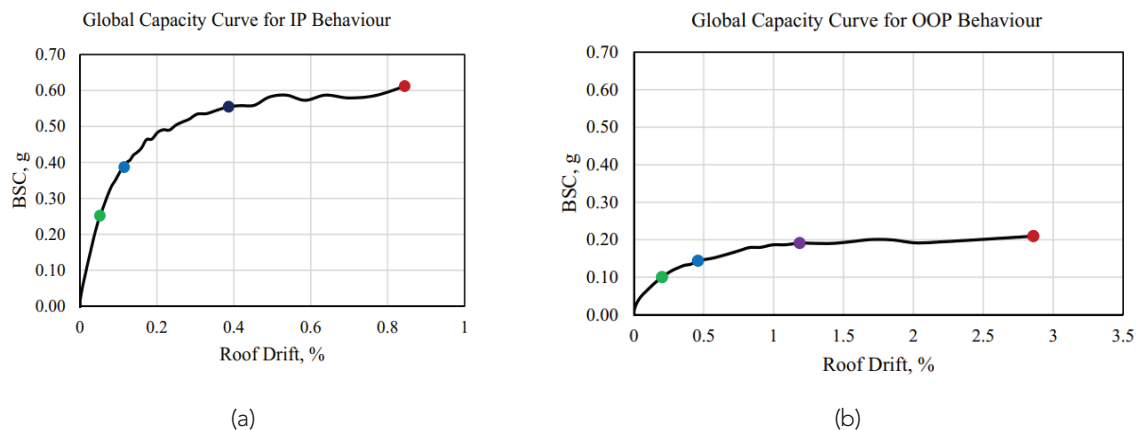



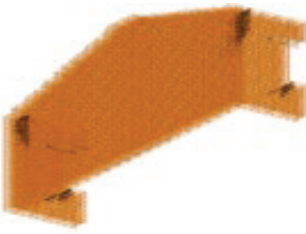
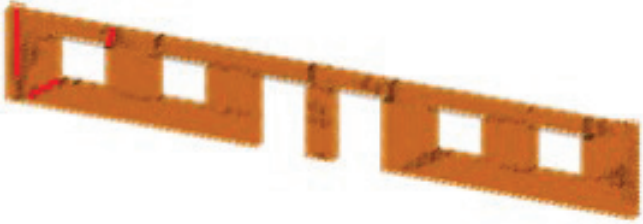
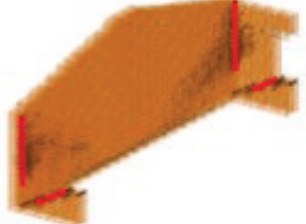

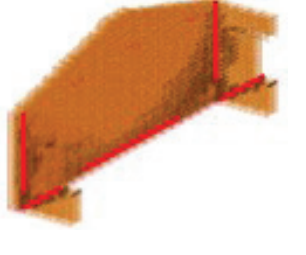


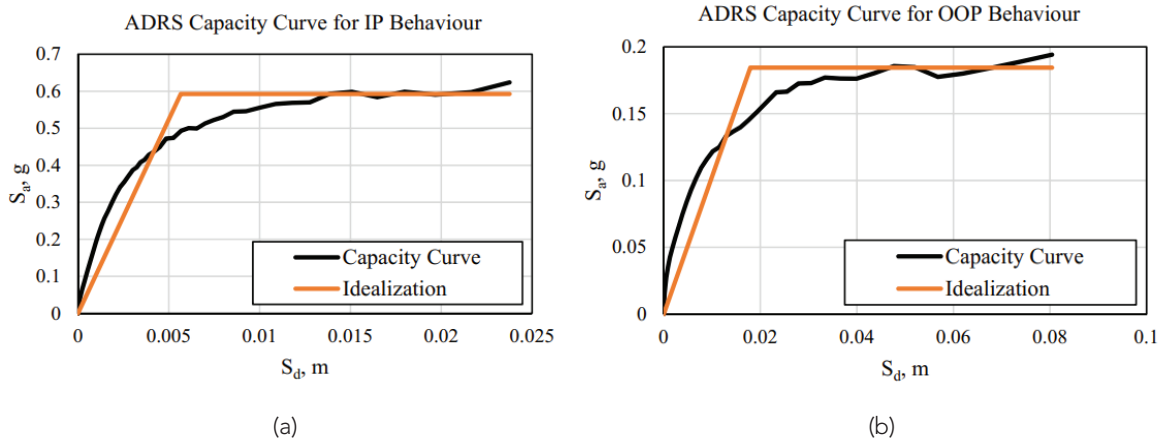
Table 10. Damage (Crack Pattern, Width and Extent) progression during seismic loading.

IP Behavior	OOP Behavior
	
<p>OP Threshold: Hairline cracks (black) of a maximum width of 0.35 mm appeared at a few corners of the openings.</p>	<p>OP Threshold: Minor cracks (black) of a 0.5 mm maximum width appeared at the connection with the in-plane wall.</p>
	
<p>IO Threshold: Hairline to minor cracks (black) of a maximum width of 1 mm developed at most of the corners of the openings, left most pier and spandrel start to develop shear and flexural cracks, respectively.</p>	<p>IO Threshold: Minor cracks (black) with a maximum width of 3 mm started to extend downwards at the connection between IP walls, minor shear cracks (black) of 1 mm started in the IP walls.</p>
	
<p>LS Threshold: The left pier has developed an extensive shear crack (red) of a 12.5 mm maximum width. The left spandrel has also developed an extensive flexural crack (red). Major shear cracks (red) of a maximum width of 10 mm as well as horizontal (flexural) cracks (red) with a maximum opening of 2 mm appear through most of the piers.</p>	<p>LS Threshold: The full combined mechanism started with major cracks (red) of a 12.5 mm maximum width at the IP walls connections through half of the wall height, and shear cracks (red) of a 12.5 mm width developed in IP walls. A minor horizontal crack at the bottom layer extended to full length, with a maximum crack opening of 1 mm.</p>
	
<p>CP Threshold: Most piers and spandrels developed extensive shear cracks (with a width of more than 12.5 mm) and flexural cracks (crack openings of 4 mm maximum) (red). The left pier and spandrel are on the verge of collapse.</p>	<p>CP Threshold: The cracks (vertical, red) at the IP wall connection become extensive with a maximum width of more than 12.5 mm, and extend through the full wall height. An extensive shear crack (diagonal, red) with a width of more than 12.5 mm has developed in the IP walls. A horizontal crack extended through the wall with a maximum crack opening of 4 mm.</p>

3.1.4 N2 Analysis

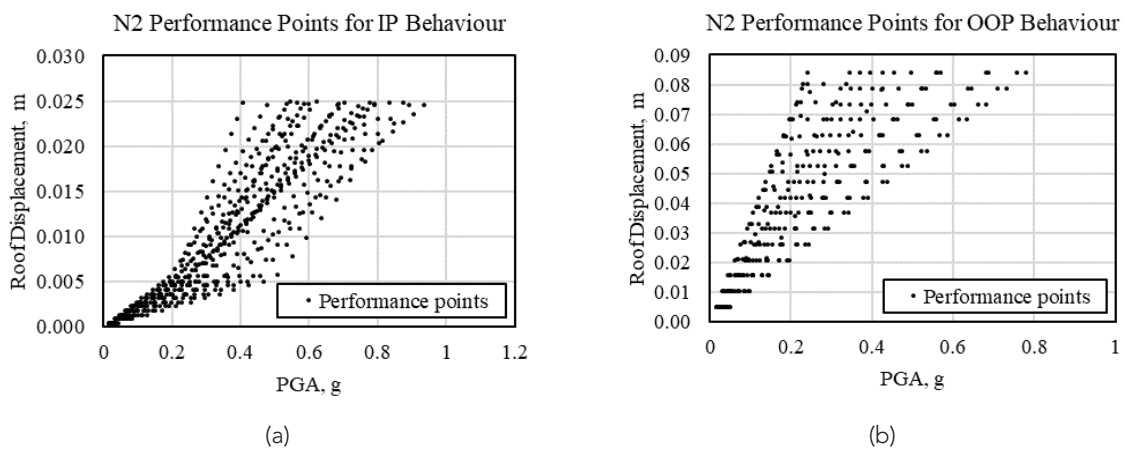
Figure 32 shows the bilinear idealization of the capacity curves for global IP and OOP behavior, respectively.

Figure 32. Bilinear idealization of the capacity curves with respect to (a) IP behavior and (b) OOP behavior.



The performance point cloud (IM vs EDP) obtained for the IP and OOP behavior using the 22 set (each scaled) of ground motions are shown in Figure 33.

Figure 33. Performance points (IM vs EDP) for OOP behavior (left) and IP behavior (right),

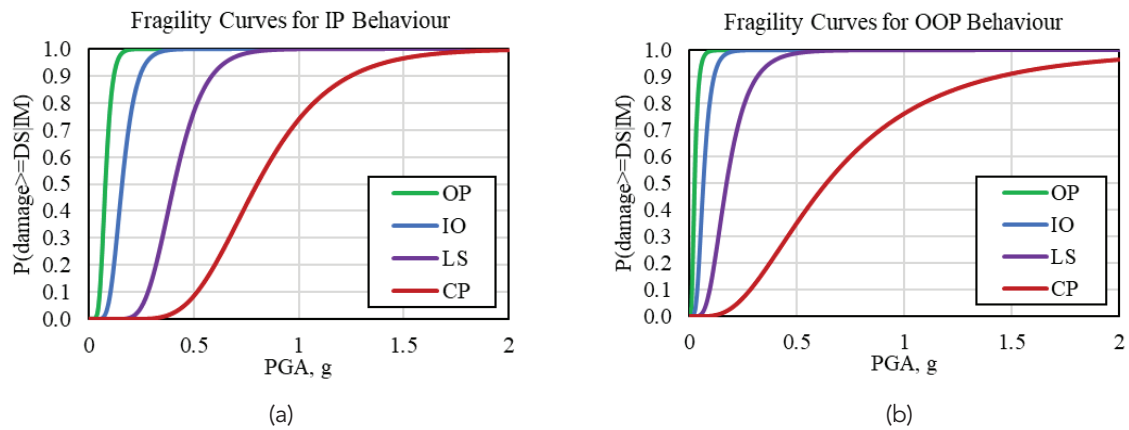


3.1.5 Fragility Analysis

Figure 34 present the fragility curves for each damage

state computed using the least squares methodology. A PGA of 2g is considered as the upper limit of the IM.

Figure 34. Fragility curves for UCM-URM7 IB for a) global IP behavior and b) global OOP behavior.

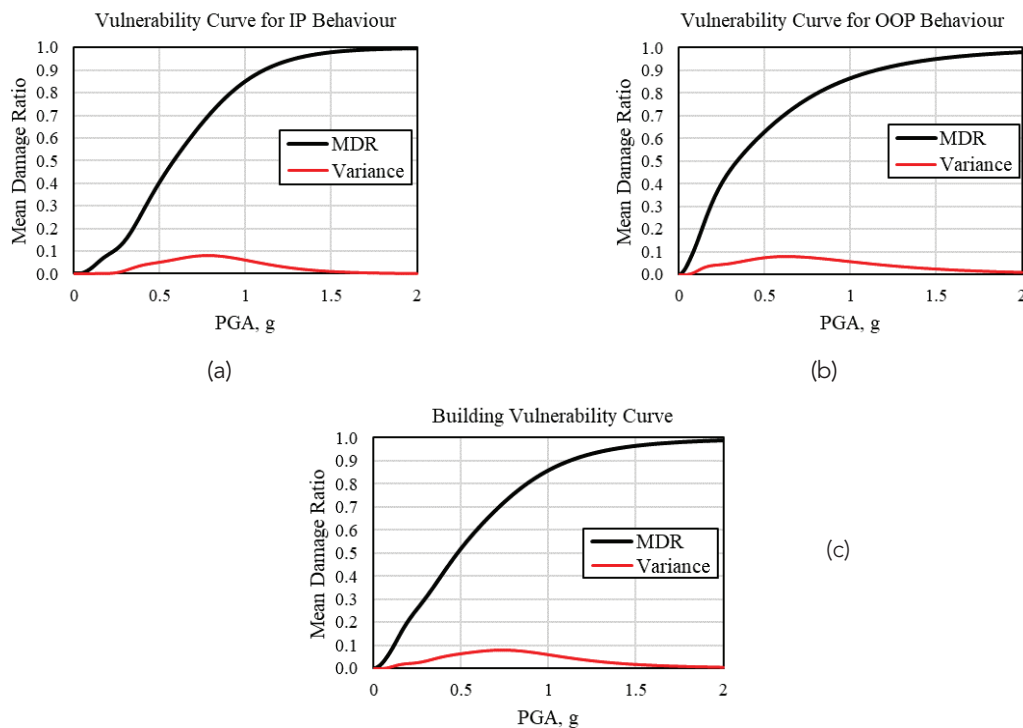


3.1.6 Vulnerability Analysis

Figures 35 a) and b) show the vulnerability functions with respect to global IP and global OOP behavior. Finally, Figure 35 c) presents the building's total vulnerability

curve obtained by combining the vulnerability curves with respect to global IP and global OOP behavior. The combination is based on the contribution factor of walls under IP behavior and walls under OOP behavior (50% each in this case) to the total building vulnerability.

Figure 35. Vulnerability curves with respect to a) IP behavior, b) OOP behavior, and (c) building total vulnerability curve for the UCM-URM7 IB.



3.2 Example Analysis of an RC Index Building

3.2.1 Hazard Definition

The group of far field records indicated are selected

for the analysis. Figure 36 presents seismic record response spectra from the proposed group.

3.2.2 Index Building Definition

Table 11 presents and summarizes the main parameters of the IB selected for illustration purposes.

Figure 36. Far field ground motion response spectrum.

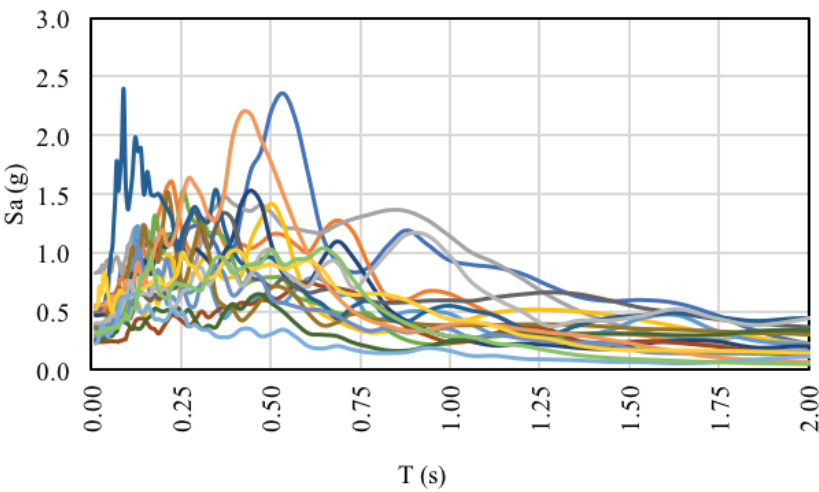


Table 11. IB taxonomy parameter.

Building Type	GLOSI Taxonomy String
RC1/MR/PD	RC3/MR/LD/RD/NI/SS/SW/RF/NP/OS/GC/VN

Table 12 shows intrinsic geometric characteristics for the Index Building in consideration.

Table 12. Intrinsic geometric.

Characteristic	Value
Building plane area (m2):	299.25
Building total area (m2):	598.5
Number of stories:	2
Story height (m):	3
Number of spans in X direction:	7
Typical span length in X direction (m):	4.5
Number of spans in Y direction (m):	3
Typical span length in Y direction (m):	3.5
Foundation system:	CISF
Typical column dimensions (cm x cm):	25X25
Typical beam dimensions (cm x cm):	20X30
Typical shear wall dimensions (cm x cm):	-
Typical bracing member section (cm x cm):	-

Table 13 presents material properties used in the modelling. It includes the concrete, reinforcement steel and masonry in the infills.

Table 13. Material properties.

Concrete	f'c (MPa):	17	Ec (GPa):	19
Reinforcement	fy (Mpa):	420	Es (GPa):	200
Masonry	f'm (MPa):	8	γ :.....	-

3.2.3 Numerical Modelling and Pushover Analysis

The modelling was made following ASCE 41-17 recommendations for bare frame structures; infill

walls are not considered in this IB. Table 14 shows the modelling considerations, the loads assigned and the analysis considerations for this specific example.

Table 14. Modelling considerations.

Modelling considerations:				
Plasticity model:	Lumped			
Infill walls modelling approach:	Equivalent frame			
Roof Diaphragm:	Rigid			
Foundation:	Rigid			
Loads:				
Over imposed design dead load (D) (kN/m2):	1.2			
Design Live load (L) (kN/m2):	2.0			
Load combination in non-linear analysis:	D+0.25L			
Average load per square meter (kN/m2):	8.7			
Analysis considerations:				
Global P-Delta effects:	Yes			
Rigid zones:	Yes			
Initial effective stiffness:	Beams	0.35	Columns	0.30
Analysis direction:	X			
Analysis orientation:	(+)X			

Figure 37 shows the mathematical model developed for the structural analysis.

Figure 37. RC IB structural model.

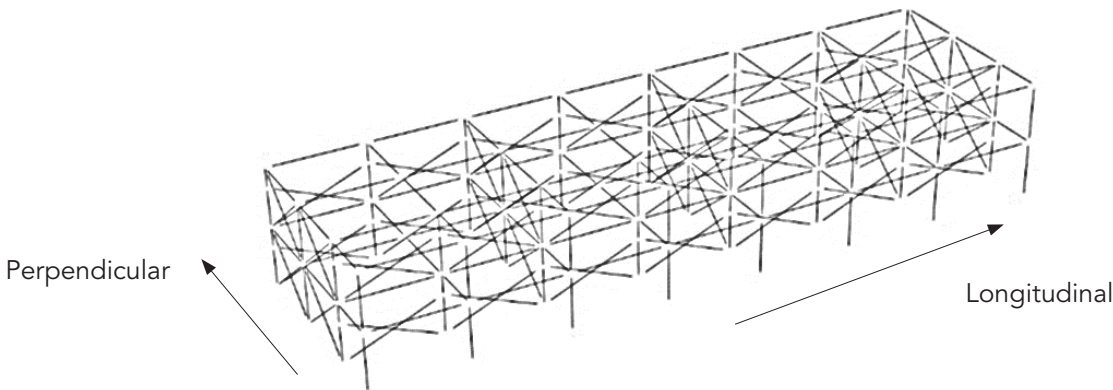
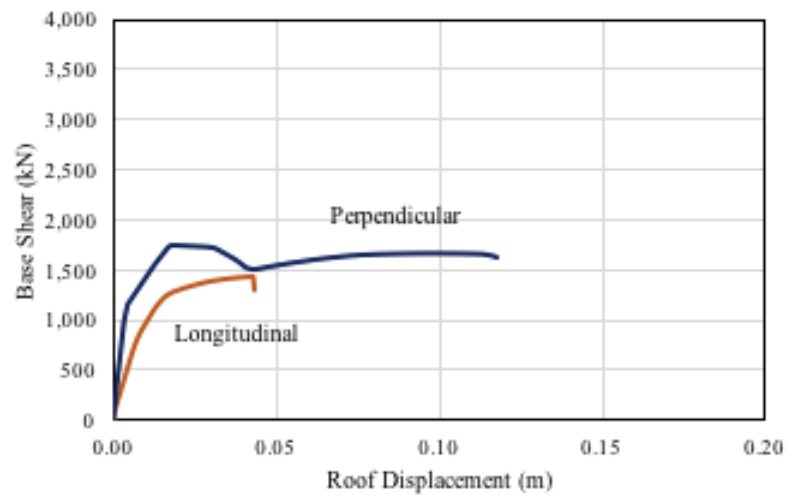


Figure 38 presents the pushover curve for the selected IB.

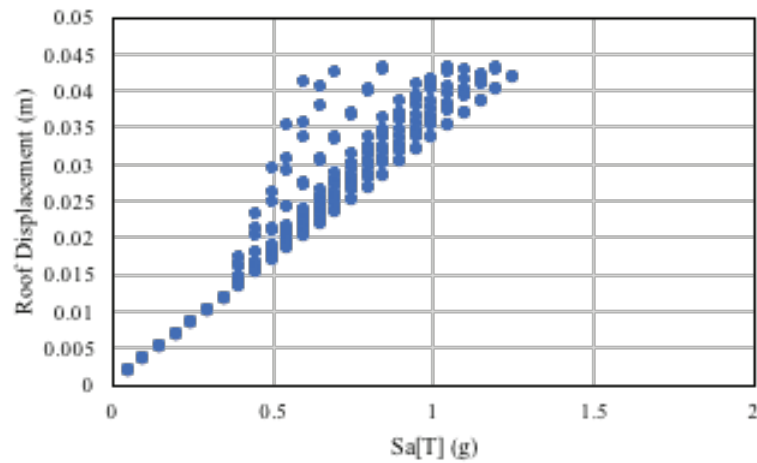
Figure 38. RC IB pushover curve.



3.2.4 N2 Analysis

Figure 39 presents the EDPs obtained using the N2 non-linear static methodology.

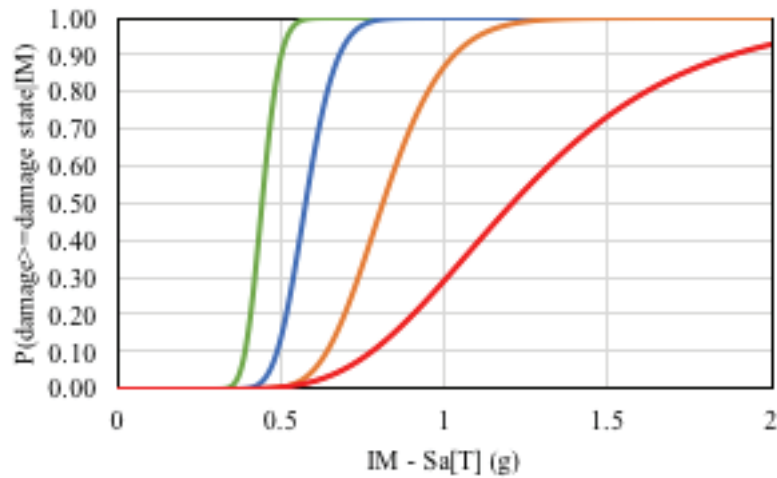
Figure 39. RC IB EDPs.



3.2.5 Fragility Analysis

Figure 40 presents the fragility curves for each damage state computed using the least squares methodology.

Figure 40. RC IB fragility function.



3.2.6 Vulnerability Analysis

The component model used is shown in Table 15.

Table 15. Component model.

Story	Group	Subgroup	Description	Unit	Quantity	Fragility curve	EDP	Correlation
1	E	C1	Column-one beam	Node	8	B1041.091a	Drift	0
1	E	C2	Column-two beams	Node	21	B1041.091b	Drift	0
1	A	F2	Masonry facade	5m x 3m	14	C1011.006a	Drift	1
1	A	M4	Masonry wall	5m x 3m	6	C1011.006b	Drift	1
1	C	S2	Contents	5m x 5m	13	E2022.010a	Drift	0
2	E	C1	Column-one beam	Node	8	B1041.091a	Drift	0
2	E	C2	Column-two beams	Node	21	B1041.091b	Drift	0
2	A	F2	Masonry facade	5m x 3m	14	C1011.006a	Drift	1
2	A	M4	Masonry wall	5m x 3m	6	C1011.006b	Drift	1
2	C	S2	Contents	5m x 5m	13	E2022.010a	Drift	0

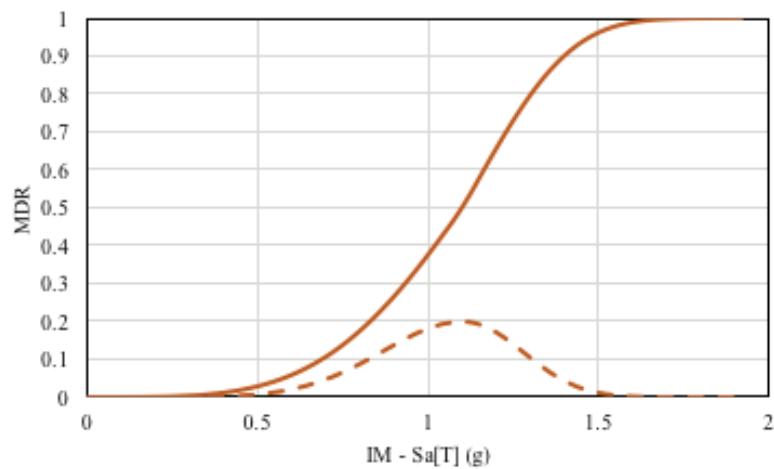
Table 16 shows the FUNVUL phase's parameters used in this example.

Table 16. FUNVUL calculation parameters.

Phase I:				
Beta model uncertainty:			0.3	
Number of iterations for model uncertainty:			15	
Number of iterations for damage states uncertainty:			15	
Number of iterations for cost and time uncertainty:			15	
Scale factor for cost:		Yes	No	x
Phase II:				
Lower intensity to no damage (g/g):			0.1	
Maximum allowable residual drift for demolition (%):			1.5	
Percentage of building replacement value (%):			100	
Bidirectional factor for total cost model:			1	
Intensity level for building evacuation (g/g):			2	

Figure 41 shows the vulnerability function obtained using the FUNVUL methodology as explained above.

Figure 41. RC IB Vulnerability function.



4. Catalog of Fragility/Vulnerability Assessment Results

A special form has been designed to organize, use,

and disseminate the final information obtained in relation to the F/V assessment. Figure 42 and Figure 43 present two different illustrative forms, one for LBM and one for a RC building. The F/V forms for all IBs analyzed are documented in GLOSI.

Figure 42. Example of an F/V Assessment Form for an LBM IB.

THE WORLD BANK		GFDRR		Universidad de los Andes		UCL	
FRAGILITY/VULNERABILITY ASSESSMENT				Date: 09/03/2015			
ABRIDGE MASONRY INDEX BUILDING				Building Type: LBM			
				Author: UCL			
				Sheet: 1 of 4			
GENERAL INFORMATION							
1. Main structural system: <input type="checkbox"/> Steel <input type="checkbox"/> Concrete <input type="checkbox"/> Masonry <input type="checkbox"/> Timber <input type="checkbox"/> Other							
2. Height range: <input type="checkbox"/> Low (L) <input type="checkbox"/> Medium (M) <input type="checkbox"/> High (H)							
3. Seismic design level: <input type="checkbox"/> Low (L) <input type="checkbox"/> Medium (M) <input type="checkbox"/> High (H)							
4. Displacement Type: <input type="checkbox"/> Flexible (F) <input type="checkbox"/> Rigid (R) <input type="checkbox"/> Vertical (V) <input type="checkbox"/> Both (B)							
5. Structural Irregularity: <input type="checkbox"/> No (N) <input type="checkbox"/> Yes (Y)							
6. Wall Panel Length: <input type="checkbox"/> Long (L) <input type="checkbox"/> Short (S)							
7. Wall Opening: <input type="checkbox"/> Small (S) <input type="checkbox"/> Large (L) <input type="checkbox"/> Rigid (R)							
8. Foundation Type and Flexibility: <input type="checkbox"/> Flexible (F) <input type="checkbox"/> Rigid (R) <input type="checkbox"/> Vertical (V) <input type="checkbox"/> Both (B)							
9. Seismic Penetration: <input type="checkbox"/> No (N) <input type="checkbox"/> Yes (Y)							
10. Seismic Reinforcement: <input type="checkbox"/> Original (O) <input type="checkbox"/> Retrofit (R) <input type="checkbox"/> Good (G) <input type="checkbox"/> Poor (P)							
11. Structural Health Condition: <input type="checkbox"/> Fair (F) <input type="checkbox"/> Poor (P) <input type="checkbox"/> Very Poor (VP)							
12. Non-Structural Components: <input type="checkbox"/> Vulnerable (V) <input type="checkbox"/> Non-Vulnerable (NV)							
EXTENSIVE CHARACTERISTICS							
Building Plan Area (m ²): 100							
Building Total Floor Area (m ²): 100							
Number of Stories: 1							
Typical Span Length in X Direction: 2.0							
Typical Span Length in Y Direction (m): 2.0							
Number of Spans in X Direction (m): 2							
Typical Span Length in Y Direction (m): 2							
Wall Thickness (mm): 200							
Roof Construction: Tile							
No. of Windows: 10							
MODELING PARAMETERS							
3D Model							
Modeling Approach: 2-D Element by Element							
Mass Modeling Approach: Simplified Mass Modeling							
Roof Dead Load (kN/m ²): 0.5							
Design Live Load (kN/m ²): 0.5							
Load Combination for Seismic Analysis: 1.2D+1.6L+0.5W							
Average Load per Square Meter (kN/m ²): 0.5							
Analysis Considerations: <input type="checkbox"/> Viscous <input type="checkbox"/> No <input type="checkbox"/> Yes							
Global P-Delta Effects: <input type="checkbox"/> No <input type="checkbox"/> Yes							
Analysis Direction: <input type="checkbox"/> X <input type="checkbox"/> Y <input type="checkbox"/> Z							
Analysis Orientation: <input type="checkbox"/> X <input type="checkbox"/> Y <input type="checkbox"/> Z							
SEISMIC EVALUATION							
Seismic Weight of IP Walls (kN): 800							
Seismic Weight of OOP Walls (kN): 720							
Fundamental Time Period of IP Walls (sec): 0.14							
Fundamental Time Period of OOP Walls (sec): 0.36							
Performance Curves with Damage State Thresholds							
Global Performance Curve for IP Behavior				Global Performance Curve for OOP Behavior			

IB1_LBM_A_LR_LD

THE WORLD BANK		GFDRR		Universidad de los Andes		UCL	
FRAGILITY/VULNERABILITY ASSESSMENT				Date: 09/03/2015			
ABRIDGE MASONRY INDEX BUILDING				Building Type: LBM			
				Author: UCL			
				Sheet: 2 of 4			
Damage of Crack Patterns, Width and Spacing Progression							
IP Wall Behavior				OOP Wall Behavior			
IP Threshold: Horizontal cracks (black) of maximum width 0.5 mm appear at low corners of openings.				OOP Threshold: Horizontal cracks (black) appear at the top corners with the top face with max crack width 0.5 mm.			
IP Threshold: Horizontal cracks (black) of maximum width 2 mm developed at almost all the corners of the openings, few pins and spacers start to develop shear and flexural cracks, respectively.				OOP Threshold: Minor cracks (black) start to develop at the IP connections, max crack width 2 mm, a minor horizontal crack of maximum opening 1 mm started at the bottom corner.			
IP Threshold: Right most spigot and pin start to damage in flexure and shear respectively, with a maximum crack width (red) of 4 mm. Minor to major shear cracks (red) of 2 to 4 mm width appear in most of the pins.				OOP Threshold: Minor to major (red) cracks of 3 mm maximum width with the IP walls connections. A horizontal crack (red) of maximum opening 1.2 mm at the bottom appears.			
IP Threshold: Most pins developed major shear cracks (red) of 3 mm maximum width.				OOP Threshold: Wall on the verge of collapse. Connections with the IP walls damaged with major cracks (red) of width more than 3 mm. Horizontal cracks (red) of maximum opening 1.2 mm at the bottom.			

IB1_LBM_A_LR_LD

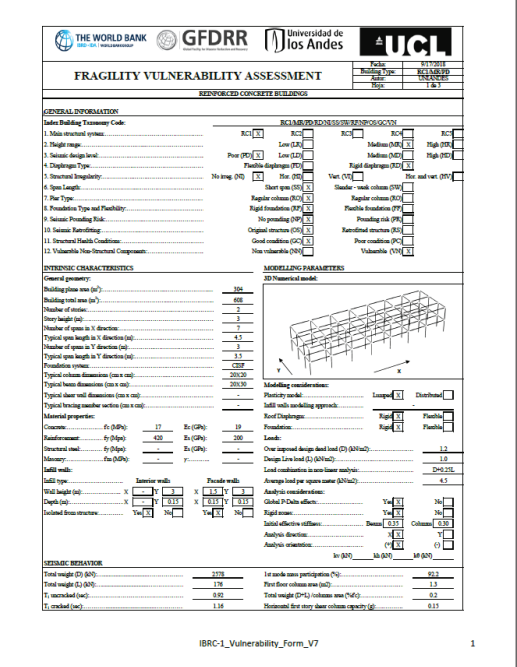
THE WORLD BANK		GFDRR		Universidad de los Andes		UCL	
FRAGILITY/VULNERABILITY ASSESSMENT				Date: 09/03/2015			
ABRIDGE MASONRY INDEX BUILDING				Building Type: LBM			
				Author: UCL			
				Sheet: 3 of 4			
SEISMIC PERFORMANCE ASSESSMENT							
Analysis Methodology: <input type="checkbox"/> Static Analysis (NZ Method) <input type="checkbox"/> Non-Linear (NL Method)							
Engineering Demand Parameter (EDP): <input type="checkbox"/> Roof Drift <input type="checkbox"/> Other							
Seismic Ground Motion: FEMA P695 - 22 Far Field Ground Motion							
Intensity Measure (IM): <input type="checkbox"/> PGA <input type="checkbox"/> Other							
Building Factor: <input type="checkbox"/> 1.0 <input type="checkbox"/> Other							
Minimum IM: <input type="checkbox"/> 0.1 <input type="checkbox"/> Other							
Maximum IM: <input type="checkbox"/> 1.0 <input type="checkbox"/> Other							
Seismic Modification							
ADRS Capacity Curve for IP Behavior				ADRS Capacity Curve for OOP Behavior			
EDP Calculation							
NZ Performance Points for IP Behavior				NZ Performance points for OOP Behavior			
FRAGILITY ASSESSMENT							
Integration Methodology: <input type="checkbox"/> Least Square Method <input type="checkbox"/> Other							
Fragility Functions				Fragility Functions			
Mean: <input type="checkbox"/> 0.07 <input type="checkbox"/> 0.17 <input type="checkbox"/> 0.25 <input type="checkbox"/> 0.51				Mean: <input type="checkbox"/> 0.07 <input type="checkbox"/> 0.17 <input type="checkbox"/> 0.25 <input type="checkbox"/> 0.51			
Standard Deviation: <input type="checkbox"/> 0.20 <input type="checkbox"/> 0.42 <input type="checkbox"/> 0.40 <input type="checkbox"/> 0.50				Standard Deviation: <input type="checkbox"/> 0.20 <input type="checkbox"/> 0.42 <input type="checkbox"/> 0.40 <input type="checkbox"/> 0.50			

IB1_LBM_A_LR_LD

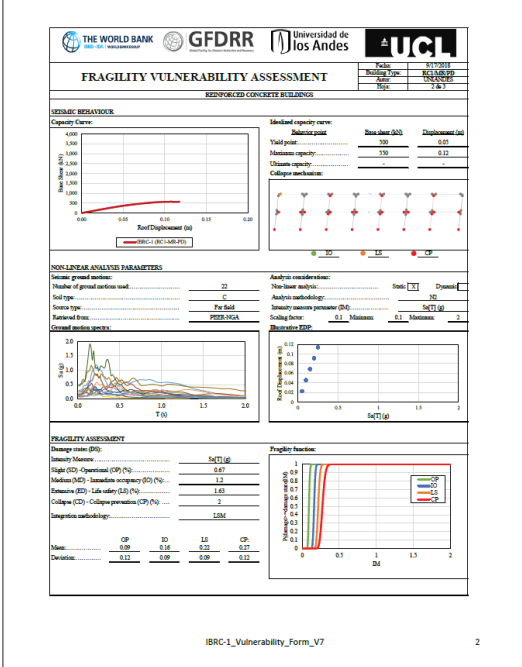
THE WORLD BANK		GFDRR		Universidad de los Andes		UCL	
FRAGILITY/VULNERABILITY ASSESSMENT				Date: 09/03/2015			
ABRIDGE MASONRY INDEX BUILDING				Building Type: LBM			
				Author: UCL			
				Sheet: 4 of 4			
VULNERABILITY ASSESSMENT							
Damage to Loss Function:							
IP (No): 2 IO (No): 10 LS (No): 43.5 CP (No): 100							
Vulnerability Function:							
GLOSSARY							
IP = In Plane IO = Out of Plane LS = Life Safety CP = Collapse Prevention							
OP = Operational SD = Structural Occupancy LS = Life Safety CP = Collapse Prevention							
IM = Intensity Measure EDP = Engineering Demand Parameter							
ADRS = Acceleration Displacement Response Spectra							
Se = Spectral Acceleration SA = Spectral Displacement							
PGA = Peak Ground Acceleration							
T = Time (seconds)							
REFERENCES							
Global Library of School Infrastructure (GLSI)							
Building Vulnerability for LBM and RC School Buildings - (GLSI Technical Report (Deliverable 2))							
FEMA P695							
ASCE E-17							
NZ Method (FEMA, 2000)							
GFDRR Vulnerability Assessment Guidelines (2014) (GLSI, 2015)							
FUNDRA (www.fundra.org)							

IB1_LBM_A_LR_LD

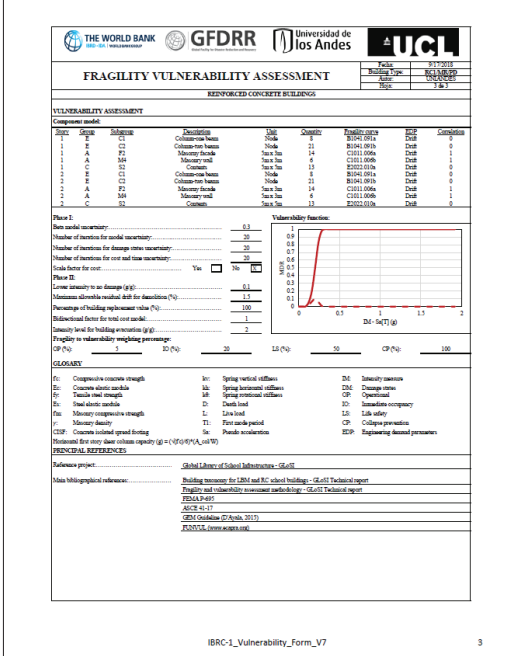
Figure 43. Example of an F/V Assessment Form for an RC IB.



IBRC-1_Vulnerability_Form_V7



IBRC-1_Vulnerability_Form_V7



IBRC-1_Vulnerability_Form_V7

5. Sensitivity Analysis

The different construction characteristics of a building (i.e. the vulnerability parameters) pose a considerable amount of uncertainties, from the actual material properties of masonry components to variations in geometry and layout. It is worth noting that the fragility and vulnerability functions derived are expected to be of international and global applicability. Therefore, it is of great importance to quantify the variability of these parameters in practice, the resulted uncertainty associated with any of the functions derived, and its remit of applicability to a given taxonomy class.

To this end, sensitivity analyses are conducted for one LBM and one RC building type to understand and quantify the effect of the different vulnerability parameters and their associated attributes on the seismic performance and seismic vulnerability of the corresponding construction type.

5.1 Load Bearing Masonry

A sensitivity analysis is conducted for the UCM-URM7/LR building type to understand and quantify the effect of the different vulnerability parameters and their associated attributes on its seismic performance and seismic vulnerability. It should be noted that in most of the cases, only a single relevant parameter is changed at a time, keeping all the others constant (this method of sensitivity analysis is known as the one-at-a-time (OAT) method).

Detailed information on the baseline model (UCM-URM7/LR/LD) is provided in the illustrative example section, and the full taxonomy string is repeated in Table 17. This building type represents an UCM-URM7 school construction, which is typical in Nepal. As the building is weaker in its longer direction, the seismic analysis for all different models is carried out in the longitudinal direction unless otherwise specified.

Table 17. Baseline model taxonomy parameters.

Building Type	GLOSI Taxonomy String
UCM-URM7/LR/LD	UCM-URM7/LR(1)/LD/FD/NI/LP/LO/RF/NP/OS/PC/VN

Table 18 gives the details of the parameters used in the sensitivity analysis. The attributes highlighted in

red represent the attributes of the sensitivity parameter being considered.

Table 18. Sensitivity parameters, attributes and associated taxonomy strings.

S.N.	Parameters	Range (Attributes)	Taxonomy String	Expected Range Covered
1	Seismic Design Level	Poor Design (PD)	UCM-URM7/LR(1)/PD/FD/NI/LP/LO/RF/NP/OS/PC/VN	Yes
		Low Design (LD)	UCM-URM7/LR(1)/LD/FD/NI/LP/LO/RF/NP/OS/PC/VN	
		Medium Design (MD)	UCM-URM7/LR(1)/MD/FD/NI/LP/LO/RF/NP/OS/PC/VN	
		High Design (HD)	UCM-URM7/LR(1)/HD/FD/NI/LP/LO/RF/NP/OS/PC/NN	
2	Diaphragm Type	Flexible Diaphragm (FD)	UCM-URM7/LR(1)/LD/FD/NI/LP/LO/RF/NP/OS/PC/VN	Yes
		Rigid Diaphragm (RD)	UCM-URM7/LR(1)/LD/RD/NI/LP/LO/RF/NP/OS/PC/NN	
3	Irregularity	No Irregularity (NI)	UCM-URM7/LR(1)/LD/FD/NI/LP/LO/RF/NP/OS/PC/VN	No (Vertical and Combined Irregularities not covered)
		Horizontal Irregularity (HI)	UCM-URM7/LR(1)/LD/FD/HI/LP/LO/RF/NP/OS/PC/VN	
4	Wall Panel Length	Long Panel (LP)	UCM-URM7/LR(1)/LD/FD/HI/LP/LO/RF/NP/OS/PC/VN	Yes
		Short Panel (SP)	UCM-URM7/LR(1)/LD/FD/HI/SP/LO/RF/NP/OS/PC/VN	
5	Wall Opening	Large Openings (LO)	UCM-URM7/LR(1)/LD/FD/HI/SP/LO/RF/NP/OS/PC/VN	Yes
		Small Openings (SO)	UCM-URM7/LR(1)/LD/FD/HI/SP/SO/RF/NP/OS/PC/VN	
6	Effective Seismic Retrofitting	Original Structure (OS)	UCM-URM7/LR(1)/LD/FD/HI/SP/SO/RF/NP/OS/PC/VN	Yes
		Retrofitted Structure (RS)	UCM-URM7/LR(1)/LD/FD/HI/SP/SO/RF/NP/RS/PC/NN	
7	Structural Health Condition	Poor Condition (PC)	UCM-URM7/LR(1)/LD/FD/HI/SP/SO/RF/NP/OS/PC/VN	Yes
		Good Condition (GC)	UCM-URM7/LR(1)/LD/FD/HI/SP/SO/RF/NP/OS/GC/VN	

5.1.1 Seismic Design Level

The seismic design level is an important parameter that highly influences the seismic behavior of a building. Four different seismic design levels are considered, viz. Poor Design (PD), Low Design (LD), Medium Design (MD) and High Design (HD). The PD model represents a masonry building that has poor material quality and poor connections between the orthogonal walls. The LD model represents a building that has poor material qualities, but the orthogonal walls are well connected in an English bond pattern. The MD model represents the buildings that have

good material quality and a lintel level band beam to improve the global building behavior. Finally, the HD model represents the buildings that are relatively new (e.g. built in the school reconstruction program after the 2015 Nepal earthquake), were built with good quality materials, and have a sufficient number of seismic enhancement measures, such as the sill level band, lintel level band, roof level band, and intermediate ties in the walls. Figure 44 shows the numerical models for the UCM-URM7 typology with different seismic design levels.

Figure 44. Numerical models of UCM-URM7 index buildings with different seismic design levels.

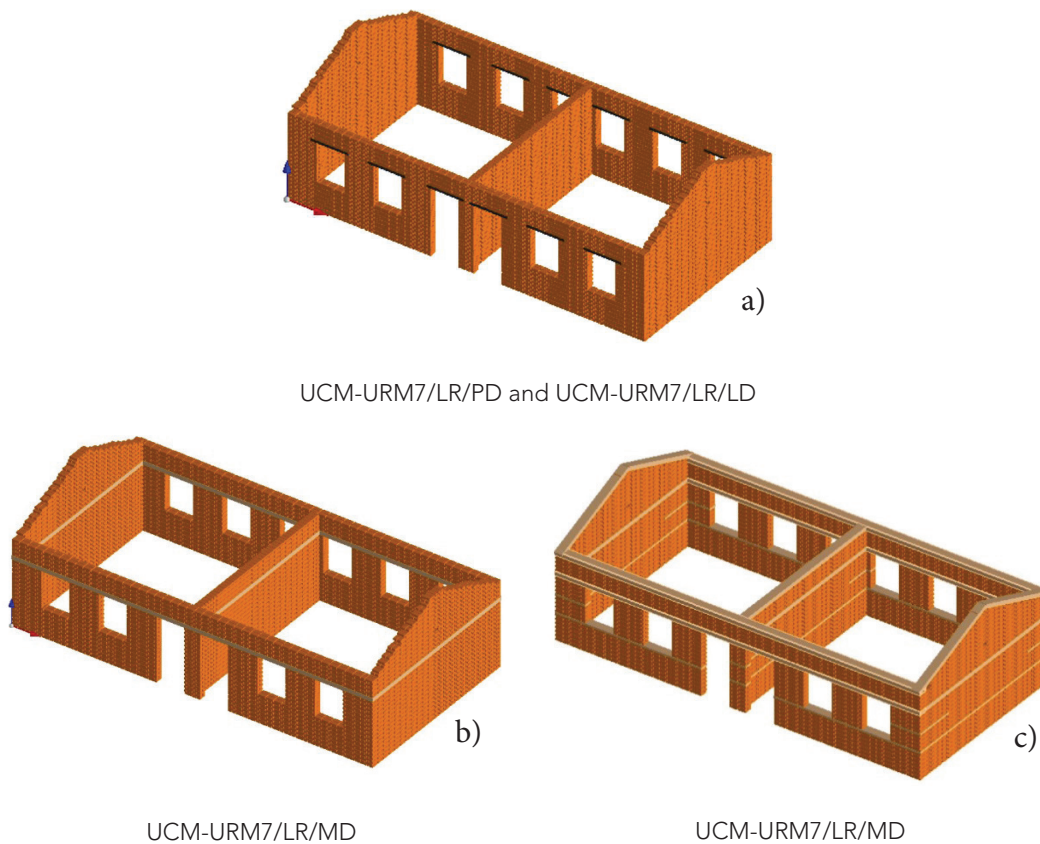


Figure 45 shows the final collapse mechanisms of each different index building. The OOP walls are highly vulnerable and tend to be detached (from IP walls) and overturn in the case of PD and LD models. On the other hand, in the case of MD, the global seismic behavior is improved due to the box-like behavior provided by the lintel band beam (which binds all the

walls together). However, in the MD model, the gables are not confined and hence are highly vulnerable and can overturn easily. In the case of HD, the behavior is highly improved through mitigating the local failure modes of OOP walls. In both the MD and HD model, the global collapse is due to the shear failure of piers in the IP walls.

Figure 45. Collapse mechanisms of UCM-URM7 index buildings with different seismic design levels. The blue lines represent the extensive cracks of a width of more than 12.5 mm (only extensive cracks are shown).

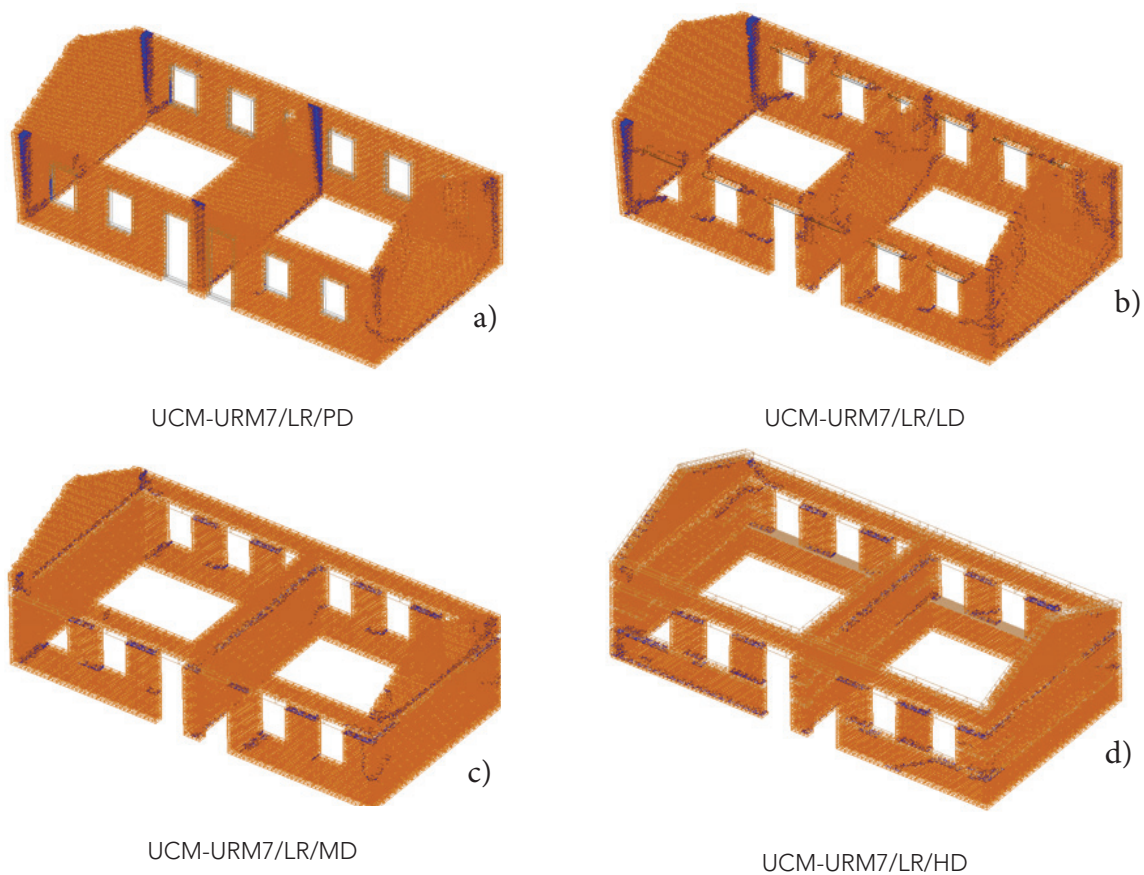


Figure 46 shows the capacity curves along with the different damage state thresholds marked along the capacity curves. For the models which do not have a global behavior (PD and LD), the capacity curves under

IP and OOP behavior are plotted separately. It can be seen from the capacity curves that both the strength and displacement capacity are increased with the increase in seismic design level.

Figure 46. Comparison of capacity curves for the index buildings with different seismic design levels. The colored dots represent the threshold of different damage states: Green = Slight Damage, Blue = Moderate Damage, Purple = Extensive Damage and Red = Collapse.

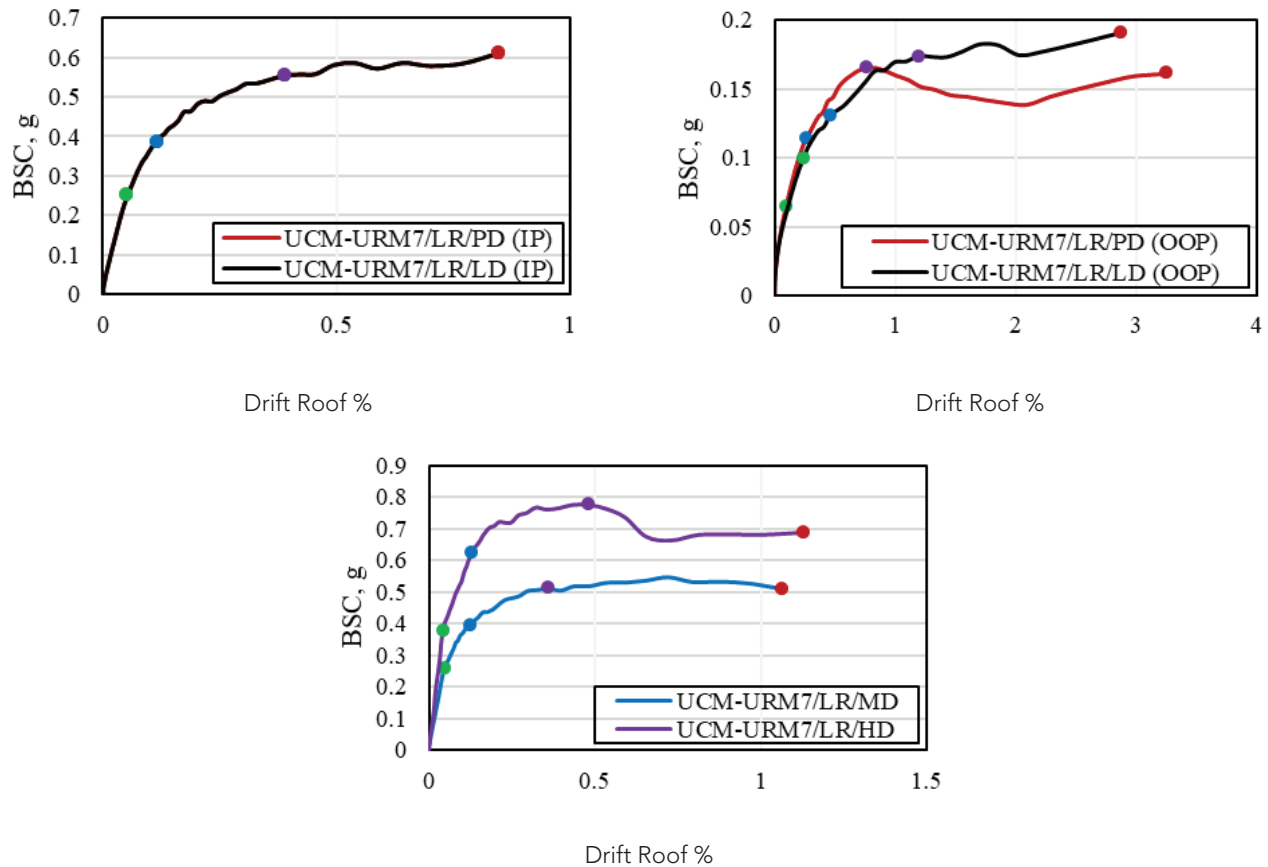
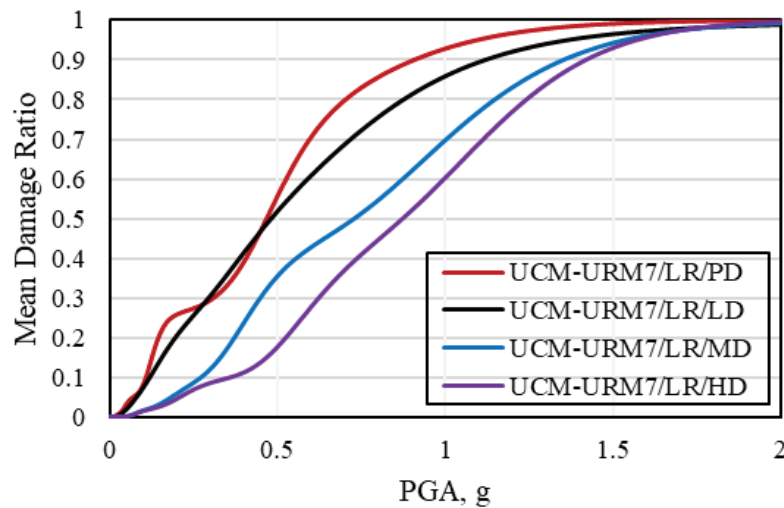


Figure 47 shows the vulnerability curves for the index buildings with different seismic design levels. It can be seen that even the introduction of the lintel band beam only (MD) highly reduces the seismic vulnerability of the UCM-URM7/LR buildings. This is due to the

restriction of OOP walls failure and the improvement of the global behavior. Vulnerability is further reduced when more seismic enhancements are introduced (in case of HD).

Figure 47. Comparison of vulnerability curves for the index buildings with different seismic design levels.



For a single-story UCM-URM7 building with the same geometrical characteristics, the results show that the seismic behavior and failure mode as well as the vulnerability curves are unique to each different seismic design level. These results support the appropriateness of having four different attributes (i.e. poor, low, medium and high design levels) for the seismic design level.

5.1.2 Diaphragm Type

Roof and floor diaphragm action is also a critical parameter that influences seismic performance. The building typically has a better global seismic performance (especially in terms of OOP wall behavior) when all the walls are well connected at the roof/floor

level by a stiff structure (e.g. an RC slab) along with a ring beam properly connected to the masonry walls.

Figure 48 shows the numerical models of the index buildings with flexible diaphragm and rigid diaphragm. The flexible diaphragm (FD) model consists of a light roof frame structure (not modelled, i.e. the stiffness of the roof structure is neglected) while the rigid diaphragm (RD) type model consists of a ring beam and an RC slab. Here, the depth of both the slabs and the ring beams is 150 mm and the slabs are provided as a flat structure without gables, considering that this is the usual construction practice in many developing countries (e.g. Nepal) for a building structure with RC slab.

a)

b)

UCM-URM7/LR/FD

UCM-URM7/LR/RD

final collapse mechanism is formed due to the shear failure of IP wall piers.

a)

b)

UCM-URM7/LR/LD/FD

UCM-URM7/LR/LD/RD

Figure 50 shows the capacity curves along with the different damage state thresholds marked along the capacity curves. It can be seen from the capacity curves that both the strength (with respect to the

OOP wall of FD model) and displacement capacity (with respect to the IP wall of FD model) are improved when the diaphragm action is rigid.

Figure 50. Comparison of capacity curves for the index buildings with different diaphragm types. The colored dots represent the threshold of different damage states: Green = Slight Damage, Blue = Moderate Damage, Purple = Extensive Damage and Red = Collapse.

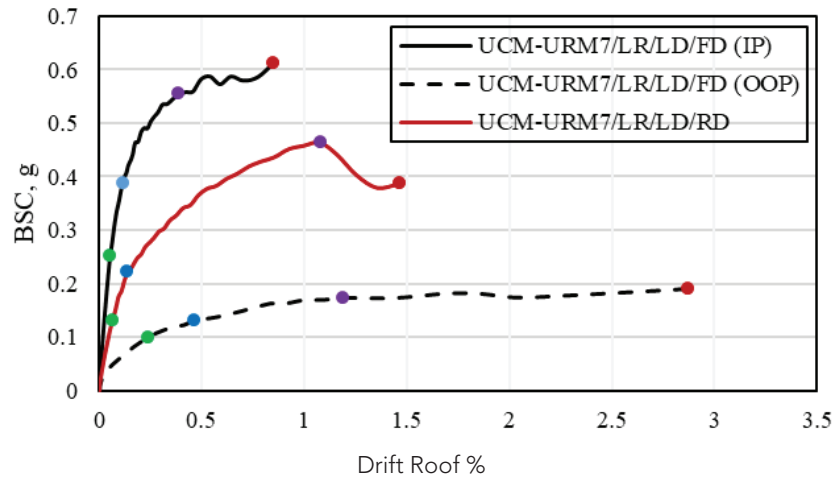
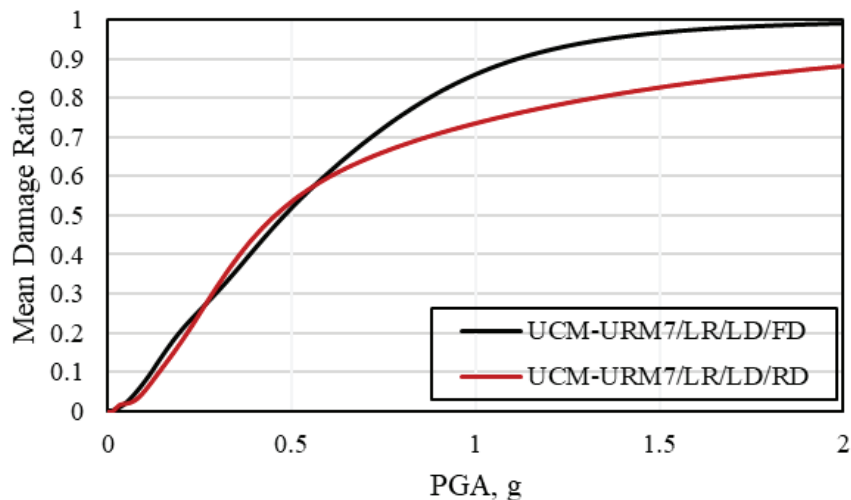


Figure 51 shows the vulnerability curves for the index buildings with different diaphragm types. Although the vulnerability reduction at lower IM is not significant,

there is considerable reduction in higher IM range. This is due to the prevention of OOP wall failure and the improvement of the global behavior.

Figure 51. Comparison of vulnerability curves for the index buildings with different diaphragm types.



5.1.3 Irregularities

Different types of horizontal and vertical irregularities can be present in a school building. It is difficult and unrealistic to introduce much irregularity in the case study building without changing the plan dimensions. Here, a horizontal irregularity imposed by the openings (size, location and distribution) is considered. The opening (%) in the front wall is increased to 65%

compared to 46% in the back wall. The opening irregularity can also be introduced when there are no openings at all in the back wall (solid wall), or when window openings are introduced in the shorter walls. But those are not very common in real school buildings and hence are not studied here. Figure 52 shows the numerical models of UCM-URM7/LR building with no irregularity and horizontal irregularity.

Figure 52. Numerical models of UCM-URM7 index buildings with no irregularity and horizontal irregularity (imposed by the openings). /-/ in the taxonomy string indicates that some parameters are truncated in the string.

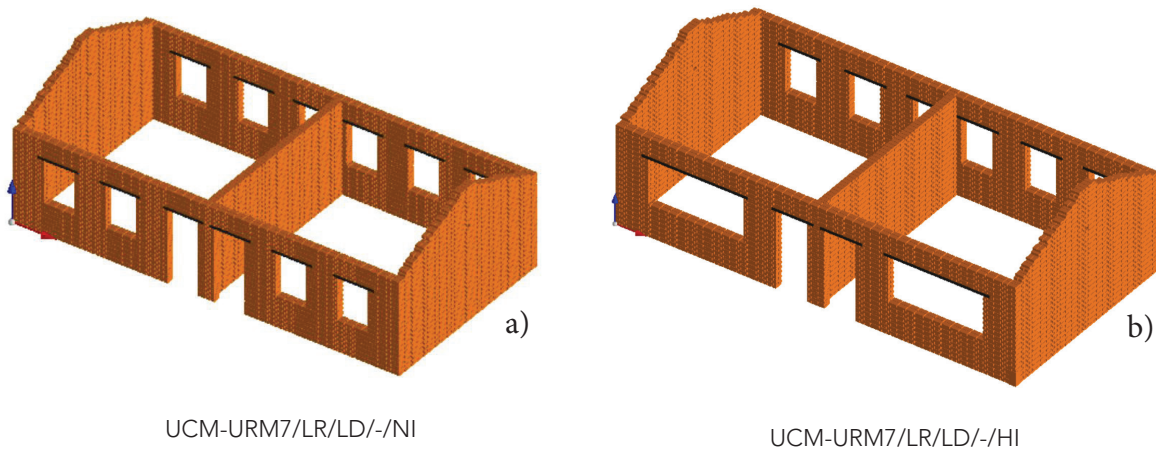


Figure 53 shows the collapse mechanisms of the two (NI and HI) index buildings. It is noticeable that in the case of the HI model, the weaker wall (front IP wall) is

subjected to more damage than the stronger back IP wall.

Figure 53. Collapse mechanisms of UCM-URM7 index buildings with no irregularity and horizontal irregularity. The blue lines represent the extensive cracks of a width of more than 12.5 mm (only extensive cracks are shown).

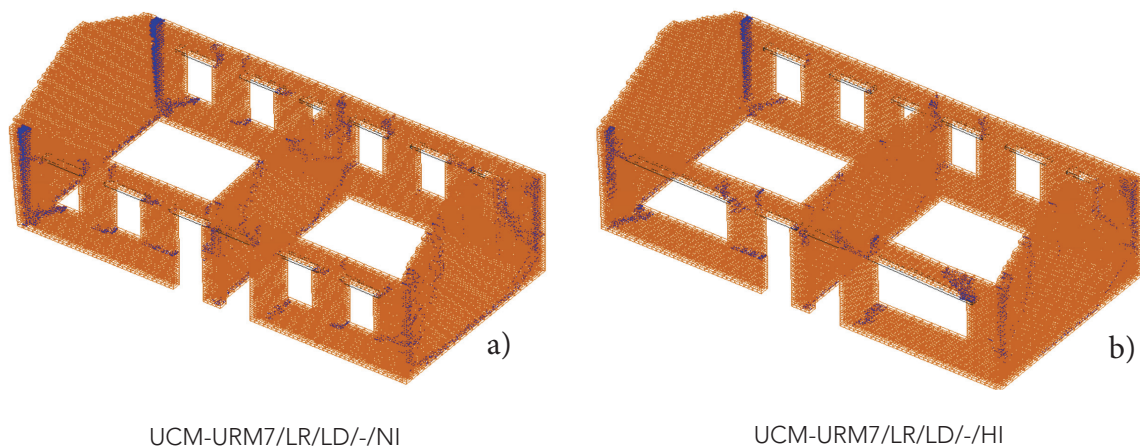


Figure 54 shows the capacity curves along with the different damage state thresholds marked along the capacity curves. In the case of the HI model, there

is noticeable reduction in both the strength and the displacement capacity.

Figure 54. Comparison of capacity curves for the index buildings with no irregularity and horizontal irregularity. The colored dots represent the threshold of different damage states: Green = Slight Damage, Blue = Moderate Damage, Purple = Extensive Damage and Red = Collapse.

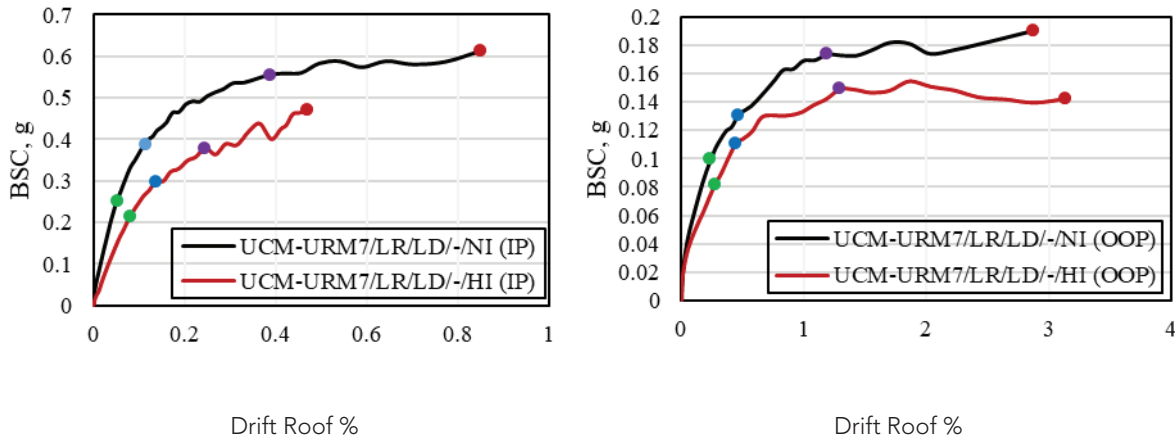
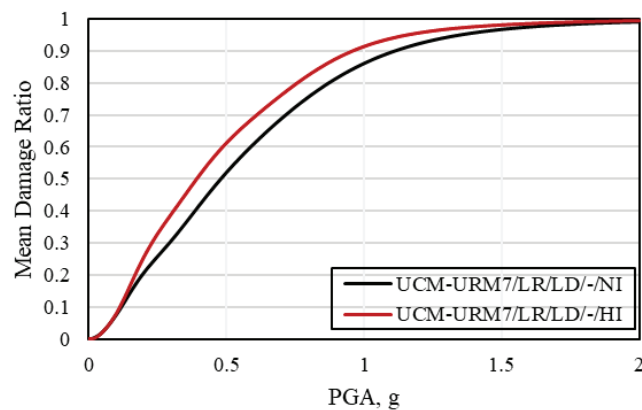


Figure 55 shows the vulnerability curves for the index buildings with no irregularity and horizontal irregularity. There is a modest increase in the seismic vulnerability due to the presence of horizontal irregularity in this

case. However, other types of horizontal irregularities (such as plan shape irregularities) can significantly increase the vulnerability.

Figure 55. Comparison of vulnerability curves for the index buildings with no irregularity and horizontal irregularity.

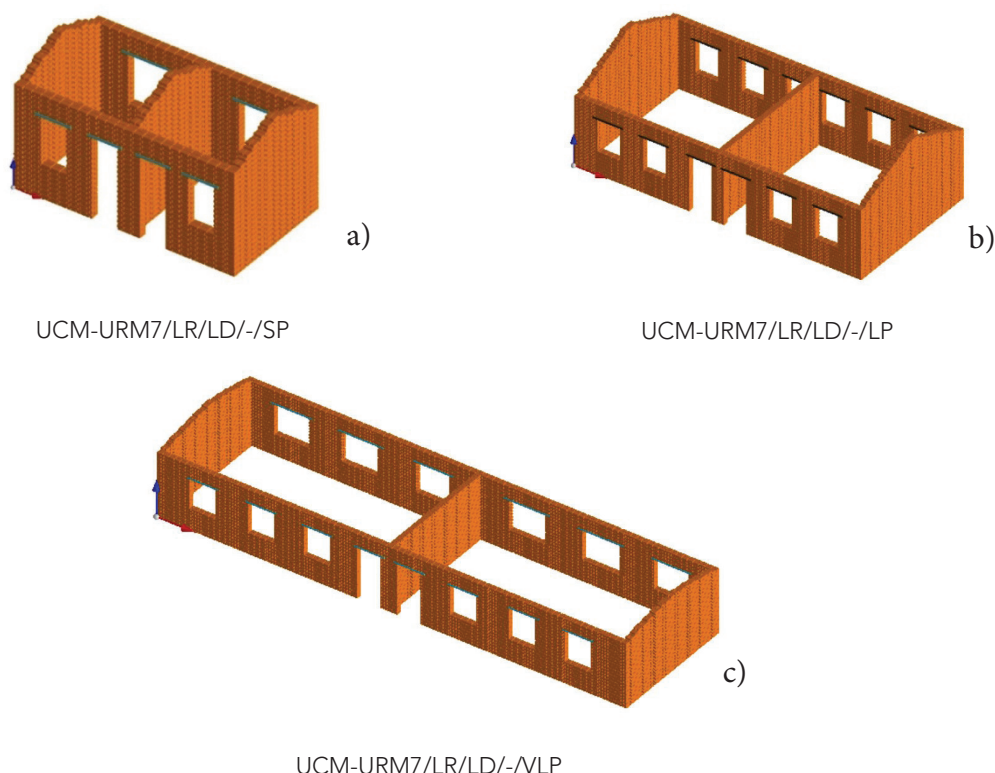


5.1.4 Wall Panel Length

The vulnerability of a building increases with the increase in unrestrained length of a wall panel, mainly under OOP seismic loading. Here, three different models are considered with different unrestrained panel lengths of the long walls, i.e. the short panel length (SP) model, long panel length (LP) model, and very long panel length (VLP) model. The SP model

has an unrestrained wall panel length of 3 m, which is less than 12 times the wall thickness. The LP and VLP models have unrestrained wall panel lengths of 5.7 m and 10 m, respectively, both of which are larger than 12 times the wall thickness. Figure 56 shows the numerical models of the index buildings with different wall panel lengths.

Figure 56. Numerical models of UCM-URM7 index buildings with different lengths of unrestrained wall panel.



When the wall panels are very large (as in the case of the VLP model), the analysis should be carried out in both directions, as the longitudinal walls might become more vulnerable to OOP failure than the gable walls (short walls). Figure 57 shows the comparison of capacity curves for OOP walls when loaded in longitudinal and transverse direction. It can be seen

that although the initial stiffness of the OOP capacity curve associated to the transverse (short) direction loading is higher, the ultimate strength and ultimate drift are both lower in comparison to the OOP capacity curve associated with the longitudinal loading. Hence, the building is weaker in the OOP failure when loaded in the shorter direction.

Figure 57. Capacity curves for the UCM-URM7/LR/VLP building under OOP behavior when loaded in the two principal directions.

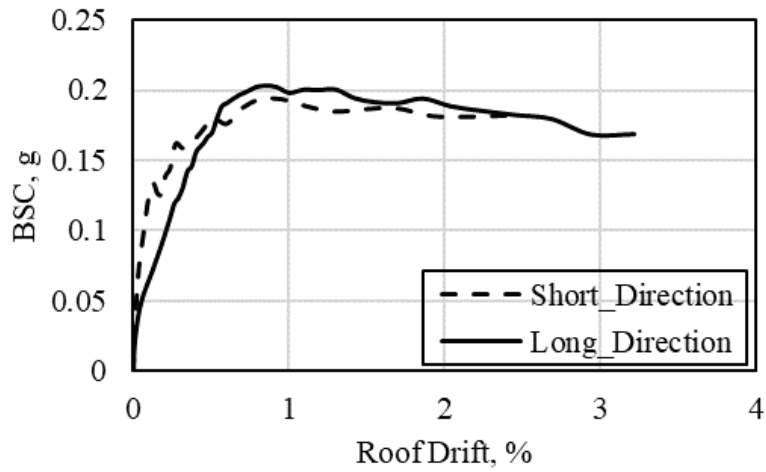


Figure 58 shows the collapse mechanisms of the index buildings with different unrestrained wall panel lengths. The SP model has a box-like global behavior

and thus improved seismic performance, while the VLP model has very weak long unrestrained walls under OOP direction when loaded in the shorter direction.

Figure 58. Collapse mechanisms of UCM-URM7 index buildings with different unrestrained wall panel lengths. The blue lines represent the extensive cracks of a width of more than 12.5 mm (only extensive cracks are shown). Note that the VLP model is loaded in the transverse direction.

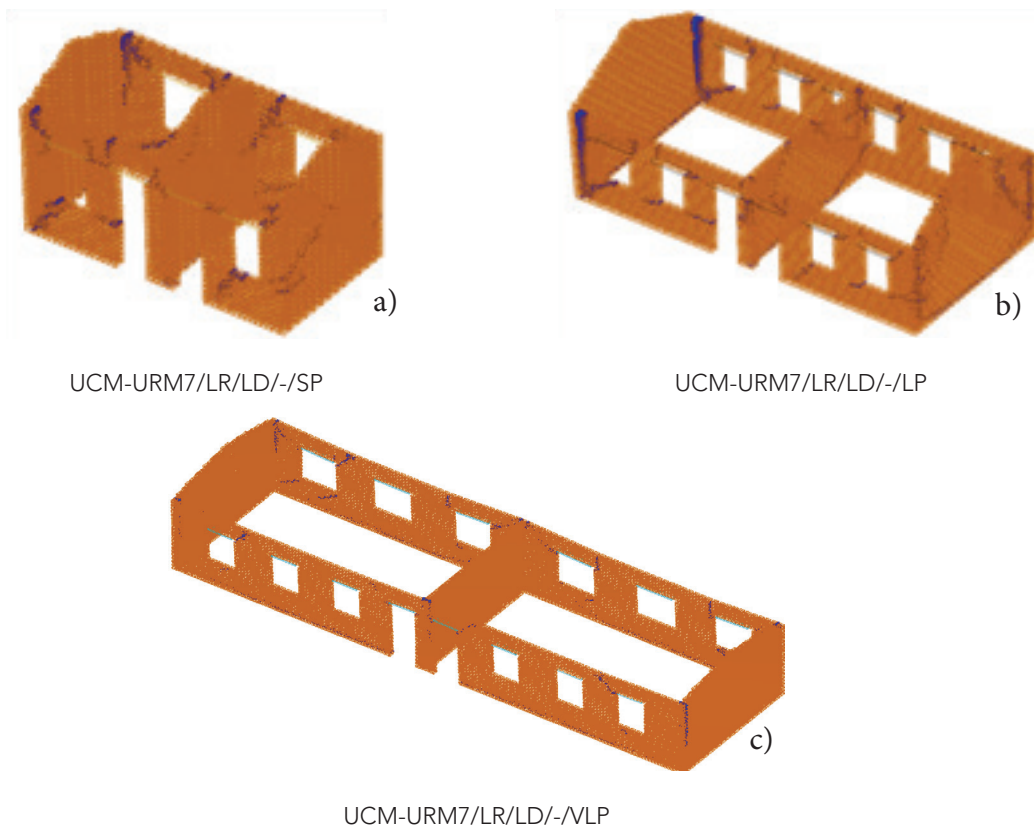


Figure 59 shows the capacity curves along with the different damage state thresholds marked along the capacity curves. As explained before, the building total capacity curve (instead of separate IP and OOP capacity curves) is plotted for the SP model because of the controlled displacement at the roof level due to the box-like behavior; while for the LP and VLP

models, the capacity curves under OOP behaviors are plotted as the OOP behavior controls the collapse. The OOP capacity curve for VLP has higher initial stiffness and strength but the displacement capacity is reduced compared to the LP model because of the large unrestrained wall panel.

Figure 59. Comparison of capacity curves for the index buildings with different unrestrained wall panel lengths. The colored dots represent the threshold of different damage states: Green = Slight Damage, Blue = Moderate Damage, Purple = Extensive Damage and Red = Collapse.

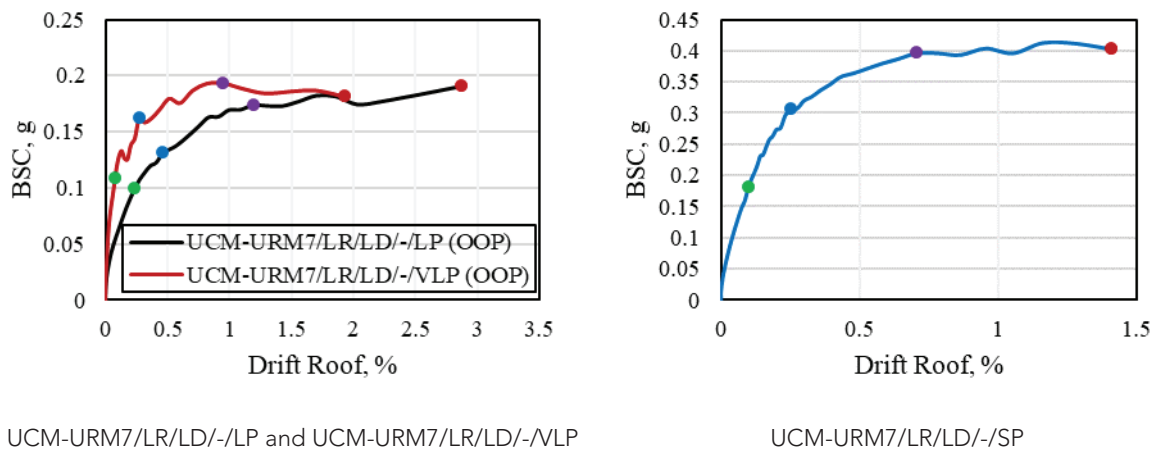
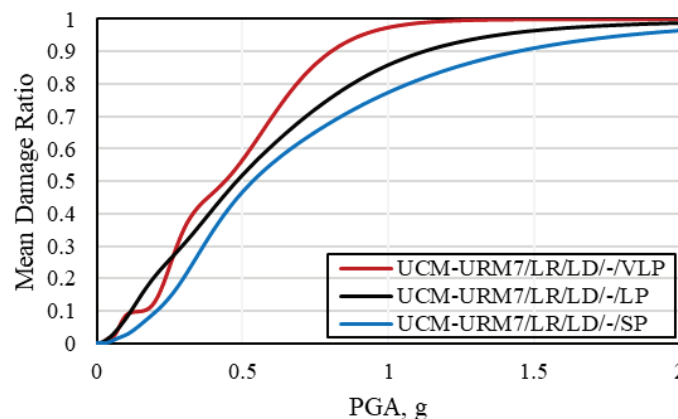


Figure 60 shows the vulnerability curves for different index buildings with different wall panel lengths. For the VLP index building, the vulnerability is considerably

higher, while the vulnerability reduces noticeably when the wall panels are short (SP model).

Figure 60. Comparison of vulnerability curves for the index buildings with different wall panel lengths.



5.1.5 Wall Opening

The openings (number, size and layout) can greatly reduce the shear/flexural capacity of masonry walls. The opening is considered small when the total width of opening in an unrestrained wall panel is less than 50% of the wall length. Two different percentages

of wall openings are considered here: one with 46% opening (small opening, SO model) and another with 65% opening (large opening, LO model). Figure 61 presents the numerical models of UCM-URM7 index buildings with different opening configurations.

Figure 61. Numerical models of UCM-URM7 index buildings with different wall opening configurations.

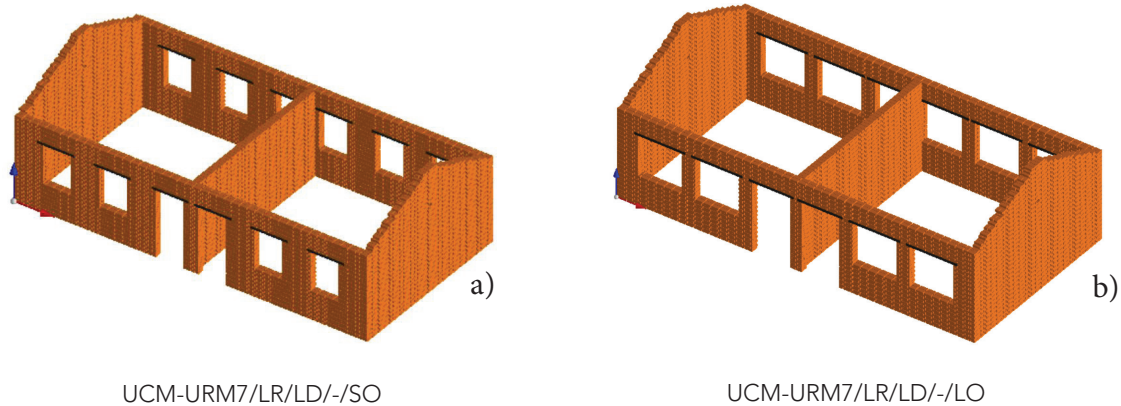


Figure 62 shows the collapse mechanisms of the index buildings with different opening configurations. The building with large openings has very weak and

slender piers in the IP walls, and the OOP walls easily develop the combined mechanism by detaching the portion of weaker connections with IP walls.

Figure 62. Collapse mechanisms of UCM-URM7 index buildings with different opening configurations. The blue lines represent the extensive cracks of a width of more than 12.5 mm (only extensive cracks are shown).

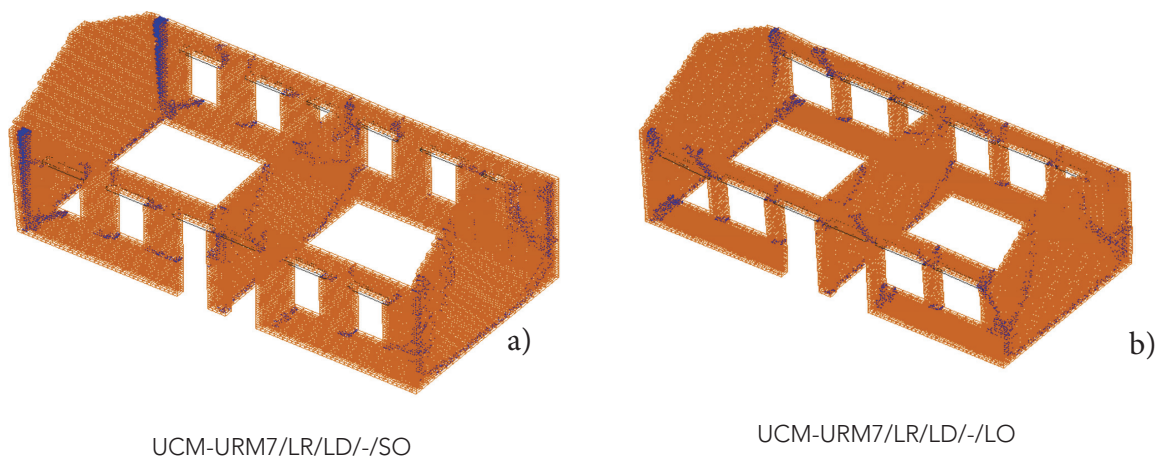


Figure 63 shows the capacity curves along with the different damage state thresholds marked along the capacity curves. For the LO model, the initial

stiffness, strength and the displacement capacity are considerably reduced compared to the SO model.

Figure 63. Comparison of capacity curves for the index buildings with different wall opening configurations. The colored dots represent the threshold of different damage states: Green = Slight Damage, Blue = Moderate Damage, Purple = Extensive Damage and Red = Collapse.

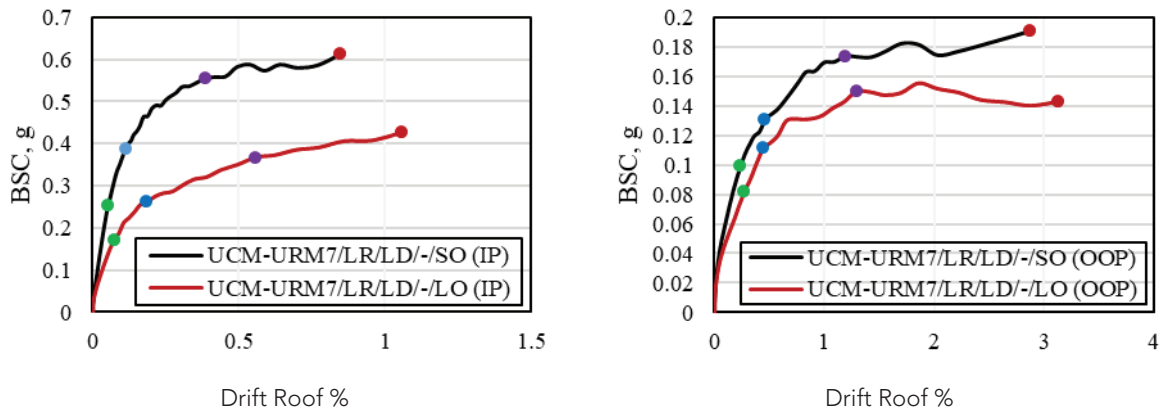
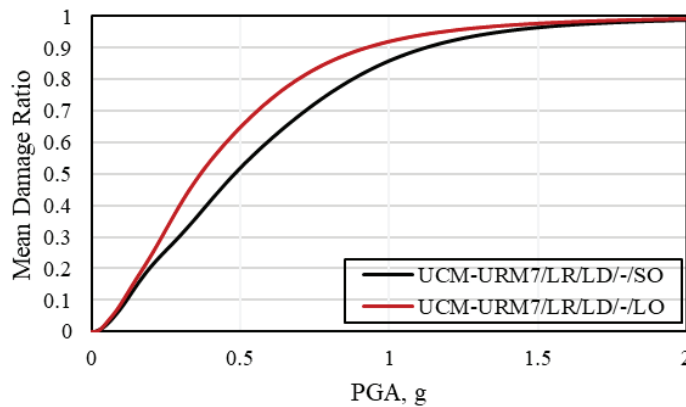


Figure 64 shows the vulnerability curves for different index buildings with different opening configurations.

For the LO index building, the vulnerability noticeably increases compared to the SO index building.

Figure 64. Comparison of vulnerability curves for the index buildings with different wall opening configurations.



5.1.6 Effective Seismic Retrofitting

The seismic performance of the poorly designed older masonry buildings can be improved by applying effective seismic retrofitting. Here, one of the most common strengthening methods, i.e. the addition of the roof level RC band beam, is employed to determine the improvement in the seismic behavior of the building. As shown previously in the cases of the MD and HD models, the roof level band beam will control the OOP wall failures, thus improving the

global seismic behavior. However, care should be taken when applying such retrofitting intervention, considering that the high difference in the stiffness of the original structure and applied retrofitting measures can degrade the seismic performance. For example, if the units or mortar quality in the existing building is poor (or deteriorated), the structure cannot take the overburden due to the addition of retrofitting elements.

Figure 65. Numerical models of UCM-URM7 index buildings: original building and retrofitted building.

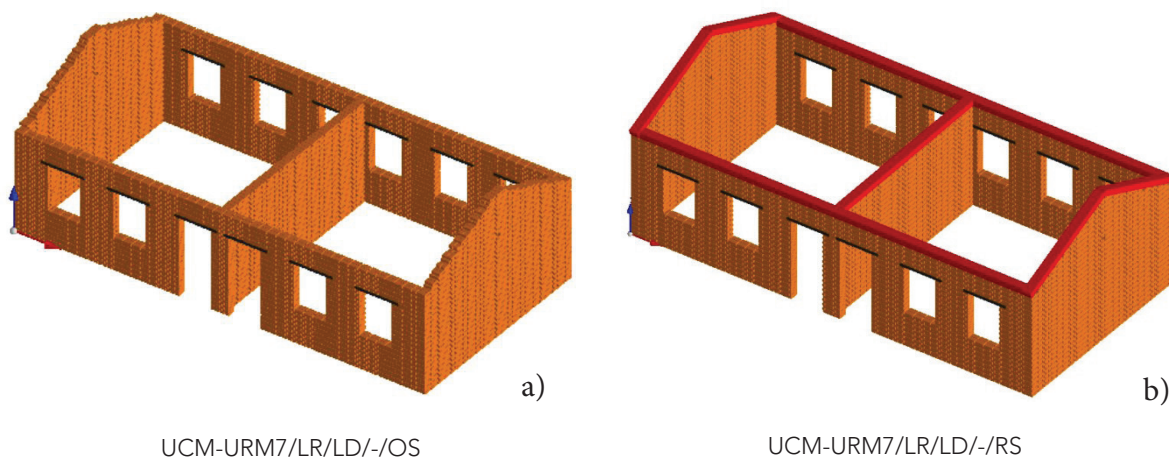


Figure 66 shows the capacity curves along with the different damage state thresholds marked along the capacity curves. It can be seen from the capacity curves that both the strength (with respect to the OOP wall of

FD model) and displacement capacity (with respect to the IP wall of FD model) are improved in the case of retrofitted structures (RS).

Figure 66. Comparison of capacity curves for the index buildings: original structure and retrofitted structure. The colored dots represent the threshold of different damage states: Green = Slight Damage, Blue = Moderate Damage, Purple = Extensive Damage and Red = Collapse.

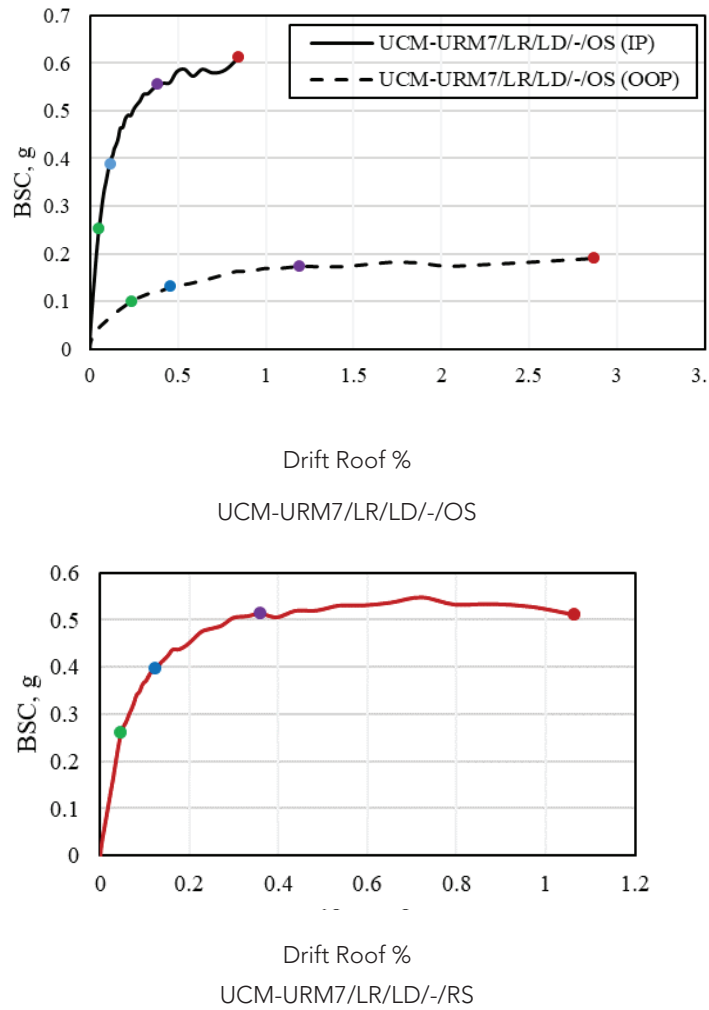
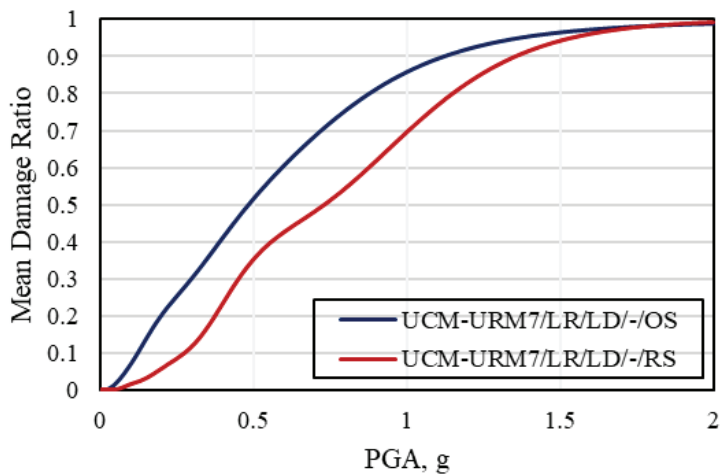


Figure 67 shows the vulnerability curves for different index buildings with and without seismic retrofitting measures. In the case of the RS index building, the

vulnerability greatly reduces compared to the OS index building.

Figure 67. Comparison of vulnerability curves for the original and retrofitted index buildings.



5.1.7 Structural Health Condition

The structural health condition is the current condition of a building with respect to its material quality, existing damages, etc. The quality of construction materials and present deterioration condition highly influence the seismic capacity and performance of a masonry building and vary greatly from one building to another. Thus, a comparison of the analysis results for three different index buildings with different material qualities is presented. The very poor condition (VPC) building model has 40% lower values of material properties than those of the baseline model (poor condition, PC whose material properties are presented in Table 9),

while the good condition (GC) model has 100% better values of material properties than those of the baseline model. However, it should be noted that in reality the material properties in the same building typology can vary drastically from one building to another within a country, or from one country to another.

Figure 68 shows the capacity curves along with the different damage state thresholds marked along the capacity curves. As the material quality increases, the initial stiffness, strength and the displacement capacity also increase. The effect is more pronounced in the IP seismic behavior.

Figure 68. Comparison of capacity curves for the index buildings with different material quality. The colored dots represent the threshold of different damage states: Green = Slight Damage, Blue = Moderate Damage, Purple = Extensive Damage and Red = Collapse.

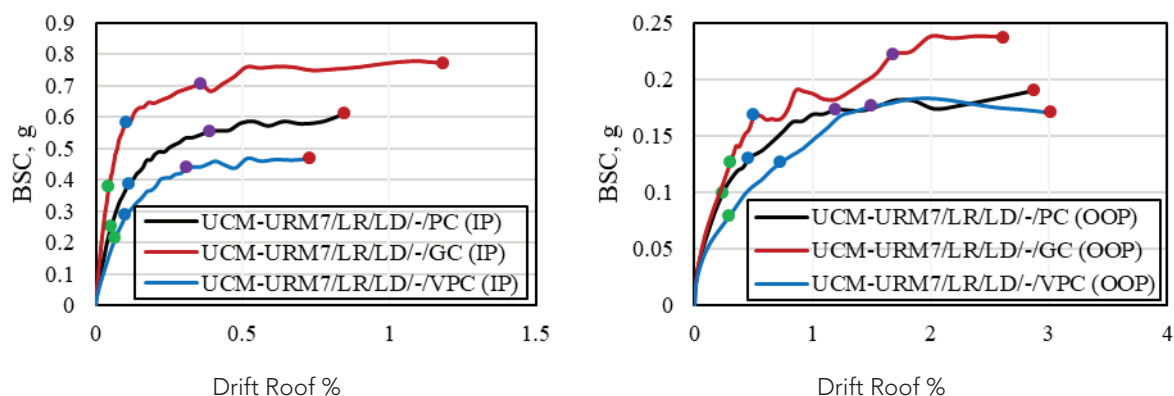
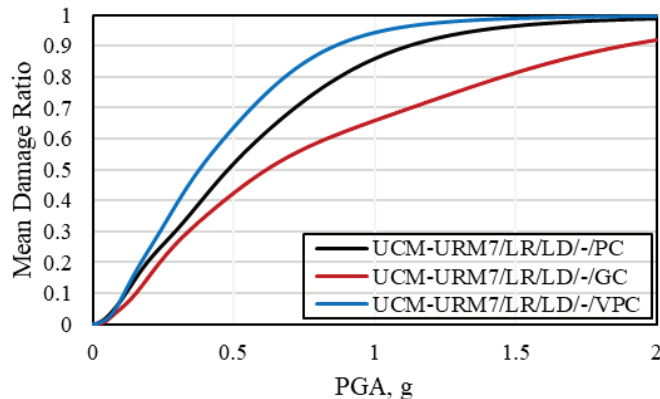


Figure 69 shows the vulnerability curves for different index buildings with different material quality. Buildings with poor quality materials (in the original

construction or deteriorated) are highly vulnerable, while the vulnerability can be greatly reduced if good quality materials are used in the building construction.

Figure 69. Comparison of vulnerability curves for the index buildings with different material quality.



To sum up, the seismic performance and vulnerability are highly sensitive to the different vulnerability parameters and their attributes (range):

Figure 70 compares the vulnerability curves for different index buildings of the UCM-URM7 building type. It is obvious that the vulnerability varies greatly with

considerable dependence on all different sensitivity parameters. As expected, the model representing the high design (HD) case shows the lowest vulnerability, while the models with large openings (LO) and poor material qualities (PC) show the highest vulnerability in a realistic PGA range.

Figure 70. Comparison of all vulnerability curves for different index buildings considered in the sensitivity analysis.

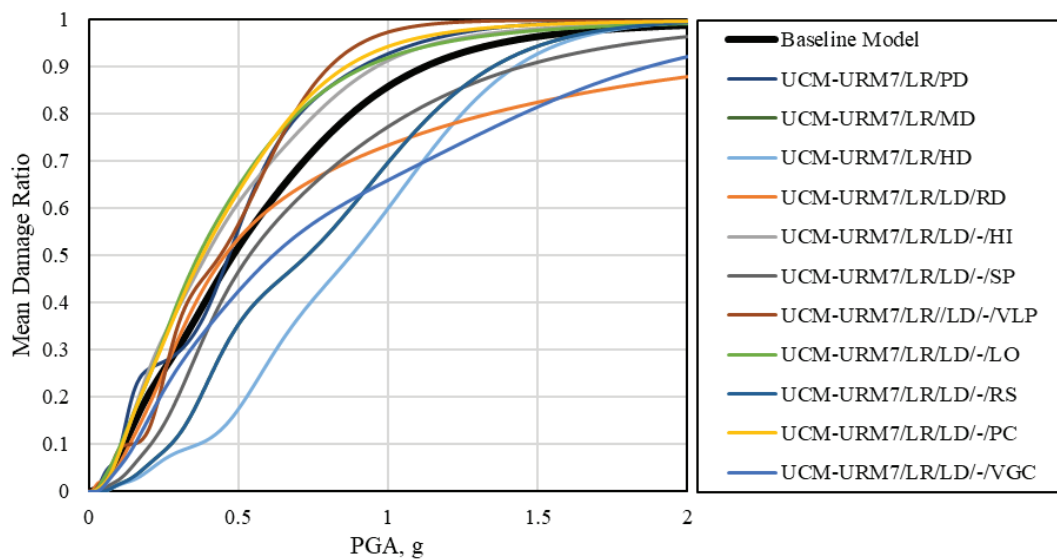


Figure 71. Mean, confidence boundary and the standard deviation of all different vulnerability functions for the UCM-URM7 school building class.

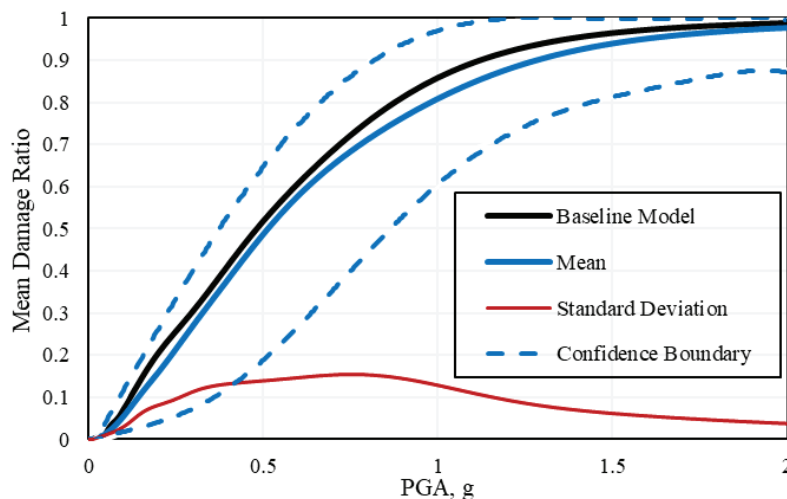


Figure 71 presents a more concise and clear plot of the vulnerability curves, in which the vulnerability curve of the baseline model, mean (of all different vulnerability curves), confidence boundary as well as the standard deviation are depicted. It is interesting to note that the mean vulnerability curve and the vulnerability curve for the baseline model are similar, which proves that the baseline model (UCM-URM7/LR/LD) represents a building with average construction characteristics

and was a good choice for the reference model. The confidence boundaries provide the variability of the vulnerability values at a given IM (i.e. PGA), which is very useful for decision making.

Table 19 presents the summary of the results with respect to the changes in seismic behavior, damage indicators, and vulnerability.

Table 19. Summary of sensitivity analysis results for UCM-URM7 IB.

Parameter	Attributes	Global box-like behavior	Collapse Mechanism	% change with respect to the baseline case			
				Initial Stiffness	Ultimate Capacity	Ultimate Roof Drift	PGA at 50% MDR
Seismic Design Level	Poor Design (PD)	No	Collapse of OOP walls	0%	-15%	0%	-11%
	Low Design (LD) Reference	No	Collapse of OOP walls	-	-	-	-
	Medium Design (MD)	Yes	Shear failure of IP piers	1174%	168%	25%	58%
	High Design (HD)	Yes	Shear failure of IP piers	1893%	311%	33%	96%
Diaphragm Type	Flexible Diaphragm (FD) Reference	No	Collapse of OOP walls	-	-	-	-
	Rigid Diaphragm (RD)	Yes	Shear failure of IP piers	363%	167%	73%	0%
Irregularity	No Irregularity (NI) Reference	No	Collapse of OOP walls	-	-	-	-
	Horizontal Irregularity (HI)	No	Collapse of OOP walls	-46%	-23%	-45%	-22%
Wall Panel Length	Very Long Panel (VLP)	No	Collapse of OOP walls	212%	11%	-33%	-10%
	Long Panel (LP) Reference	No	Collapse of OOP walls	-	-	-	-
	Short Panel (SP)	Yes	Shear failure of IP piers	310%	130%	66%	15%
Wall Opening	Large Opening (LO)	No	Collapse of OOP walls	-52%	-34%	9%	-25%
	Small Opening (SO) Reference	No	Collapse of OOP walls	-	-	-	-
Effective Seismic Retrofitting	Original Structure (OS) Reference	No	Collapse of OOP walls	-	-	-	-
	Retrofitted Structure (RS)	Yes	Shear failure of IP piers	1174%	168%	25%	58%
Structural Health Condition	Very Poor Condition (VPC)	No	Collapse of OOP walls	-31%	-33%	-14%	-24%
	Poor Condition (PC) Reference	No	Collapse of OOP walls	-	-	-	-
	Good Condition (GC)	No	Collapse of OOP walls	74%	17%	39%	27%

With respect to the seismic design level, the initial stiffness, ultimate capacity, and ultimate drift are improved the most when the seismic design level is medium and high (MD and HD), in comparison to poor and low design (PD and LD) cases. Similarly, the PGA level for 50% MDR is also significantly improved. In the same way, the introduction of a rigid diaphragm (RD) or seismic strengthening (RS) also improve the seismic behavior noticeably. Global box-like behavior is obtained when the seismic design level is MD and HD, the diaphragm is an RD type, and the structure is effectively retrofitted (RS).

When the openings are large (LO) or when there is a horizontal irregularity (HI) introduced due to the difference in opening, the seismic capacity as well as the PGA for 50% MDR are noticeably reduced. When the unrestrained panels (VLP) are very long, although the initial stiffness and ultimate capacity are higher, the ultimate drift capacity is reduced, and vulnerability increases. However, when the unrestrained wall panels are short (SP), the building develops a box-like global behavior and the vulnerability reduces. With respect to the structural health condition, the seismic capacity improves when the material quality is good (GC), in comparison to the case when the material quality is poor (VPC and PC). The vulnerability can be further reduced by using better quality construction materials.

5.2 Reinforced Concrete

This section presents the sensitivity analysis for Reinforced Concrete school buildings. The main

objective of these analysis is to understand the impact on the final vulnerability assessment with the expected variation in critical parameters. The following variables were considered:

- Geometrical variations: three different geometries considering 2, 3 and 5 classrooms
- Ground motion records for different soil types: hard, medium and soft
- Foundation-soil flexibility: combinations of different soil and foundation types
- Masonry infill quality: high, medium and poor
- Non-structural vulnerable elements: ductile and fragile behavior
- Analysis type: N2 method vs. incremental dynamic analysis (IDA)

These analyses were performed using the same methodological approach described above, and the results are illustrated in the following sections.

5.2.1 Geometrical variations

The first sensitivity analysis is made for eventual and expected geometrical variations of the school's layouts. Analysis was performed using the computer model of index building IBRC-2 (RC1-MR-LD) as a basis. Three different layouts were selected for the analysis as illustrated in Figure 72, representing three (the most common), two and four typical classrooms. All models were considered as two-story.

Figure 72. School buildings modules.

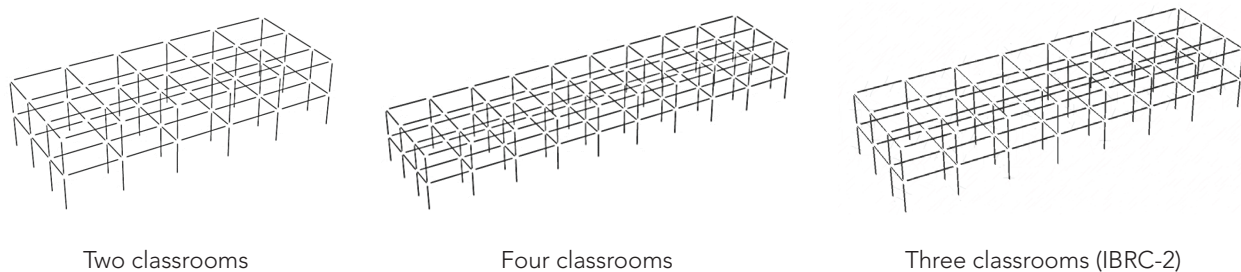
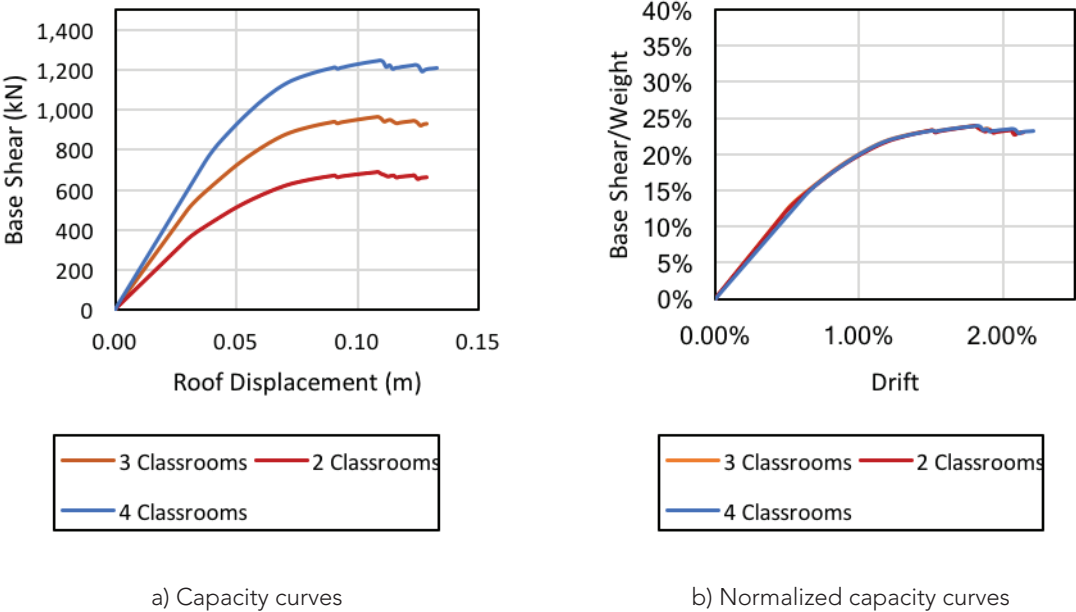


Figure 73 presents the capacity curves relating the maximum roof displacement associated to different total base shear forces. Normalized pushover curves are also included, in order to compare relative behavior between the different models considered. As it is shown in these figures, the normalized capacity curves for the three models do not present significant variations from each other. Considering that the Engineering Demand

Parameters (EDP) are obtained using the N2 method in GLOSI, no significant variations are expected in the final vulnerability functions for the three models. Therefore, it is concluded that the derived vulnerability function for the three-classroom model is representative of other general plan layouts, as long as no irregularities or other critical structural behavior is generated with alternative layouts.

Figure 73. Capacity curves for different geometries.



5.2.2 Ground motion records for different soil types

Ground motion sensitivity analysis was performed using the computer model developed for index building IBRC-3 (RC1-MR-HD). Three different

ground motion sets were obtained analytically for the following representative soil profiles: stiff soil (rock), intermediate, and soft soils. Figure 74 shows the acceleration response spectra for each set of records.

Figure 74. Ground motions acceleration response spectra for different soil profiles.

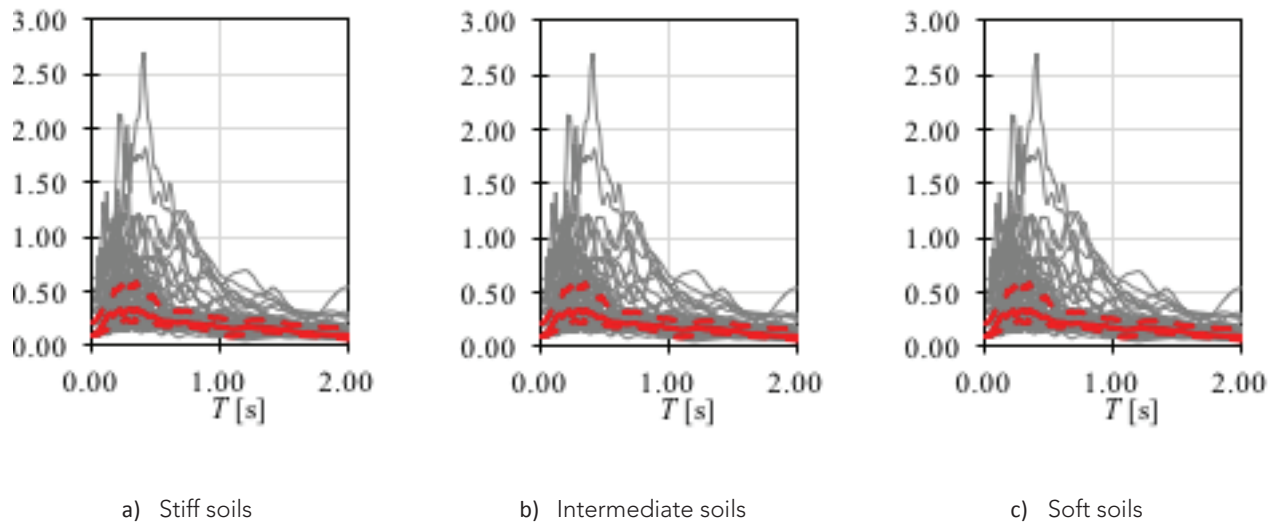


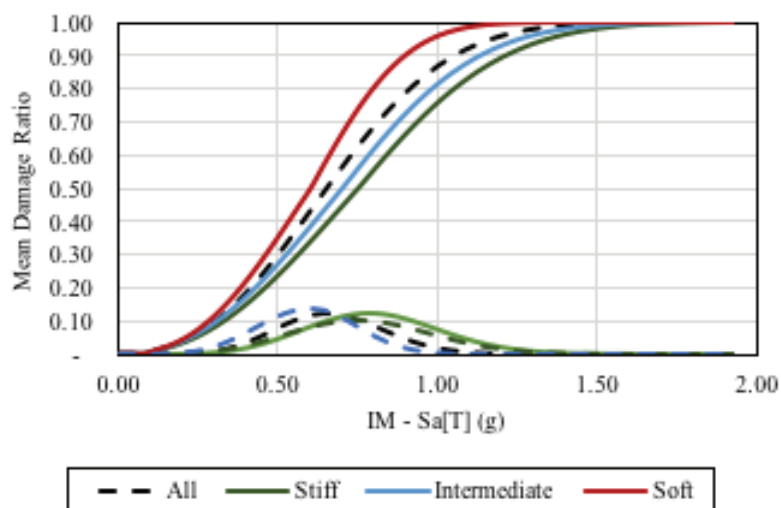
Figure 75 presents the resulting vulnerability functions for the same Index Building, but using the abovementioned ground motion sets. From these results, the following can be concluded:

- No significant variations are obtained in the mean damage ratio for low seismic intensities ($S_a(T)$ less than 0,5 g).
- For larger intensities, maximum variations of about 20% are obtained in the mean damage ratio when

using soft soil typical records as compared to stiff soil ones.

- Soft soil records tend to generate greater expected building level damages.
- Using only stiff soil records can underestimate the building damage for high seismic intensities. In case that the soil profile conditions are unknown, it is recommended to use a combination of stiff and soft soil typical ground motions.

Figure 75. Vulnerability functions for the same building in different type of soils.



5.2.3 Foundation-soil flexibility

To assess the possible variations in the vulnerability functions when the soil-foundation stiffness is considered, index building model IBRC-3 was used

as reference for the analysis. Two different foundation configurations were tested (1.0 m by 1.0 m (Z1) and a 0.5 m by 0.5 m. (Z2) isolated footings) when combined with four different soil types as indicated in Table 20.

Table 20. Soil properties for foundation stiffness calculation.

Type	G/G0	Soil	Density _{sat} (kN/m ³)	Vs30 (m/s ²)	ν
C	0.9	Lime	22	500	0.35
D	0.81	Clay	18	300	
E	0.47	Clay	18	200	
F	0.32	Clay	18	100	

Resulting capacity curves are presented in Figure 76 for all possible combinations of foundation configuration

and soil type. Corresponding vulnerability functions are presented in Figure 77.

Figure 76. Capacity curves with foundation in different soil types.

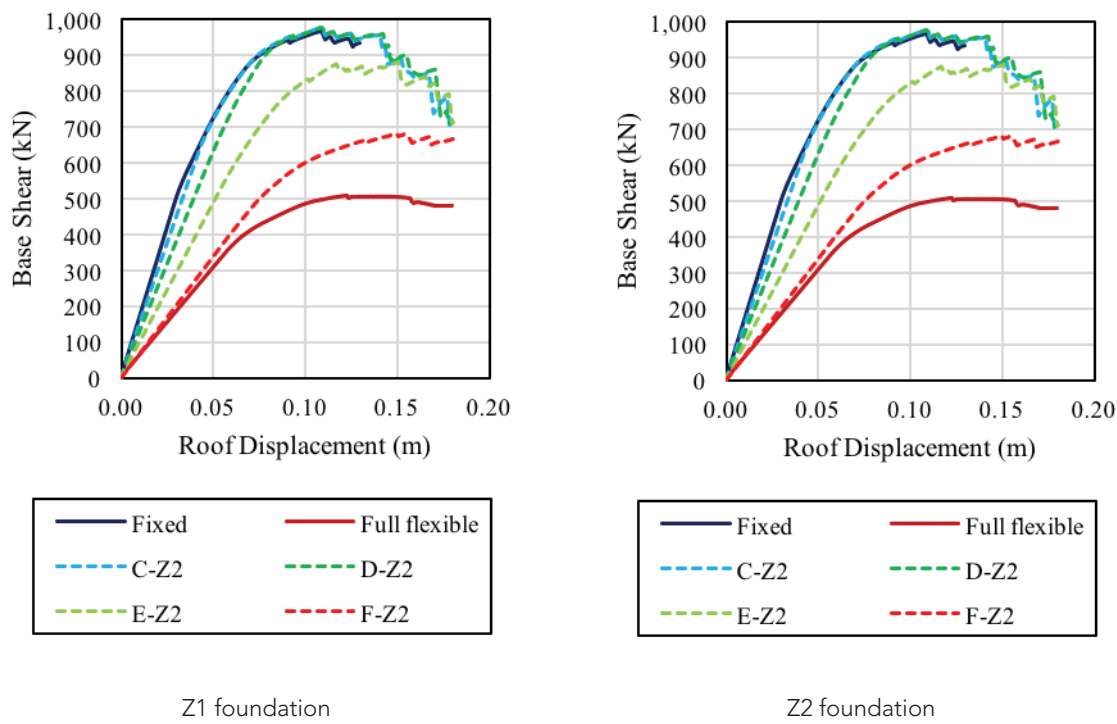
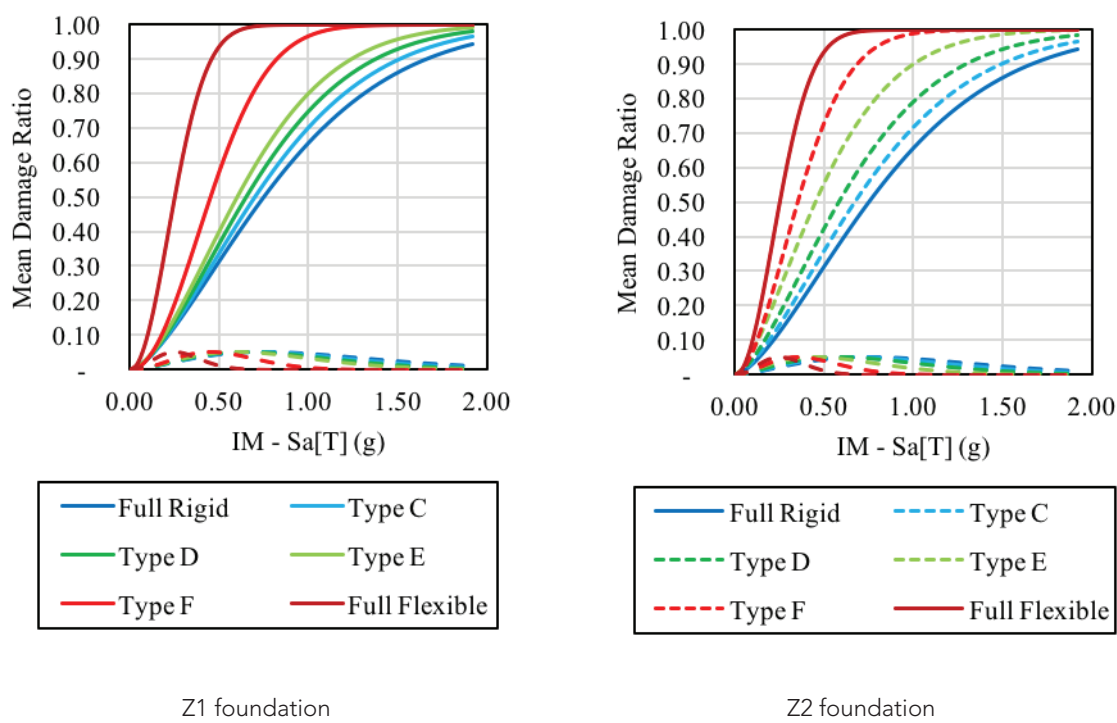


Figure 77. Vulnerability functions with different foundation stiffness.



The following conclusions can be drawn from these results:

- Good foundation configurations (represented by Z1 footings) lead to pushover curves and vulnerability functions in close relation to the rigid base model, except for a considerable flexible soil, in which case some significant variations in response would be expected.
- For relatively weak foundation configurations (represented by Z2 footings), considerable variations would be expected for different soil types. For stiff soil profiles (soil types A, B, C or D in the previous table) the expected behavior will approximate the fixed base assumption. On the other hand, for flexible soil profiles (soil types E, or F in the previous table) the expected behavior will approximate the hinged base assumption.

- In general, the most common assumption of rigid base behavior can be sustained only when a relatively good foundation configuration is expected in medium or stiff soil profiles. In the cases where there is evidence of soft soil profiles with probable deficiencies in the foundation configuration, flexible support conditions shall be considered in the assessment, given that those conditions will generate a higher vulnerability condition for the building under consideration.

5.2.4 Masonry infill quality

To test the relevance of masonry infill quality in the final vulnerability assessment, different masonry properties are selected as it described in Table 21 to perform a sensitivity analysis. In this case, index building model IBRC-9 (RC2/MR/LD) was selected.

Table 21. Masonry properties.

Quality	Age	Country	Block Material	Dimensions (bxLxt)	f_v (Mpa)	E (Mpa)	Friction coefficient
High	New	Colombia	Clay brick	10x20x6	0.9	8700	0.7
Medium	Intermediate	USA	Clay brick	10x28x6	0.13	1050	
Poor	Old	Colombia	Clay tile	11x30x20	0.1	1560	

Figure 78 presents the capacity curves obtained using the three previous masonry quality conditions as compared to the bare frame (no masonry infills) conditions. From the figure, it is clear that masonry infills, when not isolated from the structure, can heavily affect the expected structural behavior of the

building. Also, the collapse mechanism of the building can significantly change, as more resistant but fragile behavior can be obtained. In some cases, a weak floor failure mechanism can be generated when the first-floor infill walls fail under horizontal seismic loading.

Figure 78. Capacity curves using different masonry qualities.

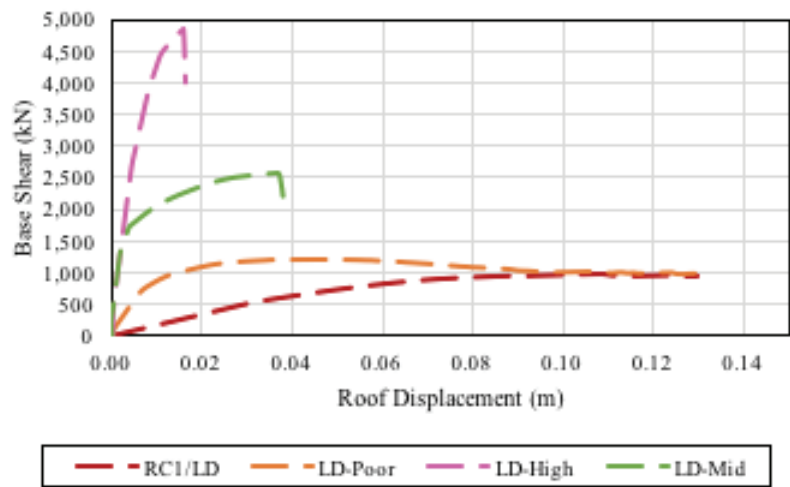
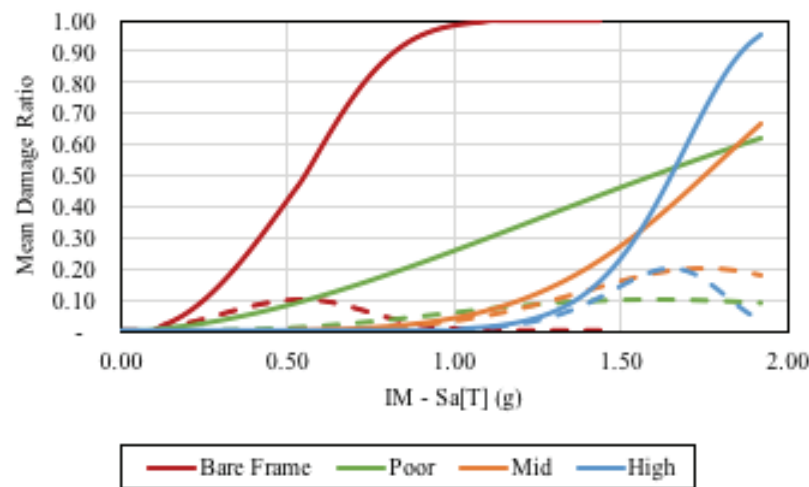


Figure 79 illustrates that a great variability of results is expected for the range of masonry infill qualities considered. It is worth noting that the curves are not directly comparable because the building’s

structural predominant period will significantly change depending on the quality of the masonry infills and therefore different intensity parameters will be used for the risk assessment.

Figure 79. Vulnerability functions using different masonry qualities.



In conclusion, the quality of the masonry infills in a school building, if not isolated from the main structure, will have a significant impact on the final vulnerability of the building. Therefore, it is highly recommended to consider the quality of the masonry infills as a critical variable for the assessment.

5.2.5 Non-structural vulnerable elements

The objective of this sensitivity analysis is to identify

the effect of considering non-structural elements (NEE) in the loss calculation process. To that end, the index building model IBRC-3 (RC1/MR/HD) is selected. The following three conditions are considered: (i) No non-structural elements; (ii) poor quality fragile non-structural elements, and; (iii) high quality ductile non-structural elements. Table 22, Table 23 and Table 24 present the component models for these three conditions.

Table 22. Only structural elements component model.

Story	Group	Subgroup	Description	Quantity	Fragility curve	EDP	Correlation
1	E	C1	Column-one beam	8	B1041.091a	Drift	0
1	E	C2	Column-two beams	21	B1041.091b	Drift	0
2	E	C1	Column-one beam	8	B1041.091a	Drift	0
2	E	C2	Column-two beams	21	B1041.091b	Drift	0

Table 23. Poor quality component model.

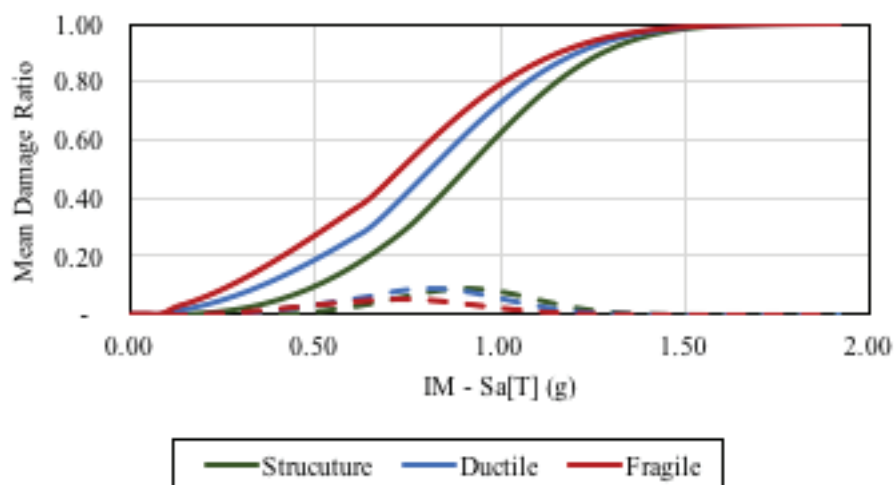
Story	Group	Subgroup	Description	Quantity	Fragility curve	EDP	Correlation
1	E	C1	Column-one beam	8	B1041.091a	Drift	0
1	E	C2	Column-two beams	21	B1041.091b	Drift	0
1	A	F2	Masonry facade	14	C1011.006a	Drift	1
1	A	M4	Masonry wall	6	C1011.006b	Drift	1
1	C	S2	Contents	13	E2022.010a	Drift	0
2	E	C1	Column-one beam	8	B1041.091a	Drift	0
2	E	C2	Column-two beams	21	B1041.091b	Drift	0
2	A	F2	Masonry facade	14	C1011.006a	Drift	1
2	A	M4	Masonry wall	6	C1011.006b	Drift	1
2	C	S2	Contents	13	E2022.010a	Drift	0

Table 24. High quality component model.

Story	Group	Subgroup	Description	Quantity	Fragility curve	EDP	Correlation
1	E	C1	Column-one beam	8	B1041.001a	Drift	0
1	E	C2	Column-two beams	21	B1041.001b	Drift	0
1	A	F2	Masonry facade	14	C1011.001a	Drift	1
1	A	M4	Masonry wall	6	C1011.001a	Drift	1
1	C	S2	Contents	13	E2022.010a	Drift	0
2	E	C1	Column-one beam	8	B1041.001a	Drift	0
2	E	C2	Column-two beams	21	B1041.001b	Drift	0
2	A	F2	Masonry facade	14	C1011.001a	Drift	1
2	A	M4	Masonry wall	6	C1011.001a	Drift	1
2	C	S2	Contents	13	E2022.010a	Drift	0

Figure 80 presents the vulnerability curves for each of the cases explained above.

Figure 80. Vulnerability functions using different component models.



From the previous results, it can be concluded that variations on the order of 20% in the mean damage ratio could be expected when considering fragile NEE as compared with a building with no NEE for the lower ranges of seismic intensities. In addition, lower relative variations are expected in the higher range of seismic intensities, due to the fact that global building collapses would control the losses in the higher intensity range.

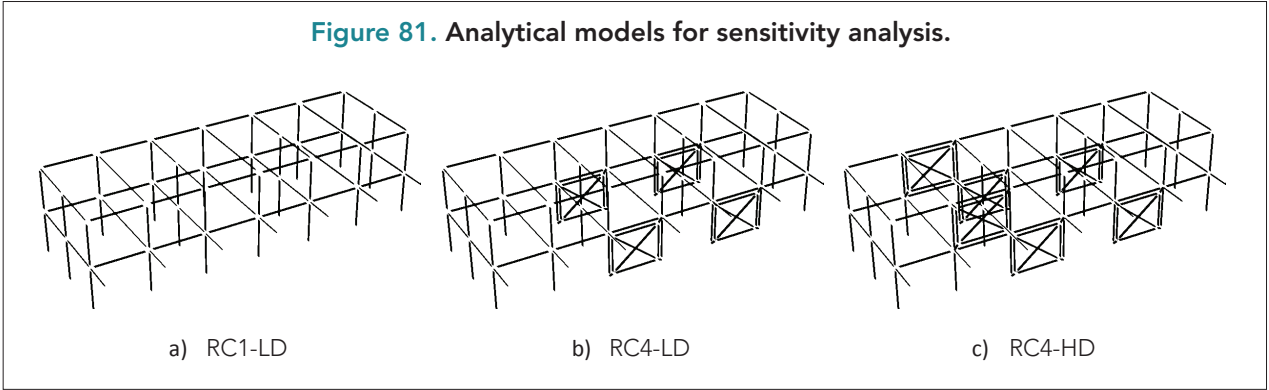
As a general recommendation, NEE shall be included in the vulnerability assessment when they represent

a significant replacement value as compared to the structure itself, and when they are expected to observe a fragile behavior and significant damage after an earthquake (e.g. no seismic design for NEE). The consideration of the NEE in those cases will generate a significant increase in the mean damage ratio of the global building especially for the low range of seismic intensities, and will therefore affect significantly the expected annual losses in the risk assessment process.

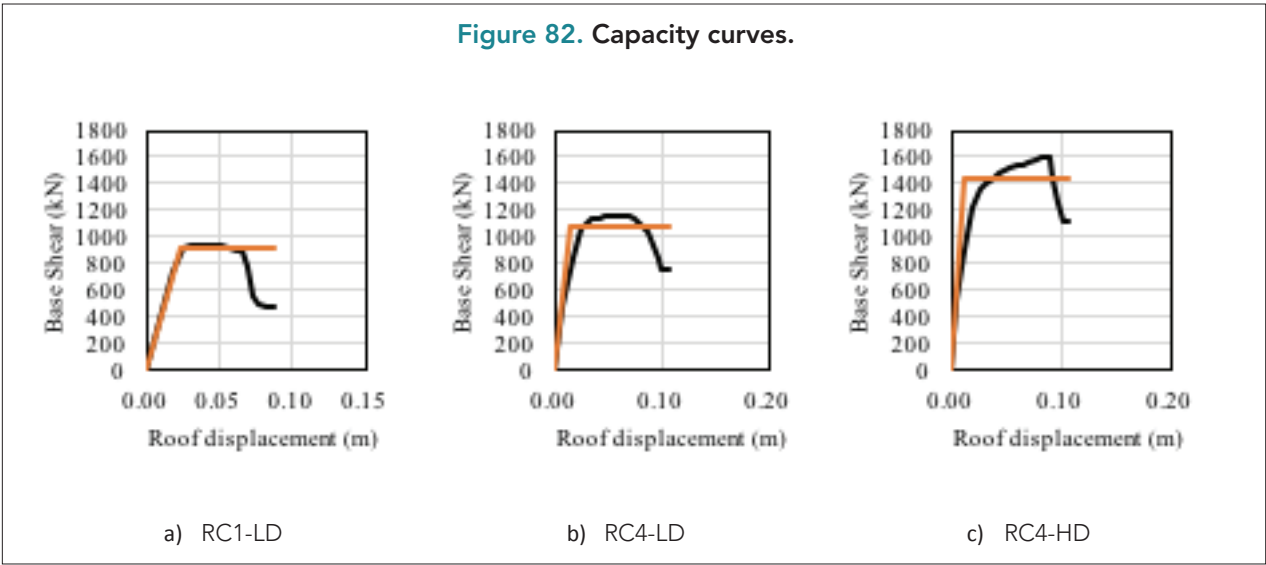
5.2.6 Analysis type

In order to establish the reliability of the N2 method used here, results are compared with equivalent incremental dynamic analysis (IDA). For this application,

three different models are considered, one RC1 model and two RC4 models (RC4-LD and RC4-HD), as shown in Figure 81.

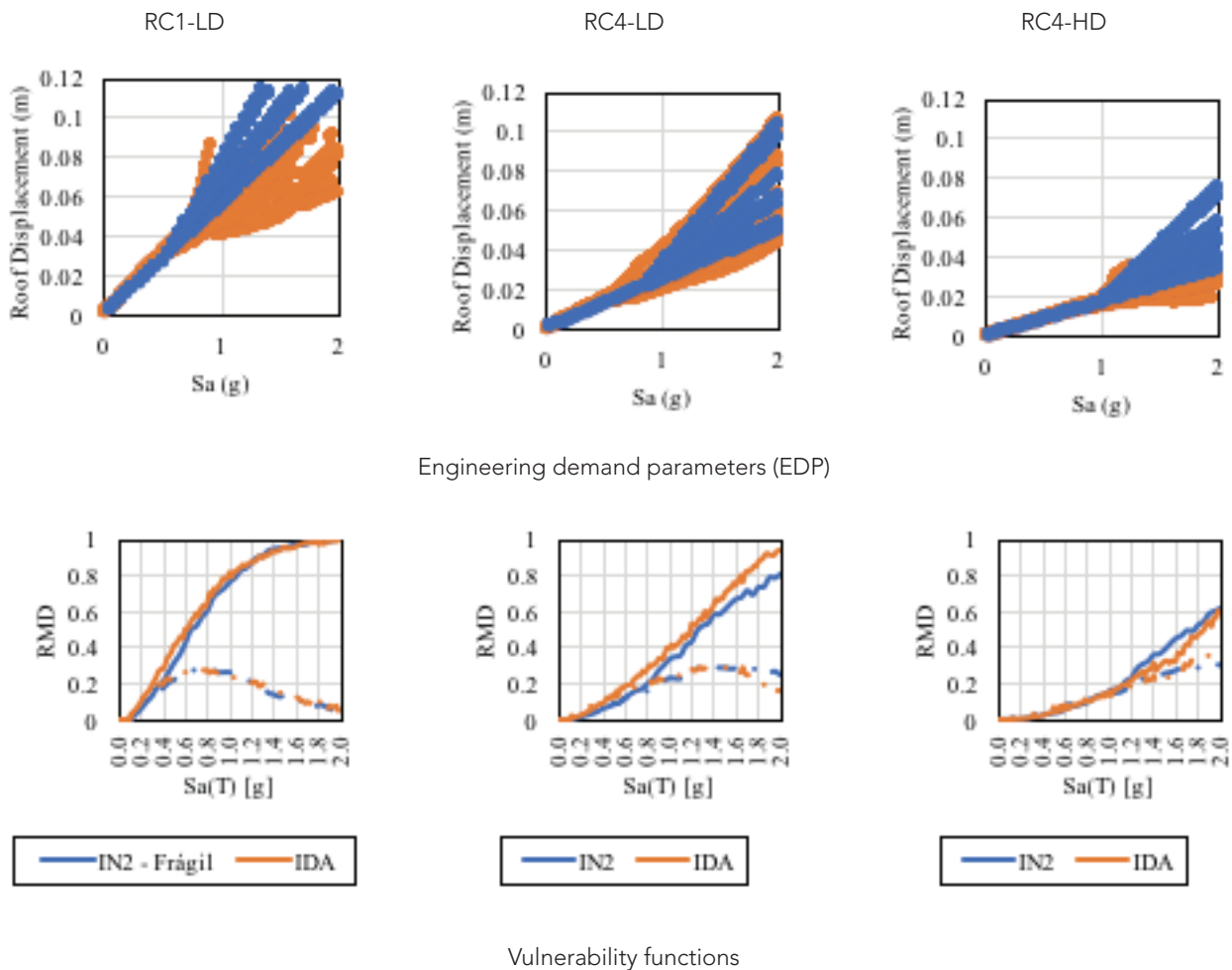


Capacity curves for these three models are presented in Figure 82. These were obtained using the methodological approach explained in detail in Section 2:



Engineering demand parameters (EDP) and the corresponding vulnerability functions are presented in Figure 83.

Figure 83. EDP and vulnerability curves.



From those results it can be concluded that the N2 method, which in general is much simpler and faster to run, gives comparable results with the more refined and time-consuming IDA method of analysis. Both methodologies generate similar mean and dispersion values. For the vulnerability assessment of typical

school buildings, the N2 method is clearly a reliable option for EDP calculations. Caution shall be exerted when considering non-typical school buildings, the behavior of which may be influenced by irregularities, variations in height, combined structural systems or any other special characteristic.

References

- ABAQUS (2013) Finite Element Analysis (Theory manual), Dassault Systèmes Simulia Corporation, Providence, USA.
- ASCE (2013) ASCE/SEI 41-13: Seismic Evaluation and Retrofit of Existing Buildings, American Society of Civil Engineers, Virginia, USA.
- Applied Technology Council (1985) ATC-13: Earthquake Damage Evaluation Data for California, Applied Technology Council, California, USA.
- Arya, S., Boen, T., & Ishiyama, Y. (2013) Guidelines for Earthquake Resistant Non-Engineered Construction, UNESCO, France.
- ARUP (2017) Measuring Seismic Risk in Kyrgyz Republic, The World Bank Report, ARUP, London.
- ASI (2018) Extreme Loading for Structures, Applied Science International, LLC, North Carolina, USA.
- CEN (2004) EC 8: Design of structures for earthquake resistance—Part 1: General rules, seismic actions and rules for buildings (EN 1998-1: 2004).
- Chopra Anil, K. (1995) Dynamics of structures: Theory and Application to Earthquake Engineering. Prentice Hall, New Jersey, USA.
- D'Ayala, D., Meslem, A., Vamvatsikos, D., Porter, K., Rossetto, T. (2015) Guidelines for Analytical Vulnerability Assessment - Low/Mid-Rise. GEM Technical Report, GEM Foundation, Pavia, Italy.
- D'Ayala, D.F., (2008) Numerical Modelling of Masonry Structures, Structures & Construction in Historic Building Conservation, pp. 151–172. doi: 10.1002/9780470691816.ch9.
- Decreto Ministeriale del 14/01/2008 (2008) Norme Tecniche per le Costruzioni. Gazzetta Ufficiale della Repubblica Italiana, 29., Rome
- De Luca F, Vamvatsikos D., Iervolino I. (2013) Improving Static Pushover Analysis by Optimal Bilinear Fitting of Capacity Curves. In: Papadrakakis M, Fragiadakis M, Plevris V (eds) Computational Methods in Earthquake Engineering. Springer
- De Luca F, Vamvatsikos D, Iervolino I (2013b) Near-optimal piecewise linear fits of static pushover capacity curves for equivalent SDOF analysis. Earthq Eng Struct Dyn 42:523–543 . doi: 10.1002/eqe.2225
- ERN (2009) Central American Probabilistic Risk Assessment (CAPRA) User Manual.
- Fajfar, P (2000) A nonlinear analysis method for performance-based seismic design. Earthquake Spectra 16.3: 573-592.
- FEMA (2005) Improvement of nonlinear static seismic analysis procedures, FEMA 440. Washington, D.C.
- FEMA (2012) Hazus – MH 2.1 Technical Manual, Washington D.C.
- Guragain, R. (2015), Development of Earthquake Risk Assessment System for Nepal, PhD thesis, The University of Tokyo, Japan.
- Karbassi, A. and Nollet, M. J. (2013) Performance-based seismic vulnerability evaluation of masonry buildings using applied element method in a nonlinear dynamic-based analytical procedure, Earthquake Spectra, 29(2), pp. 399–426. doi: 10.1193/1.4000148.
- Lang, K., (2002) Seismic Vulnerability of Existing Buildings, Doctoral Thesis, Swiss Federal Institute of Technology Zurich, Switzerland.
- Lagomarsino, S., Penna, A., Galasco, A. and Cattari, S., (2013) TREMURI program: an equivalent frame model for the nonlinear seismic analysis of masonry buildings. Engineering Structures, 56, pp.1787-1799.
- Maganes, G. (2006) Masonry Building Design in Seismic Areas: Recent Experiences and Prospects from a European Standpoint, First European Conference on Earthquake Engineering and Seismology, Geneva, Switzerland

- MARN (2012) Modelacion Probabilistica de Escenarios de Reiso Sismico Para el Area Metropolitana de San Salvador, Incluye Analisis de Los Portafolios de Educacion, Salud y Gobierno. Ministerio de Medio Ambiente y Recursos Naturales, El Salvador. (In Spanish)
- Meguro, K., and Tagel-Din, H. (2000) Applied Element Method for Structural Analysis, Doboku Gakkai Ronbunshu, 2000(647), 31-45.
- Mouroux, P., and Benoit, L.B. (2006) Presentation of RISK-UE Project, Bulletin of Earthquake Engineering, 4:323-339.
- Pandey, B. H. and Meguro, K. (2004) Simulation of brick masonry wall behavior under in-plane lateral loading using applied element method, 13th World conference on earthquake engineering, Vancouver, BC, Canada, August, pp. 1–6.
- Pannell, D. J. (1997) Sensitivity analysis of normative economic models: theoretical framework and practical strategies. *Agricultural economics*, 16(2), 139-152.
- Rossetto T., D'Ayala D., Ioannou I., Meslem A. (2014) Evaluation of Existing Fragility Curves. In: Pitilakis K., Crowley H., Kaynia A. (eds) SYNER-G: Typology Definition and Fragility Functions for Physical Elements at Seismic Risk. *Geotechnical, Geological and Earthquake Engineering*, vol 27. Springer, Dordrecht
- Shome, N. and Cornell, C. A.. (1999) Probabilistic Seismic Demand Analysis of Nonlinear Structures. Reliability of Marine Structures Program Technical Report RMS-35. Stanford Digital Repository. Available at: <http://purl.stanford.edu/qp089qb1141>
- Yamin, L., Hurtado, A., Barbat, A. H., & Cardona, O. D. (2014) Seismic and wind vulnerability assesment for the GAR-13 global risk assessment. *International Journal of Disaster Risk Reduction*, 10, 425–460.
- Yamin, L. E., Hurtado, A., Rincon, R., Dorado, J. F., & Reyes, J. C. (2017) Probabilistic seismic vulnerability assessment of buildings in terms of economic losses. *Engineering Structures*, 138, 308-323.

Learn more about us
gps.worldbank.org

Contact information
gps@worldbank.org





GLOSI THE GLOBAL LIBRARY OF SCHOOL INFRASTRUCTURE

Learn more about us

gpss.worldbank.org

Contact information

gpss@worldbank.org